Robotic High-Throughput Screening for the Optimization and Prediction of Recombinant Protein Expression in Microscale

Automatisiertes Hochdurchsatzscreening zur Optimierung und Vorhersage der rekombinanten Proteinexpression im Mikromaßstab

Von der Fakultät für Maschinenwesen der Rheinisch-Westfälischen Technischen Hochschule Aachen zur Erlangung des akademischen Grades einer Doktorin der Ingenieurwissenschaften genehmigte Dissertation

vorgelegt von

Martina Julia Mühlmann

Berichter: Universitätsprofessor Dr.-Ing. Jochen Büchs
Universitätsprofessor Dr.-Ing. Andreas Kremling

Tag der mündlichen Prüfung: 07.12.2018

Danksagung

Die vorliegende Arbeit ist während meiner Tätigkeit als wissenschaftliche Mitarbeiterin am Lehrstuhl für Bioverfahrenstechnik innerhalb der Aachener Verfahrenstechnik (AVT.BioVT) an der Fakultät für Maschinenwesen der RWTH Aachen im Zeitraum von Februar 2014 bis März 2018 entstanden. Das Projekt wurde durch die Deutsche Forschungsgemeinschaft (DFG) im Rahmen des Exzellenzclusters “Tailor made fuels from biomass” gefördert.

Mein besonderer Dank gilt Prof. Dr.-Ing. Jochen Büchs für die gute fachliche Betreuung meiner Arbeit und der Möglichkeit zur Promotion am Lehrstuhl für Bioverfahrenstechnik. Seine wertvollen Anregungen und Diskussionen haben maßgeblich zum Erfolg dieser Arbeit beigetragen. Weiterhin möchte ich mich bei Prof. Dr.-Ing. Andreas Kremling für die Übernahme des Koreferats bedanken. Ebenso gilt mein Dank Prof. Dr.-Ing. Dirk Müller für die Übernahme des Prüfungsvorsitzes.

Den zahlreichen Studierenden, die mich als HiWis, Forschungspraktikanten oder im Rahmen einer Bachelor- oder Masterarbeit während meiner Promotion unterstützt haben und einen großen Beitrag zu dieser Arbeit geleistet haben, danke ich ebenfalls recht herzlich: Erik Böhm, Bertram Geinitz, Pia Händel, Diana Noffke, Jennifer Goldmanns, Niklas Knaup, Xenia Steurer, Sarah Stachurski, Eva Forsten und Saskia Noack. Mark Broderius, André Schmeing und Frederik Erkens danke ich für die langjährige Unterstützung als HiWis bei der RoboLector Programmierung.

Bei meinen Kollegen und Freunden der AVT.BioVT möchte ich mich für die großartige Zeit am Lehrstuhl bedanken. Die Hilfsbereitschaft und die stets sehr angenehme Arbeitsatmosphäre habe ich sehr zu schätzen gewusst. Für die Unterstützung bei der Vorbereitung und Korrektur von Veröffentlichungen und Vorträgen möchte ich mich ganz besonders bei meinen Bürokollegen Kira Kauffmann und Betram Geinitz bedanken, sowie bei Nina Ihling, Timm Keil und Robin Lamm.

Mein ganz besonderer Dank gilt meinen Eltern und meiner Schwester, die immer an mich geglaubt haben und mich nicht nur während meiner Promotionszeit bedingungslos unterstützt haben. Meinem Freund Chris danke ich für die unendliche Geduld mit mir, den Glauben an mich und in das Gelingen der Arbeit.

München, im Januar 2019 Martina Mühlmann

Publications

This work was performed during my doctoral research at the chair of Biochemical Engineering, RWTH Aachen University as part of the “Tailor made fuels from biomass” (TMFB) project EXC236 which was funded by the German Research Foundation (DFG).

By the time of submission, main aspects and passages of this thesis have already been published. This is in agreement with my supervisor Prof. Dr.-Ing. Jochen Büchs.

- Mühlmann M[§], Kunze M[§], Ribeiro J, Geinitz B, Lehmann C, Schwaneberg U, Commandeur U, Büchs J (2017) Cellulolytic RoboLector - towards an automated high-throughput screening platform for recombinant cellulase expression. Journal of Biological Engineering 11:1

- Mühlmann M, Forsten E, Noack S, Büchs J (2017) Optimizing recombinant protein expression via automated induction profiling in microtiter plates at different temperatures. Microbial Cell Factories 16:220

- Mühlmann M, Büchs J (2018) Automatisiertes Klonscreening und Vorhersage der Expressionsleistung. BioSpektrum 24:46–49

- Mühlmann M, Forsten E, Noack S, Büchs J (2018) Prediction of recombinant protein production by *Escherichia coli* derived online from indicators of metabolic burden. Biotechnology Progress 34:1543-1552

[§]Authors contributed equally to the respective publication.

Other contributions to publications during this PhD thesis:

- Lara AR, Jaén KE, Sigala J, Mühlmann M, Regestein L, Büchs J (2016) Characterization of endogenous and reduced promoters for oxygen-limited processes using *Escherichia coli*. ACS synthetic biology. 6:344-356.

- Ladner T, Mühlmann M, Schulte A, Wandrey G, Büchs J (2017) Prediction of *Escherichia coli* expression performance in microtiter plates by analyzing only the temporal development of scattered light during culture. Journal of Biological Engineering 11:20

Zusammenfassung

Im Rahmen dieser Arbeit wurden sowohl Methoden für ein reproduzierbares Klonscreening, als auch Methoden zur Erhöhung und Vorhersage der rekombinanten Proteinproduktion in *Escherichia coli* entwickelt.

Automatisierte Hochdurchsatzscreenings mit kombinierbaren Modulen aus Upstream- und Downstreamprozessen konnten realisiert werden. Dabei wurde sowohl nach optimierten Stämmen gescreent, als auch nach optimierten Kultivierungs- und Induktionsbedingungen. Als Basis diente eine Roboterplattform (RoboLector), die neben einem Liquid Handling System zusätzlich mit einem BioLector ausgestattet ist. Standardprozeduren für die manuelle Medienpräparation, Zelllyse, Proteinquantifizierung, Detektion von Enzymaktivität und Probenahme wurden auf automatisierbare Protokolle transferiert.

Viele Parameter beeinflussen die rekombinante Proteinexpression. In dieser Arbeit wurden die Temperatur, die Induktorkonzentration und der Induktionszeitpunkt genauer untersucht. Mit Hilfe des RoboLectors wurden Induktionsprofile in 48-Well Flowerplates erstellt und zudem mit Schüttelkolben Experimenten in der RAMOS (Respiration Activity Monitoring System) Anlage verglichen. Es zeigte sich sowohl in den Daten der Biomasse, als auch in den Daten der Sauerstofftransferraten (*oxygen transfer rate* - OTR), dass der Metabolismus durch die Induktion mit dem Lactose-Analogon Isopropyl-β-D-thiogalactopyranosid (IPTG) bei hohen Temperaturen deutlich stärker belastet war, als bei geringen Temperaturen. Außerdem reichten bereits geringe Induktorkonzentrationen (0.5 - 0.1 mM IPTG) aus, um eine hohe Produktbildung zu erzielen.

OTR Daten liefern viele Information über den metabolischen Zustand einer Kultur. Bisher ist die Messung in Mikrotiterplatten in kommerziell verfügbaren Geräten aber nicht möglich. Die sichtbaren Zusammenhänge von OTR und Biomasse-basiertem Streulicht wurden deshalb im Rahmen der Arbeit genauer untersucht. Für *E. coli* konnte gezeigt werden, dass die erste Ableitung der Streulichtverläufe proportional zu den OTR Verläufen ist. Die Streulichtdaten können somit in vielen Fällen zur Interpretation von physiologischen Zuständen dienen. Die Nicotinamidadenindinukleotid (NADH) Fluoreszenz der Zellen konnte als zusätzliches Signal für die metabolische Belastung identifiziert werden. Zudem wurden zwei verschiedene Ansätze zur Vorhersage der rekombinanten Proteinbildung entwickelt. Aufwändige Analysetests sind für eine erste Abschätzung nicht mehr notwendig.

Short version

The aim of this work was to develop methods for a reproducible clone screening as well as methods to increase and predict recombinant protein production in *Escherichia coli*.

Automated high-throughput screenings (HTS) with combinable modules from upstream and downstream processes were realized. It was screened for optimized strains as well as for optimized cultivation and induction conditions. Therefore, a robotic platform (RoboLector), which is equipped with a liquid handling system and a BioLector, was applied. Standard procedures for manual media preparation, cell lysis, protein quantification, enzyme activity detection and sampling have been transferred to automatable protocols

Many parameters affect the recombinant protein expression. In this work, temperature, inducer concentration, and induction time were investigated in more detail due to the lack of broad studies. With the help of the RoboLector, induction profiling was carried out at temperatures of 28°C - 37°C in 48-well Flowerplates. Data were additionally compared with shake flask experiments in the RAMOS (Respiration Activity Monitoring System) device. Both, the biomass measurements and the oxygen transfer rate (OTR) data, indicated a stronger metabolic burden from induction at high temperatures than at low temperatures. In addition, even low inducer concentrations (0.5 - 0.1 mM IPTG) were sufficient to achieve high product formation.

OTR data provide a lot of information about the metabolic state of a culture. So far, the measurement of OTR in microtiter plates is not possible in commercially available devices. Therefore, the recognized correlations between OTR and biomass-based scattered light were examined in more detail in the context of this work. The first derivative of the scattered light course revealed to be proportional to the OTR trend for *E. coli*. Thus, the scattered light data can serve for the interpretation of physiological states in many cases. The nictotinamide adenine dinucleotide (NADH) fluorescence of the cells could be identified as an additional signal for metabolic burden. Moreover, two different approaches to predict recombinant protein formation have been developed.

Kurzfassung

In der Bioverfahrenstechnik werden Mikroorganismen und Enzyme als Biokatalysatoren zur Herstellung hochwertiger Produkte eingesetzt. Teile des großen Produktspektrums umfassen dabei Fein- und Grundchemikalien, Biokraftstoffe, Impfstoffe und Wirkstoffe in der Medizin, aber auch Lebensmittel wie Bier und Joghurt für den täglichen Gebrauch. Viele der Produkte können allerdings nicht auf natürlichem Wege in Mikroorganismen produziert werden. Deshalb spielen rekombinante Expressionssysteme eine große Rolle. Der populärste prokaryotische Wirt ist hierbei *Escherichia coli (E. coli)* aufgrund seiner einfachen Skalierbarkeit, hoher Expressionsraten und kosteneffizienter Kultivierung.

In der Forschung und Entwicklung gilt es zudem stetig nach neuen und verbesserten Biokatalysatoren und Kultivierungsbedingungen zu suchen (bzw. zu screenen), um höhere Ausbeuten zu erzielen oder neue Produkte auf den Markt zu bringen. Solche primären Screenings werden herkömmlicherweise im Kleinkulturmaßstab durchgeführt, um den experimentellen Durchsatz zu erhöhen. Dabei kommen neben Schüttelkolben vor allem Mikrotiterplatten zum Einsatz, welche in Kombination mit einem Liquid-Handling Roboter eine Automatisierung zulassen. Oft geht das Herunterskalieren mit dem Verlust von Prozessinformationen zu den einzelnen Kultivierungen einher. Dies kann beispielsweise zu deutlichen Nachteilen in einem Klonscreening, bei welchem genmodifizierte Mikroorganismen in Bezug auf ihr exprimiertes Produkt verglichen werden, führen. Besonders bei induzierbaren Expressionssystemen spielt die Biomassekonzentration zum Zeitpunkt der Induktion eine große Rolle in Bezug auf die final gebildeten Produktkonzentrationen. Sofern die Biomassekonzentration nicht online überprüft werden kann, sind die Endergebnisse möglicherweise nicht vergleichbar. Neue Technologien und Methoden sind deshalb notwendig, um eine ausreichende Prozessüberwachung und -kontrolle zu garantieren. Ein bereits etablierter und in dieser Arbeit eingesetzter Mikrobioreaktor ist der sogenannte BioLector, welcher eine

optische Echtzeitmessung von Biomasse, pH, O_2 und fluoreszierenden Molekülen in Mikrotiterplatten ermöglicht.

Im Rahmen dieser Arbeit wurden sowohl Methoden für ein reproduzierbares Klonscreening, als auch Methoden zur Erhöhung und Vorhersage der rekombinanten Proteinproduktion in *Escherichia coli* entwickelt. Die Expression der Produkte wurde hierbei immer mit dem Lactose-Analogon Isopropyl-β-D-thiogalactopyranosid (IPTG) induziert.

Es wurden automatisierte Hochdurchsatzscreenings (engl. *high-throughput screening* - HTS) mit kombinierbaren Modulen aus Upstream- und Downstreamprozessen realisiert. Dabei wurde sowohl nach optimierten Stämmen gescreent, als auch nach optimierten Kultivierungs- und Induktionsbedingungen. Als Basis diente eine Roboterplattform (RoboLector), die neben einem Liquid Handling System zusätzlich mit einem BioLector ausgestattet ist. Standardprozeduren für die manuelle Medienpräparation, Zelllyse, Proteinquantifizierung, Detektion von Enzymaktivität und Probenahme wurden auf automatisierbare Protokolle transferiert. Die Methoden wurden entweder mit dem Modelorganismus *E. coli* oder der sekretierenden Hefe *Kluyveromyces lactis* (*K. lactis*) evaluiert. Durch Methoden zur Vorkultursynchronisation und biomasse-spezifischen Induktion konnte die Zuverlässigkeit des finalen Klonrankings in einem Klonscreening garantiert werden. Dies wurde anhand 46 *E. coli* BL21(DE3) Stämmen, die unterschiedliche Varianten einer Cellulase exprimierten, gezeigt. Zudem wurde eine Mutante identifiziert, deren volumetrische Enzymaktivität im Vergleich zum nichtmodifizierten Enzym um das 6-fache erhöht war.

Es existieren viele Parameter, die die rekombinante Proteinexpression beeinflussen. In dieser Arbeit wurden die Temperatur, die Induktorkonzentration und der Induktionszeitpunkt genauer untersucht, da hier breite Studien fehlen. Mit Hilfe des RoboLectors wurden Induktionsprofile bei Temperaturen von 28°C - 37°C in 48-Well Flowerplates erstellt. Die speziellen Mikrotiterplatten ermöglichen einen erhöhten Sauerstoffeintrag und somit eine Vergleichbarkeit zu Schüttelkolbenexperimenten. In Schüttelkolben kann die Sauerstofftransferrate (*oxygen transfer rate* - OTR) mit der RAMOS (Respiration Activity MOnitoring System) - Technologie gemessen werden. Parallelansätze im BioLector und in der RAMOS Anlage ermöglichten die genaue Untersuchung der optimalen Induktionsbedingungen für aerobe Batch-Kultivierungen des Stamms *E. coli* Tuner(DE3) FbFP. Es hat sich sowohl in den Messwerten der Biomasse, als auch in den OTR-Daten gezeigt, dass der Metabolismus durch die Induktion mit IPTG bei hohen Temperaturen deutlich stärker belastet war, als bei

geringen Temperaturen. Außerdem waren bereits geringe Induktorkonzentrationen (0.5 - 0.1 mM IPTG) ausreichend, um eine hohe Produktbildung zu erzielen.

OTR Daten liefern viele Information über den metabolischen Zustand einer Kultur. Bisher ist die Messung in Mikrotiterplatten in kommerziell verfügbaren Geräten aber nicht möglich. Die sichtbaren Zusammenhänge von OTR und Biomasse-basiertem Streulicht wurden deshalb im Rahmen der Arbeit genauer untersucht. Für *E. coli* konnte gezeigt werden, dass die erste Ableitung der Streulichtverläufe proportional zu den OTR Verläufen ist. Die Streulichtdaten können somit in vielen Fällen zur Interpretation von physiologischen Zuständen dienen. Die Nicotinamidadenindinukleotid (NADH) Fluoreszenz der Zellen konnte als zusätzliches Signal für die metabolische Belastung identifiziert werden. Zudem wurden zwei verschiedene Ansätze zur Vorhersage der rekombinanten Proteinbildung entwickelt. Die erste Methode nutzt alleine die Streulichtableitung, um Vorhersagen über die maximal erreichte relative rekombinante Proteinmenge zu treffen. Aufwändige Analysetests sind für eine erste Abschätzung nicht mehr notwendig. Die zweite Methode ist komplexer und benötigt mehr Daten (Streulicht und OTR), es werden aber erste Möglichkeiten einer zeitaufgelösten Vorhersage präsentiert.

Zusammenfassend zeigen die Ergebnisse dieser Arbeit das Potential einer automatisierten Hochdurchsatzplattform mit integrierter Echtzeitüberwachung im Kleinstmaßstab. Im Gegensatz zu herkömmlichen „blinden“ Screeningverfahren, können reproduzierbare und verlässliche Ergebnisse erzielt werden. Die rekombinante Proteinproduktion konnte durch geeignete Stammauswahl und Optimierung der Kultivierungs- und Induktionsbedingungen in vielen Anwendungen erhöht und vorhergesagt werden. Die etablierten Methoden stellen einen wichtigen Schritt in Richtung vollautomatisierte Optimierung in der Bioprozessentwicklung dar.

Abstract

Microorganisms and enzymes are used in bioprocess engineering as biocatalysts for the production of high-quality products. Parts of the large product range include fine and basic chemicals, biofuels, vaccines and active ingredients in medicine as well as foods such as beer and yoghurt for daily use. However, many of the products cannot be produced naturally, thus recombinant expression systems play a major role. The most popular prokaryotic host is *Escherichia coli* (*E. coli*) due to its simple scalability, high expression rates, and cost-effective cultivation.

In research and development, it is important to constantly screen for new and improved gene variants and cultivation conditions in order to achieve higher yields or provide new products to the market. Such primary screenings are conventionally performed in small scale cultures to increase experimental throughput. Thus, shake flasks and in particular microtiter plates are applied and can further be combined with a liquid handling robot to allow for automation. Scale-down is often accompanied by the loss of process information of the individual cultivations. This can, for example, lead to significant disadvantages in a clone screening in which gene-modified microorganisms are compared with respect to their expressed product. Particularly in the case of inducible expression systems, the biomass concentration at the time of induction plays a major role regarding final product concentrations. If the biomass concentration cannot be checked online, the final results might not be comparable. New technologies and methods are therefore necessary to guarantee adequate process monitoring and control. A well-established microbioreactor is the so-called BioLector, which is applied in this work and allows real-time optical measurement of biomass, pH, O_2 and fluorescent molecules in microtiter plates.

The aim of this work was to develop methods for a reproducible clone screening as well as methods to increase and predict recombinant protein production in *Escherichia coli*. The

expression of the target genes was always induced with the lactose analogue isopropyl-β-D-thiogalactopyranoside (IPTG).

Automated high-throughput screenings (HTS) with combinable modules from upstream and downstream processes were realized. It was screened for optimized strains as well as for optimized cultivation and induction conditions. Therefore, a robotic platform (RoboLector), which is equipped with a liquid handling system and a BioLector, was applied. Standard procedures for manual media preparation, cell lysis, protein quantification, enzyme activity detection and sampling have been transferred to automatable protocols. The methods were evaluated either with the model organism *E. coli* or the secreting yeast *Kluyveromyces lactis* (*K. lactis*). The methods for preculture synchronization and biomass-specific induction could guarantee the reliability of final results in a clone screening. It was demonstrated on 46 *E. coli* BL21(DE3) strains expressing different variants of a cellulase. In addition, a mutant was identified whose volumetric enzyme activity was increased 6-fold compared to the unmodified enzyme.

Many parameters that affect the recombinant protein expression exist. In this work, temperature, inducer concentration, and induction time were investigated in more detail due to the lack of broad studies. With the help of the RoboLector, induction profiling was carried out at temperatures of 28°C - 37°C in 48-well Flowerplates. These special microtiter plates allow an increased oxygen transfer capacity and thus a comparability to shake flask experiments. In shake flasks, the oxygen transfer rate (OTR) can be measured using the RAMOS (Respiration Activity Monitoring System) technology. Parallel experiments in the BioLector and in the RAMOS device enabled the accurate investigation of the optimal induction conditions for aerobic batch cultivations of the strain *E. coli* Tuner (DE3) FbFP. Both, the biomass measurements and the OTR data, indicated a stronger metabolic burden from induction at high temperatures than at low temperatures. In addition, even low inducer concentrations (0.5 - 0.1 mM IPTG) were sufficient to achieve high product formation.

OTR data provide a lot of information about the metabolic state of a culture. So far, the measurement of OTR in microtiter plates is not possible in commercially available devices. Therefore, the recognized correlations between OTR and biomass-based scattered light were examined in more detail in the context of this work. The first derivative of the scattered light course revealed to be proportional to the OTR trend for *E. coli*. Thus, the scattered light data can serve for the interpretation of physiological states in many cases. The nictotinamide adenine

dinucleotide (NADH) fluorescence of the cells could be identified as an additional signal for metabolic burden. Moreover, two different approaches to predict recombinant protein formation have been developed. The first method uses only the scattered light derivative to allow predictions about the maximum achieved relative recombinant protein amount. Elaborate offline assays are no longer necessary for an initial assessment. Although the second method is more complex and requires more data (scattered light and OTR), a first approach of a time-resolved prediction is presented.

In summary, the results of this work show the potential of an automated high-throughput (HT) platform with integrated online monitoring in small-scale. In contrast to conventional "blind" screening methods, reproducible and reliable results can be achieved. Recombinant protein production could be increased and predicted by appropriate strain selection and optimization of cultivation and induction conditions in many applications. The established methods represent an important step towards fully automated optimization in bioprocess development.

Contents

Contents ..... **I**

Nomenclature ..... **IV**

List of figures ..... **VII**

List of tables ..... **XII**

1 Introduction **1**

1.1 Relevance of high-throughput screening (HTS) for biofuel production 1

1.2 Influencing parameters on recombinant protein production 3

1.3 Online monitoring of oxygen and biomass in microscale 5

1.4 Objectives and overview 6

2 Materials and methods **9**

2.1 Biological systems 9

2.2 Cultivation media 10

2.3 Cultivation of microorganism 11

2.3.1 Shake flask cultivations in RAMOS device 11

2.3.2 Microtiter plate cultivation in BioLector device 11

2.3.3 Cultivation conditions 13

2.4 RoboLector system 14

2.4.1 Components 14

2.4.2 Advanced data processing of BioLector raw files 15
2.4.3 Biomass separation 15
2.4.4 Enzyme extraction 16
2.4.5 Azo-CMC assay 16
2.4.6 Induction profiling 17
2.5 Offline analysis 18
2.5.1 Optical density, Osmolality and culture fluorescence 18
2.5.2 SDS-PAGE 18
2.5.3 4-MUC assay 18

3 Automated HTS platform for recombinant cellulase expression 21
3.1 Extended RoboLector HTS platform 21
3.2 Development of HT methods 25
3.2.1 Automated sampling from a microtiter plate 27
3.2.2 Recombinant protein extraction 27
3.2.3 Colorimetric Azo-CMC assay 30
3.2.4 Bradford protein quantification assay 32
3.3 Application of HT methods 34
3.3.1 Expression study of *K. lactis* for cellulase production 34
3.3.2 Automated HTS of recombinant cellulases 37
3.4 Conclusion 40

4 Induction profiling at different temperatures 43
4.1 Comparable oxygen supply in microtiter plates and shake flasks 43
4.2 Induction profiling covering conventional conditions 45
4.3 Comparison of selected induction conditions at 28°C and 37°C 47
4.4 Comparison of induction profiles at four temperatures 50
4.5 Induction profile with low inducer concentrations 52

4.6 Conclusion 53

5 Proportionality of OTR and dScL/dt over time for *E. coli* 55

5.1 Transformation of scattered light curves 55

5.2 Validity of proportionality between OTR and dScL/dt also for product forming cells 58

5.3 Conclusion 61

6 Prediction of the expression performance for *E. coli* 63

6.1 Categorization of OTR and dScL/dt curves and prediction of production performance 63

6.2 Predicted induction profiling 66

6.3 Time-resolved prediction of recombinant protein production 68

6.4 NADH as indicator for metabolic burden 73

6.5 Conclusion 76

7 Conclusion and outlook 79

Bibliography 85

Appendix 99

Nomenclature

Abbreviations

4-MUC	4-methylumbelliferyl-β-D-cellobioside
a.u.	Arbitrary unit
Azo-CMC	Carboxymethyl cellulose dyed with Remazolbrilliant Blue
BSA	Bovine serum albumin
cel5A	Enduglucanase from *Trichoderma reesei*
celA2	Cellulase originally isolated from a metagenome library
C. glutamicum	*Corynebacterium glutamicum*
CMC	Carboxymethyl cellulose
c_v	Relative standard deviation
DWP	Deep well plate
E. coli	*Escherichia coli*
EG	Endoglucanase
FbFP	Flavin mononucleotide (FMN)-based fluorescent protein
FMN	Flavin mononucleotide
GFP	Green fluorescent protein
HEPA	High efficiency particulate air
HT	High-throughput
HTS	High-throughput screening

HPLC	High-performance liquid chromatography
IPTG	Isopropyl β-d-1-thiogalactopyranoside
K. lactis	*Klyveromyces lactis*
max	Maximum
m	Amount of different cultivations
m_s	Maintenance coefficient
MTP	Microtiter plate
MOPS	3-(N-morpholino)-propanesulfonic acid
n	Amount of time intervals
NADH	Nictotinamide adenine dinucleotide
P. pastoris	*Pichia pastoris*
RAMOS	Respiration activity monitoring system
RT	Room temperature
SDS-PAGE	Sodium dodecyl sulfate polyacrylamide gel electrophoresis
STY	Space time yield
TB	Terrific broth
U	Enzyme unit
YP	Yeast extract peptone

Roman Symbols

c_{O2*}	Oxygen concentration in the gas phase	[mmol/L]
c_{O2}	Oxygen concentration in the liquid phase	[mmol/L]
CTR	Carbon dioxide transfer rate	[mmol/L/h]
DOT	Dissolved oxygen tension	[%-air saturation]
dScL/dt	Scattered light derivative	[a.u./h]
I	Indicator value	[a.u.]

k_La	Volumetric mass transfer coefficient	[1/h]
OD	Optical density	[a.u.]
OD_{600}	Optical density at 600 nm	[a.u.]
OTR	Oxygen transfer rate	[mmol/L/h]
OTR_{max}	Maximum oxygen transfer capacity	[mmol/L/h]
OUR	Oxygen uptake rate	[mmol/L/h]
P	Product concentration	[g/L]
q_{O2}	Specific oxygen uptake rate	[mmol/g/h]
q_p	Product formation rate	[1/h]
RQ	Respiratory quotient	[-]
rpm	Round per minute	[1/min]
ScL	Scattered light	[a.u.]
t	Time	[h]
$t_{1;\ldots;n}$	Sampling time	[h]
T	Temperature	[°C]
X	Biomass concentration	[g/L]
$Y_{P/S}$	Yield coefficient of product per substrate	[g/g]
$Y_{X/O2}$	Yield coefficient of biomass per oxygen	[g/g]
$Y_{X/S}$	Yield coefficient of biomass per substrate	[g/g]
$Y_{P/O2}$	Yield coefficient of product per oxygen	[g/g]

Greek Symbols

λ_{em}	Emission wavelength	[nm]
λ_{ex}	Excitation wavelength	[nm]
μ	Specific growth rate	[1/h]

List of figures

Figure 3-1: Automated HTS of recombinant cellulase expression applying the RoboLector platform. 22

Figure 3-2: Schematic comparison of conventional protocols and modified protocols adapted for HT application in MTPs 24

Figure 3-3: Extraction of the fluorescent model protein FbFP from *E. coli* BL21(DE3) pRhotHi-2 comparing the standard and HT protocol 29

Figure 3-4: Calibration curves for the Azo-CMC cellulase activity assay comparing the standard protocol and HT protocol at varied incubation times 32

Figure 3-5: Set-up for the automated Bradford-assay on the RoboLector platform. 33

Figure 3-6: Expression study of *K. lactis* expressing recombinant endoglucanase cel5A from *Trichoderma reesei* at varied medium composition applying the RoboLector system. 36

Figure 3-7: Primary screening of an *E. coli* clone library expressing variants of endoglucanase celA2 applying the RoboLector system. 38

Figure 4-1: Comparison of oxygen transfer rate (OTR, measured in shake flasks) and dissolved oxygen tension (DOT, measured in microtiter plates) measured by a RAMOS and a BioLector device, respectively. 45

Figure 4-2: Induction profile with automated addition of 0-1 mM IPTG solution after 1–10 h of cultivation time. 46

Figure 4-3: Comparison of selected induction conditions at 28°C and 37°C measured in a RAMOS and a BioLector device. 48

Figure 4-4: Induction profiles with automated addition of 0-0.4 mM IPTG at different temperatures..... 51

Figure 4-5: Induction profile with automated addition of 0-0.09 mM IPTG solution after 1–10 h of cultivation time. 53

Figure 5-1: Schematic illustration of the transformation procedure of the ScL signal into its first derivative and comparison with the OTRs..... 57

Figure 5-2: Categorization of cultures depending on OTR, ScL and dScL/dt patterns. 59

Figure 6-1: Relation of the progresses of dScL/dt over time and recombinant protein production. 64

Figure 6-2: Prediction of the expression performance of strains producing the cellulase celA2 and the fluorescent protein FbFP. 66

Figure 6-3: Induction profiles – predicted vs. measured data. 67

Figure 6-4: Parity plots of OTR vs. dScL/dt for non-induced *E. coli* cultures. 69

Figure 6-5: Time-resolved prediction of *E. coli* Tuner(DE3) FbFP at 30°C. 70

Figure 6-6: Comparison of old and new prediction method. 72

Figure 6-7: Redox balance of NADH. 73

Figure 6-8: Impact of product expression on NADH formation classified in three groups. 75

Figure 7-1: Controlled-loop for the automated optimization of recombinant protein production. 83

Figures in appendix

Figure A- 1: Calibration curve for Bradford-assay. 99

Figure A- 2: Online and offline analytics of *E. coli* Tuner(DE3) FbFP in an automated sampling experiment. 100

Figure A- 3: Induction profile with automated addition of 0 - 1 mM IPTG solution after 1 - 10 h of cultivation time at 30°C. 101

Figure A- 4: Comparison of induction profiles at 30°C and 37°C in 48-well plates and 96-well plates. 102

Figure A- 5: Comparison of selected induction conditions at 30°C and 34°C measured in a RAMOS and a BioLector device. 103

Figure A- 6: Comparison of selected induction conditions at 28°C and 37°C at same optical density measured in BioLector device. 104

Figure A- 7: Calibration curves for conversion of scattered light to standard optical density in 48-well and 96-well plates. 105

Figure A- 8: Simultaneous experiments of *E. coli* BL21(DE3) pET28a(+) expressing the cellulase celA2 wildtype under control of the T7-promoter in a RAMOS device and a BioLector device. 106

Figure A- 9: Simultaneous experiments of *E. coli* BL21(DE3) pET28a(+) expressing the cellulase celA2 mutant under control of the T7-promoter in a RAMOS device and a BioLector device. 107

Figure A- 10: 3D-plot of dScL/dt courses over time vs. achieved product maximum. 108

Figure A- 11: Induction profiles – predicted vs. measured data. 109

Figure A- 12: Simultaneous experiments of *E. coli* BL21(DE3) pET28a(+) celA2 expressing the cellulase celA2 wildtype under control of the Tac-promoter in a RAMOS device and a BioLector device..... 110

Figure A- 13: Induction profiles – predicted vs. measured data. 111

Figure A- 14: Simultaneous experiments of *E. coli* Tuner(DE3) FbFP in a RAMOS device and a BioLector device. 112

Figure A- 15: Induction profiles – predicted vs. measured data. 113

Figure A- 16: 48 simultaneous experiments of *E. coli* Tuner(DE3) FbFP in a device that combines the µRAMOS with the BioLector technology 114

Figure A- 17: Time-resolved prediction of *E. coli* Tuner(DE3) FbFP at 30°C (0-1 mM IPTG). 115

Figure A- 18: Time-resolved prediction of *E. coli* Tuner(DE3) FbFP at 30°C (0-0.09 mM IPTG). 116

Figure A- 19: Time-resolved prediction of *E. coli* Tuner(DE3) FbFP at 37°C. 117

Figure A- 20: Time-resolved prediction of *E. coli* Tuner(DE3) FbFP at 28°C. 118

Figure A- 21: Impact of product expression on NADH formation classified in three groups for *E. coli* BL21(DE3)pET28a(+) celA2 wildtype under control of a Tac-promoter. 119

Figure A- 22: Impact of product expression on NADH formation classified in three groups for *E. coli* Tuner(DE3)FbFP at 28°C. 120

Figure A- 23: Impact of product expression on NADH formation classified in three groups for *E. coli* Tuner(DE3)FbFP at 30°C. 121

Figure A- 24: Screenshot of the programmed BioLector plotter in MATLAB for 48-well cultivations. 122

List of tables

Table 1-1: Comparison of commercialized microbioreactors and their specifications 2

Table 2-1: Applied microorganisms for the expression of recombinant proteins. 9

Table 2-2: Optical signals and applied setup for BioLector online monitoring. 12

Table 3-1: Overview of developed or extended HT methods. 25

Table 3-2: Product, biomass and space time yield (STY) of *K. lactis* in dependency on the utilized galactose concentration in YP medium. 37

Table 6-1: Overview of applied and obtained yield coefficients for the time-resolved prediction. 71

Tables in appendix

Table A- 1: Equations for regression curves in Figure 6-2 123

Chapter 1

Introduction

1.1 Relevance of high-throughput screening (HTS) for biofuel production

Since fossil resources are limited, many current research projects are investigating the utilization of renewable resources to ensure the sustainable production of platform chemicals and biofuels (Fiorentino et al. 2016). Most of these approaches have focused on producing alcohols from starch-containing plant material which competes with the food supply chain. Moreover, these approaches waste most of the plant biomass. New research is focusing on utilizing ligno-cellulose as the prime raw material for biofuel production (Ragauskas et al. 2006; Hayes 2013; Sharma et al. 2013) and constructing new biocatalysts for this purpose (Dellomonaco et al. 2010).

As the cellulose de-polymerization performed by different kinds of cellulases is the rate-limiting step for the whole hydrolysis (Percival Zhang et al. 2006; Garvey et al. 2013), efficient cellulases have to be identified and characterized regarding their performance. Mutagenesis procedures are a common way to modify existing enzymes in order to improve their properties. Typically, such modifications end up in huge libraries of enzyme variants which need to be further investigated (Wang et al. 2012). For this task an efficient screening process is essential (Percival Zhang et al. 2006; Chandel et al. 2012). To handle this immense workload, a high-throughput screening (HTS) system is necessary, which combines a miniaturized mode of operation with an advanced automation concept (Davids et al. 2013).

Table 1-1: Comparison of commercialized microbioreactors and their specifications

Microbioreactor	**Monitoring parameter**	**Volume [mL] / Quantity [-]**	**Mixing / Aeration**	**k_La [1/h] / OTR [mmol/L/h]**	**Compatibility with a robot**
BioLector, m2p-Labs (Samorski et al. 2005)	Biomass, O_2, pH, fluorescence	0.1 – 0.2 / 96 0.8 – 2.4 / 48	Orbital shaker (< 1500 rpm / 3mm)	k_La < 650 OTR < 110	Yes
ambr 15, Sartorius (Hsu et al. 2012), (Bareither and Pollard 2011)	O_2, pH	10 - 15 / 24, 48	Stirred and aerated	k_La < 30	Already integrated
Growth profiler 960 www.enzyscreen.com	Biomass	0.2 – 4 / 960	Orbital shaker (< 225 rpm / 50 mm)	OTR < 40	No
BioReactor, 2magAG (Weuster-Botz et al. 2005)	O_2, pH	8 - 15 / 48	Stirred and aerated	k_La < 1440	Yes
micro-Matrix, applikon www.applikon-bio.com	O_2, pH	1 - 5 / 24	Orbital shaker (< 400 rpm / 25 mm)	OTR < 250	No
SensorDish Reader, Presens (Kensy et al. 2005), (Hortsch and Weuster-Botz 2011)	O_2, pH	0.2 - 10 / 6, 24, 96	Need for extra shaker	Dependent on selected shaker	Yes

Automated high-throughput (HT) concepts for single steps such as measurement of optical density, pH, metabolites (Knepper et al. 2014), protein purification (Lesley 2001; Scheich et al. 2003; Meng et al. 2008) and different enzyme activity assays (Decker et al. 2003; Navarro et al. 2010; Knepper et al. 2014) have been reported. Additionally, many microbioreactors equipped with online or at-line monitoring tools have been evolved. The most prominent and already commercialized systems are given in Table 1-1.

Advanced HT concepts combine single methods to a semi or even fully automated operation. Dörr et al. 2016 recently presented a robotic platform for HT enzyme library screening. It enables automated colony picking, at-line monitoring of biomass growth, induction, subsequent

enzyme purification steps and biochemical assay. However, this platform lacks in an online monitoring tool to follow the biomass growth without interruption of shaking. In particular, constant oxygen transfer rates (OTR) are necessary for reproducible cultivations. Huber et al. 2009b combined the BioLector technology (Samorski et al. 2005) and a robotic liquid handling system to overcome this issue. A similar set-up was later used by Hemmerich et al. 2014 who performed an online monitored fed-batch clone screening of *P. pastoris*. However, the automation was restricted to the feeding and harvest procedure. Both, the preculture and the subsequent enzyme activity assay was conducted manually. A more complex clone screening was carried out with *C. glutamicum* by Unthan et al. 2015. They integrated an automated biomass triggered sampling with subsequent separation of supernatant by centrifugation and a following freezing step. An independent assay was used for the analysis of samples. Unfortunately, no conditioning of the preculture was attempted since these authors inoculated directly from cryo cultures into the main culture.

The major challenge is the comparability of screening results amongst different plates. Clone screening commonly starts from 96-well cryo cultures whose biomass concentrations are neither individually determined nor adjusted. Without the application of online measurement tools, this may lead to non-recognized differences in the onset of growth, when comparing different variants. Thereupon, especially microorganisms which have to be induced undergo non-comparable enzyme expression (Kensy et al. 2009b; Huber et al. 2010). Additionally, it is important to distinguish technical replicates from biological replicates. A small standard error in technical replicates doesn’t reflect the reliability of the whole experimental procedure. It provides only information about the reliability of the last measurement step. Moreover, there is a difference in using one microtiter plate (MTP) for producing replicates at the same time and the repetition of a whole experiment in many plates at different times.

1.2 Influencing parameters on recombinant protein production

In 1982, the recombinant protein technology achieved the great breakthrough with Humulin, a recombinant human insulin expressed in *Escherichia coli* (*E. coli*), which was the first approved biopharmaceutical (FDA 1982). Since that time, more than 400 recombinant proteins were introduced to the market (Sanchez-Garcia et al. 2016). *E. coli* is still the most popular host

organism for heterologous protein production due to its well-known genetics, high growth rates on inexpensive media, and a wide range of possible expression vectors (Terpe 2006).

Recombinant protein production always implicates a perturbation of the host cell metabolism, which typically leads to lower biomass growth rates (Betenbaugh et al. 1989; Miao and Kompala 1992; Basan et al. 2015). This stems from high maintenance requirements for the replication of inserted plasmids and from the resources needed for the transcription of target genes (Bentley et al. 1990; Bhattacharya and Dubey 1995; Bienick et al. 2014). Particularly, high copy number plasmids can overburden the cell and induce a metabolic collapse, which results in low product yields or even cell death (Durrschmid et al. 2008; Rosano and Ceccarelli 2014; Rahmen et al. 2015b). Thus, a good balance of biomass growth and product formation associated with unavoidable cell stress has to be found to achieve high productivity. Therefore, many parameters have to be individually optimized. This involves not only the choice of vector and promoter system, but also composition of the medium, oxygen supply, cultivation temperature and induction conditions (Donovan et al. 1996; Berrow et al. 2006; Terpe 2006; Diederichs et al. 2014; Marini et al. 2014; Morowvat et al. 2014; Rosano and Ceccarelli 2014).

The reduction of cultivation temperature is one of the common approaches to prevent formation of inclusion bodies by correct folding of the molecule (Schein and Noteborn 1988; Vera et al. 2007; Dragosits et al. 2011). Unfortunately, this comes along with prolonged cultivation times. A fast approach to investigate temperature effects in microtiter plates by using a special temperature profiling device is described by Kunze et al. 2014.

One of the most frequently used expression systems is the *E. coli* T7 system under control of the *lac* operon, present in pET and pRhot vectors. The expression of the target protein can be induced with lactose or the non-degradable analog isopropyl β-D-thiogalactopyranoside (IPTG) (F.William Studier and Barbara A. Moffatt 1986; Katzke et al. 2010). Such inducible expression systems allow the precise and adjustable separation of growth and production phases by the variation of inducer concentration and induction time. However, the large space available for optimization is also coupled to high experimental effort. This can be handled with miniaturized cultivations in HT applications. A fast optimization of induction conditions can be conducted on robotic platforms (Huber et al. 2009b).

Due to the very low solubility of oxygen in aqueous solutions, the transfer of oxygen into the liquid phase is a challenging process (Rischbieter and Schumpe 1996; Garcia-Ochoa and Gomez 2009). The miniaturization of culture vessels may allow high-throughput but typically

leads to reduced oxygen transfer capacities. Sufficient supply with oxygen is important since oxygen limitations complicate scale up and lead to altered metabolism and lower product formation (Freyer et al. 2004; Peter et al. 2004; Zimmermann et al. 2006; Garcia-Ochoa et al. 2010). A good strategy is to use special 48-well flower-shaped microtiter plates. The flower shape of the wells serve as baffles allowing OTR_{max}-values of up to 100 mmol/L/h (Samorski et al. 2005; Funke et al. 2009).

1.3 Online monitoring of oxygen and biomass in microscale

Monitoring of dissolved oxygen concentrations and OTR allows for detecting oxygen limitations and strongly supports the interpretation of physiological states of microorganisms (Anderlei and Büchs 2001). It was demonstrated for *E. coli*, that the course of the OTR can indicate diauxic growth, pH-inhibition and secondary substrate limitations. Additionally, it can give hints regarding metabolic burden and product formation types (Anderlei and Büchs 2001; Kunze et al. 2012; Rahmen et al. 2015b).

While monitoring of oxygen supply in fermenters using oxygen probes is a long-standing common practice (Hitchman 1978; Suresh et al. 2009) it is rather new in small-scale bioreactors like shake flasks and microtiter plates (Tolosa et al. 2002; John et al. 2003; Anderlei et al. 2004; Jäger et al. 2012; Ladner et al. 2015; Flitsch et al. 2016b; Flitsch et al. 2016a). Anderlei et al. presented the so-called Respiration Activity MOnitoring System (RAMOS)-technology to monitor the OTR, carbon dioxide transfer rate (CTR) and the respiratory quotient (RQ) within eight parallel shake flasks (Anderlei et al. 2004). This is a non-invasive method based on partial pressure measurements in the headspace of shake flasks. The RAMOS-technology could recently be adapted to a 48-well microtiter plate format (Flitsch et al. 2016b). Another approach is the optical measurement of dissolved oxygen tension inside a culture broth. Thereby, an oxygen sensitive fluorophore spot is attached at the inside of a shake flask (Jäger et al. 2012). Since fluorophore spots can be very small in size, this method is transferable to microtiter plates (John et al. 2003). An alternative method for both, shake flask and microtiter plate, represents the application of infrared fluorescent nanoparticles within the culture broth (Ladner et al. 2015; Flitsch et al. 2016a).

Another fundamental parameter which is commonly monitored during microbial cultivations is the biomass concentration. While sampling and subsequent cell counting or optical density

measurement is still an option in stirred tank reactors, it is not practicable at increasing throughput in small-scale cultures. A popular online-monitoring device for microtiter plate cultivations is the BioLector device already mentioned (Table 1-1). Biomass and fluorescent products can simply be measured via scattered light (ScL) and fluorescence intensities, respectively (Samorski et al. 2005; Kensy et al. 2009b; Kensy et al. 2009a; Huber et al. 2010; Huber et al. 2011; Back et al. 2016; Ladd Effio et al. 2016; Koepff et al. 2017). A decisive advantage is the non-invasive procedure, which allows measurement of samples without stopping the shaking process of the microtiter plate (Samorski et al. 2005). By using special microtiter plates equipped with optodes, also oxygen or pH can be detected.

While HT monitoring of biomass is already established in microtiter plates using devices like the BioLector, OTR measurement is still restricted to larger scales like shake flasks, as long as the above mentioned µRAMOS device (Flitsch et al. 2016b) is not commercially available. The course of an OTR curve and its relative maxima reflect a lot of metabolic information. When OTR is not measured, a parameter, which is proportional to the OTR, might be sufficient for analysis in many applications.

1.4 Objectives and overview

The overall objective of this thesis was to develop, extend and apply HT methods on a robotic platform to screen for optimized microorganisms and cultivation conditions in microscale to achieve high recombinant protein yields. The work was performed as part of the Cluster of Excellence “Tailor-made fuels from biomass” (TMFB), funded by the German Research Foundation (DFG). One field of the TMFB addresses the fractionation and conversion of lignocellulosic biomass via intermediates and platform molecules into biofuels. As described in section 1.1, the hydrolysis of cellulose by enzymes is a challenging step. The need for improved enzyme variants was the reason to investigate the heterologous cellulase production in *E. coli* and *K. lactis*.

In addition to the strains with relevance for the TMFB, an *E. coli* strain expressing a fluorescent protein was applied in many cases within this work. It allows for online monitoring of product formation and consequently an easy tracking without necessary offline assays.

A robotic platform (RoboLector), introduced by Huber et al. 2009b was used to realize all HT-applications. In order to realize more complex operations, the automatic platform had to be

extended (see chapter 3). Methods for protein purification and cellulase characterization had to be adapted to and optimized for miniaturized HT operation with a special focus on automated handling. In several application examples, the potential of the extended robotic system is demonstrated. Single process steps were evaluated using different *E. coli* and *K. lactis* strains. The applied HT methods comprise also a preculture synchronization and controlled induction of *E. coli* cultivations. This is a prerequisite to obtain a fair comparison within clone library screening experiments. Finally, 46 mutants of *E. coli* expressing the cellulase celA2 were used for the evaluation of the HT screening procedure.

As described in section 1.2, many parameters strongly influence the production of recombinant proteins. The temperature, the inducer concentration and the induction time are three of them. Several studies have presented results of induction profiles in microtiter plates, hence the identification of optimal induction time and inducer concentration. However, these studies were performed either at single temperatures (Huber et al. 2009b; Rohe et al. 2012; Hemmerich and Kensy 2014; Wandrey et al. 2016) or with few data points (Baumann et al. 2015; Ladd Effio et al. 2016). The aim of chapter 4 was to comprehensively investigate the effect of temperature on optimal induction conditions in oxygen unlimited batch cultivations. Therefore, the flavin mononucleotide (FMN)-based fluorescent model protein FbFP was expressed in *E. coli* Tuner(DE3) under control of the T7 promoter. This strain has a *lacY* deletion to prevent the active transport of IPTG into the cell. Instead, IPTG enters the cell solely via concentration-dependent diffusion (Marbach and Bettenbrock 2012). Complete induction profiles with variations of IPTG concentrations and times of induction were performed in 48-well Flowerplates. In order to enable an automatic induction, the robotic platform RoboLector was used. During cultivations, biomass and product formation were detected via scattered light and fluorescence measurements, respectively. OTRs were observed in simultaneous shake flask cultivations using the Respiration Activity Monitoring System (RAMOS)-device and compared to the results obtained in microtiter plates.

Since the OTR is a very useful parameter for the interpretation of metabolic processes in microorganisms but hard to monitor in microscale (compare section 1.3), chapter 5 demonstrates an alternative signal that is easily online detectable in microtiter plates. This ScL signal is optically accessible and there is no need for additional sensor spots or nanoparticles as it is necessary for DOT monitoring. Biomass growth curves can be detected via ScL and the final course is proportional to the OTR after a mathematical transformation. In a very simple

approach, solely ScL curves from 48-well microtiter plate experiments were converted into OTR-similar courses by taking the first derivative (dScL/dt). The proportionality was validated by two model *E. coli* strains expressing recombinant proteins. A variety of induction conditions, revealing largely different OTR patterns were tested. The strain *E. coli* BL21(DE3) was applied to express variants of the cellulase celA2 under control of a T7 promoter or a Tac-promoter. The strain *E. coli* Tuner(DE3) was chosen to express the fluorescent protein FbFP. The microtiter plate cultivations in the BioLector device were always conducted in parallel to the shake flasks experiments in a conventional RAMOS device to enable a comparison of the ScL-derivative and the real OTR.

The aim of chapter 6 was to use and handle all online derivable data to find a way to estimate the performance of recombinant product formation in *E. coli*. Therefore, the transformed ScL signals described in chapter 5 were part of new methods that were developed in chapter 6. An indicator value (I) is introduced and supplies information about the relative amount of formed recombinant proteins and imposed metabolic burden. The evaluation of complete induction profiles is demonstrated. Furthermore, a first approach for a time-resolved prediction of recombinant protein formation is presented. It requires both, OTR and dScL/dt values from a microbial cultivation. It was evaluated on *E. coli* Tuner(DE3) expressing FbFP. Additionally, NADH is investigated as an alternative biomass signal and its potential to indicate metabolic burden.

Chapter 2

Materials and methods

2.1 Biological systems

The applied microorganisms with their respective vectors for recombinant protein expression as well as their selection markers are specified in Table 2-1.

Table 2-1: Applied microorganisms for the expression of recombinant proteins.

Target protein	Organism	Strain	Vector	Selection marker	Inducer
celA2-variants	*E. coli*	BL21 (DE3)	pET-28a(+)	Kanamycin	IPTG
cel5A	*K. lactis*	GG799	pKlac1	-	Galactose
FbFP	*E. coli*	BL21 (DE3)	pRhotHi-2	Kanamycin	Lactose
FbFP	*E. coli*	Tuner (DE3)	pRhotHi-2	Kanamycin	IPTG

The wildtype cellulase celA2 originates from a metagenome library derived from a biogas plant (Ilmberger et al. 2012) and was used for the production of two clone libraries in *E. coli*. The first library was created by directed evolution applying a simultaneous site-saturation mutagenesis at positions 288, 299 and 300 within the target gene sequence. Active variants that showed halos on LB agar plates supplemented with 0.125% (w/v) Azo-CMC were picked. The library was constructed and investigated by Lehmann et al. 2012. The second library was created by Yang et al. 2016 and consists of *E. coli* strains that express the wildtype cellulase

celA2 under control of different promoters. Within this work the plasmid pET-28a(+) was provided with a T7 or a Tac promoter to allow IPTG inducible high-level expression of the heterologous protein (Studier and Moffatt 1986; Katzke et al. 2010; Rosano and Ceccarelli 2014).

E. coli Tuner(DE3) strains are *lacY* deletion mutants of BL21, thus, no lactose permease is produced. The entry of IPTG is solely possible by diffusion which leads to adjustable levels of homogenous protein expression throughout the entire population (Marbach and Bettenbrock 2012). The plasmid pRhotHi-2 is provided with a T7 promoter. The recombinant protein EcFbFP is an (FMN)-binding fluorescent protein, which is codon optimized for the expression in *E. coli* and whose maturation is, compared to GFP, independent of oxygen supply (Drepper et al. 2010).

2.2 Cultivation media

Three different cultivation media were applied for *E. coli* cultivations. The complex terrific broth (TB) medium (Tartof and Hobbs 1987), a modified Wilms and Reuss medium (henceforth referred as Wilms-MOPS medium) (Wilms et al. 2001) and OvernightExpress™ (OnEx) medium (Merck, Darmstadt, Germany). For cultivation of *K. lactis*, the yeast extract peptone (YP) medium (Hahn-Hagerdal et al. 2005) was used.

TB medium consists of 12 g/L tryptone, 24 g/L yeast extract, 12.54 g/L K_2HPO_4, 2.31 g/L KH_2PO_4, and 5 g/L glycerol (all ingredients from Roth, Germany) dissolved in water. The pH value was 7.2 ± 0.2 without adjustment.

The modified **Wilms-MOPS medium** consists of 5 g/L $(NH_4)_2SO_4$, 0.5 g/L NH_4Cl, 3.0 g/L K_2HPO_4, 2 g/L Na_2SO_4, 0.5 g/L $MgSO_4 \cdot 7\ H_2O$, 0.01 g/L thiamine hydrochloride, 41.85 g/L 3-(N-morpholino)-propanesulfonic acid (MOPS, 0.2 M), 1 mL/L trace element solution and glucose as C-source. Depending on the experiment, either 15 g/L glucose or 20 g/L glucose were used (see section 2.3.3 for details). The trace element solution consists of 1.98 g/L $CaCl_2 \cdot 2\ H_2O$, 0.54 g/L $CoCl_2 \cdot 6\ H_2O$, 0.48 g/L $CuSO_4 \cdot 5\ H_2O$, 41.76 g/L $FeCl_3 \cdot 6\ H_2O$, 0.3 g/L $MnSO_4 \cdot H_2O$, 0.54 g/L $ZnSO_4 \cdot 7\ H_2O$, 33.39 g/L Na_2EDTA (Titriplex III). The pH was adjusted with 5 M NaOH to a value of 7. Additionally, 50 µg/mL kanamycin were added to the media from a 1000-fold concentrated stock solution.

YP medium consists of 10 g/L yeast extract, 20 g/L tryptone (both Carl Roth, Karlsruhe, Germany) and 10 g/L glucose for the preculture (Hahn-Hagerdal et al. 2005). The main cultures were performed in YP medium containing 10-100 g/L galactose instead of glucose. Thereby, galactose served as carbon source and inducer for recombinant protein expression.

2.3 Cultivation of microorganism

2.3.1 Shake flask cultivations in RAMOS device

The in-house manufactured Respiration Activity MOnitoring System (RAMOS) is a device for online monitoring of the oxygen transfer rate (OTR), the carbon dioxide transfer rate (CTR) and the respiratory quotient (RQ) in up to eight shake flasks. The OTR is a suitable parameter to quantify the physiological state of a culture of aerobic microorganism (Anderlei and Büchs 2001). Commercial versions of the RAMOS device can be purchased from Kühner AG, Birsfelden, Switzerland or HiTec Zang GmbH, Herzogenrath, Germany. All shake flask cultivations were conducted in 250 mL shake flasks and cultivated on an orbital shaker (ISF1-X, Kühner AG, Birsfelden, Switzerland) at a shaking frequency of 350 rpm and a shaking diameter of 50 mm.

2.3.2 Microtiter plate cultivation in BioLector device

The BioLector is an online monitoring system for measurement of biomass and product formation in microtiter plates (Samorski et al. 2005; Kensy et al. 2009b). An optical fiber is moved sequentially below each well of a shaken microtiter plate and light is transmitted from a light source into the sample. Depending on the applied optical filter or monochromator position, the scattered light (ScL, indicator for biomass) or the fluorescence of the sample (indicator for fluorescent products) can be detected. If not otherwise stated, a commercially available BioLector (m2p-labs, Baesweiler, Germany) was used in this work, for measurement of ScL, FbFP-fluorescence and dissolved oxygen tension (DOT). For DOT measurement, Flowerplates with optodes were used (MTP-48-BO, m2p-labs, Baesweiler, Germany). The corresponding excitation and emission wavelength as well as the gain factors are specified in Table 2-2. 48-well and 96-well microtiter plate cultivations were performed at a shaking frequency of 1400 rpm and 1000 rpm, respectively. In single experiments, also the in-house constructed combination of a BioLector and a µRAMOS-device (Ladner et al. 2016b) was used

with 48-roundwell plates (MTP-R48-B, m2p-labs, Baesweiler, Germany). While the commercial BioLector measurement is based on LED light sources and a filter module system, the in-house constructed BioLector is based on a spectrofluorometer (Fluoro-Max-4, HORIBA Jobin Y, Munich, Germany). The shaking diameter was always 3 mm. For ScL and fluorescence measurement the initial minimal light intensity (e.g. ScL_{min}), which is mainly attributed to such factors as the media background or the type of the MTP, was subtracted from the original measured data (e.g. ScL - ScL_{min}).

Table 2-2: Optical signals and applied setup for BioLector online monitoring.

Optical signal	λ_{ex} [nm]	λ_{em} [nm]	Gain
Biomass (ScL)	620	-	20
DOT	520	600	60
FbFP fluorescence	450	492	60
NADH fluorescence	365	460	60

To allow the conversion of ScL, measured by the BioLector device, into standard OD_{600}, calibration curves for 48-well and 96-well microtiter plates were generated. A non-induced main culture from the stationary phase was utilized. The cell culture was centrifuged at 18,000 g for 10 min, the supernatant was removed and the cell pellet was resuspended in Wilms-MOPS mineral medium (without glucose) to adjust OD_{600} values from 0.1 – 12. Cavities of a 48-well Flowerplate (singular determination of samples) and 96-well microtiter plate (triplicate determination of samples) were filled with 800 µL or 200 µL, respectively. ScL was measured at 28°C, 30°C, 34°C and 37°C applying the BioLector system with the parameters listed in Table 2-2. Data were determined from at least five consecutive measurement cycles. The used shaking frequencies were identical to the cultivation conditions. The data were fitted using linear regression with the software Origin 9.0. The results are presented in Figure A- 7. These fits were applied to calculate the OD_{600} at the respective time of induction for all induction profiles (upper x-axis of Figure 4-2**,** Figure 4-4**,** Figure 4-5, Figure A- 3, Figure A- 4, Figure A- 5). The ScL mean of all cultivations that have not been induced up to this time were used to obtain the respective OD_{600}.

2.3.3 Cultivation conditions

For the pre- and main cultivation of *E. coli* BL21(DE3) expressing celA2 variants from the site-saturation mutagenesis, Wilms-MOPS medium (15 g/L glucose) was used. Pre- and main culture were performed at 30°C within a 96-well MTP (Greiner Bio-One GmbH, Frickenhausen, Germany) that was sealed with an xPierce™ film (Z722529, Sigma-Aldrich, Munich, Germany). The expression of celA2 in *E. coli* was individually induced after exceeding the ScL value of 10 a.u. by automated adding of IPTG, resulting in a final concentration of 0.1 mM.

For *E. coli* BL21(DE3) expressing FbFP TB medium was used for preculture. If not stated differently, 10 mL of TB medium in a 250 ml shake flask were inoculated with 50 µL from a cryoculture for *E. coli* pre-cultivation, and cultures were grown for 8 h at 350 rpm (shaking diameter 50 mm) and 37°C. The main culture was conducted in OvernightExpress™ (OnEx) medium for auto-induction. Besides this, the cultivation conditions were identical to the preculture.

All experiments of *E. coli* Tuner(DE3) FbFP and the variants from the *E. coli* BL21(DE3) celA2 promoter library started with two precultivation steps in shake flasks. For the first preculture 10 mL of TB-medium were inoculated to an initial optical density of 0.05 (OD_{600}) from cryogenically preserved cultures and incubated over night at 30°C. For the second preculture 8 mL of the modified Wilms-MOPS mineral medium (20 g/L glucose) were inoculated to an initial optical density of 0.2 (OD_{600}) from the first preculture and incubated at 37°C in a RAMOS device until the OTR reached a value in between 20 and 40 mmol/L/h.

The main cultivations of *E. coli* Tuner(DE3) FbFP and the variants from the *E. coli* BL21(DE3) celA2 promoter library were carried out simultaneously in RAMOS and BioLector devices at temperatures ranging from 28°C - 37°C. To enable same starting conditions in shake flasks and microtiter plates, a *mastermix* consisting of Wilms-MOPS mineral medium (20 g/L glucose) inoculated with cells from the second preculture was prepared. The initial optical density (OD_{600}) was set to 0.1. The *mastermix* was thereupon distributed among the cultivation systems. The shake flask cultivation conditions were identical to the second preculture. Microtiter plate cultivations were conducted in 48-well Flowerplates (m2p-labs, Baesweiler, Germany) and 96-well plates (black-clear, BD-Bioscience, USA). Each well was filled either with 800 µL (48-well) or 200 µL (96-well) *mastermix* and sealed with a gas permeable perforated silicone layer

(F-GPRS48-10, m2p-labs, Baesweiler, Germany) or a gas permeable membrane (AeraSeal, Excel-Scientific, CA, USA).

2.4 RoboLector system

2.4.1 Components

The applied automated HTS platform RoboLector is identical to the system described by Huber et al. 2009b. For this work, it was extended by the following components which are commercially available from Hamilton Robotics GmbH (Martinsried, Germany): cooling carrier (PLT_CAR_L5C), MTP heater shakers (HHS), on-deck vacuum station (BVS). The extended setup is illustrated in the layout scheme in Figure 3-1 A. The cooling carrier was operated with a controllable recirculation cooler (FL300, Julabo, Seelbach, Germany) located underneath the robotic platform and connected via flexible tubes. It allows temperature set points from -20°C to 40°C. To keep the tubes from ice coating, set temperatures lower than -5°C were avoided for long-term experiments. Due to heat transfer phenomena, set temperatures and final temperatures in MTP wells differ from each other. The respective relationship was identified by experiments. For 96-deep well plates (DWP, 2.2 mL, sterile, square wells, Corning/Axygen Scientific) it is described by Eq. (2-1).

$$T_{well} = 0.75 \cdot T_{set} + 6.50°C \quad (2\text{-}1)$$

Similar experiments were performed for the heater shakers, too. The respective relationship for 96-well DWPs is described by Eq. (2-2). The maximum set temperature was 110°C. Well temperatures were determined by a CheckTemp 1 precision thermometer (G002.1, Roth, Karlsruhe, Germany).

$$T_{well} = 0.78 \cdot T_{set} + 6.45°C \quad (2\text{-}2)$$

The vacuum station was operated by a vacuum pump (ME 4C VARIO, Vacuubrand, Wertheim, Germany) equipped with pressure sensor and control unit. All devices are controlled by the VENUS three software of the pipetting robot (Microlab STAR, Hamilton Robotics, Martinsried, Germany).

2.4.2 Advanced data processing of BioLector raw files

Interaction of the robot with the BioLector is often initiated by reaching certain biomass values. In particular this applies the methods *biomass specific replication* and *biomass specific induction* which were firstly described by Huber et al. 2009b. The measured raw data derived from a BioLector measurement are without consideration of time dependent technical shifts. Thus, after each cultivation a transformation of the whole dataset is conducted to enable long-term reproducible data. Thereby, reference values are taken into account. Up to now, this referencing was ignored when BioLector data were automatically read out during the cultivation. Thus, the trigger values for biomass specific replication and induction were slightly inaccurate. Therefore, novel methods were programmed to include also the referencing at the specific inquiry intervals. In Eq. (2-3) the relation is defined as:

$$V_{ref} = V_{raw} \cdot \frac{R_{constant}}{R_{dynamic}} \tag{2-3}$$

The raw value (V_{raw}) is multiplied by the ratio of a predefined filter dependent constant reference value ($R_{constant}$) and a dynamic reference value ($R_{dynamic}$) which is automatically detected in each measurement cycle. The obtained referenced value (V_{ref}) is then used for further method dependent calculations or trigger point verifications.

2.4.3 Biomass separation

For the HT separation of whole cells or cell fragments, microfiltration was performed applying the on-deck vacuum station of the RoboLector (Figure 3-1 A**,** no. 7a-b) with AcroPrep™ 96 Filter Plates (3.0 µm Glass Fiber / 0.2 µm Bio-Inert membrane, modified hydrophilic nylon, 1 mL, part no. 5053, Pall Life Sciences, Ann Arbor, MI, USA). For the filtration an underpressure of 0.5-0.6 bar was applied. Previous experiments revealed that a filtration time of 30 min is sufficient for the complete filtration of cultivation samples with volumes up to 600 µL and OD_{600} values up to 20. For all HT filtration experiments, full plate occupancy was ensured for a homogeneous vacuum distribution.

2.4.4 Enzyme extraction

For *E. coli* cell lysis and protein extraction, the commercial kit BugBuster 10x Protein Extraction Reagent (70921, Merck-Millipore, Darmstadt, Germany) was used. It is a detergent based mixture with a small amount of lysozyme. For the standard protocol, samples were filled in 1.5 mL tubes, biomass was separated via centrifugation for 5 min at 18000 g (centrifuge 1-15K, rotor 12024-H, Sigma), and the supernatant removed with a pipette. For resuspension, the 10x Protein Extraction Reagent was diluted in acetate buffer (to 1x) and a volume equal to the original sample volume was added to the pellet. After 30 min of incubation at 900 rpm and room temperature, samples were centrifuged again for 5 min at 18000 g. The resulting supernatant containing the target protein was stored at 4°C. It must be noticed that this protocol is not in accordance with the manufacturer's guidelines since it was optimized for internal use. For the HT protocol, cultivation samples were given directly to a multiwell filter plate for microfiltration. For protein extraction, 11 µL of 10x Protein Extraction Reagent was added to each 100 µL sample volume. After 30 min of incubation at 900 rpm and room temperature, the filter plate was automatically transported by the gripper to the on-deck vacuum station of the RoboLector and filtration performed as described for microfiltrations. The filtrate was collected in a 96-well DWP and, if necessary, stored at 4°C.

2.4.5 Azo-CMC assay

Azo-CMC is a commercially available substrate for endo-1,4-β-glucanases (Megazyme, Bray, Ireland). All working solutions were prepared as given by the manufacturer's instructions. Only the acetate buffer's pH was adjusted to 4.8 instead of 4.6. For the standard protocol of the assay, 0.5 mL enzyme sample were added to 0.5 mL Azo-CMC solution in a 5 mL tube. Both, enzyme and substrate solution were pre-heated to the incubation temperature of 45°C. Incubation was done for 10 min at 900 rpm, before adding 2.5 mL precipitant solution. After thorough manual mixing, the sample was incubated at RT for 10 min. Precipitated non-hydrolyzed substrate was separated by centrifugation at 18000 g for 10 min. For measurement, 100 µL of supernatant were transferred to a flat-bottom MTP (9293.1, Roth, Germany) and absorbance was determined at 590 nm in a Synergy 4 Microplate Reader (BioTek, Winooski, VT, USA). For the HT protocol, 0.2 mL of the enzyme sample were added to 0.2 mL Azo-CMC solution in a 96-well DWP. Both, the MTP containing the samples and the MTP with the substrate solution were pre-heated on the heater shakers (Figure 3-1 A, no.6) for 15 min at 45°C. After the

incubation for 10 or 20 min, respectively, at 900 rpm, 1 mL precipitant solution was added. Mixing was done by threefold repeatedly aspirating and ejecting the solution with the pipetting robot. After 10 min incubation at RT, 300 µL of the solution were transferred to an AcroPrep™ 96 Filter Plate (0.2 µm Bio-Inert membrane, modified hydrophilic nylon, 350 µL, part no. 5042, Pall Life Sciences, Ann Arbor, MI, USA) placed on the vacuum station of the RoboLector. For complete filtration, an underpressure of 0.5-0.6 bar was applied for 15 min. To ensure homogeneous vacuum distribution, filtrations were performed with full plate occupancy. For measurement, 100 µL of filtrate were transferred from the receiver plate to a flat-bottom MTP and absorbance was determined at 590 nm in a Synergy 4 Microplate Reader (BioTek, Winooski, VT, USA). To determine calibration curves, a commercially available endo-1,4-β-D-glucanase (EGII) from *Trichoderma longibrachiatum* was used (E-CELTR, Megazyme, Bray, Ireland). By dilution in 0.1 M acetate buffer, measuring solutions were prepared with cellulase activities of 100-1000 mU/mL.

2.4.6 Induction profiling

During the main cultivation of *E. coli* Tuner(DE3) FbFP, the induction was carried out automatically for microtiter plate cultivations by the RoboLector device and manually for shake flask cultivations. An appropriate concentrated IPTG-gradient was provided in a single 96-well microtiter plate (flat-bottom, Roth, Karlsruhe, Germany) sealed with X-pierce film (XP-25, Excel Scientific, CA, USA). This plate was located outside of the BioLector on the RoboLector deck at room temperature. Within the programmed RoboLector method, the user can individually select the columns to be induced, the induction volume and time. For induction profiling, 20 µL (48-well) or 10 µL (96-well) of the provided IPTG solution were transferred column by column at predefined times by the liquid handling system into the microtiter plate standing inside the BioLector device. The IPTG concentration in each well was finally in between 0 - 1 mM. For induction with 0 mM IPTG, pure basic Wilms-MOPS mineral medium (without glucose, trace elements, magnesium sulfate, thiamine and kanamycin) was used.

2.5 Offline analysis

2.5.1 Optical density, Osmolality and culture fluorescence

OD_{600} was determined via a Genesys 20 photometer (Thermo Scientific, Dreieich, Germany) in 1.5 mL micro cuvettes (PS, Plastibrand, Roth, Karlsruhe, Germany). For values higher than 0.5, the samples were appropriately diluted with 0.9 % [m/v] NaCl solution.
Osmolality was measured by a cryoscopic osmometer (Osmomat 030, Gonotec GmbH, Berlin, Germany).
For FbFP fluorescence quantification, 100 µl of the respective sample were transferred to a cavity of a 96-well MTP (Greiner Bio-One GmbH, Frickenhausen, Germany). The measurement was done applying the BioLector system with parameters listed in Table 2-2. Each presented value is the average of at least 10 consecutive measuring values.

2.5.2 SDS-PAGE

After measuring the OD_{600} of the culture, samples were centrifuged at 18000 g for 10 min. Subsequently, the supernatant was removed, and the pellet was resuspended in water to an OD_{600} of 25. To 40 µL of this suspension, 140 µL of 2-fold concentrated sample buffer (E-PAGE Loading Buffer, Invitrogen, Germany) and 20 µL of 1 M dithiothreitol (AppliChem GmbH, Darmstadt, Germany) were added before shaking the mixture for 10 min at 1000 rpm and 70°C in a thermo shaker (MKR 10, HLC Biotech, Bovenden, Germany). For analysis, the SDS-PAGE device (Invitrogen, Germany) was equipped simultaneously with up to two gels (4–12% Bis-Tris, Invitrogen, Germany). The transferred volumes were 20 µL for the prepared samples and 15 µL for the protein marker (RotiVR -Mark Standard, Roth, Germany). The process was operated under the suggested standard settings of the manufacturer (running time 35 min, maximum current 200 V, and maximum power 0.25 W). The gels were stained in Simply Blue Staining solution (Invitrogen, Germany) at 37°C and shaken at 60 rpm overnight and were subsequently washed in water at the same temperature and shaking conditions for 2 h

2.5.3 4-MUC assay

The endoglucanase activity of the recombinant protein celA2 was measured manually with the already established fluorescence-based 4-methylumbelliferyl-β-D-cellobioside (4-MUC) assay (Lehmann et al. 2012). Some adaptions were made. A 50x 4-MUC stock solution (0.5 mM) was

prepared by dissolving the reagent in potassium phosphate buffer (0.1 M, pH 6.5) and stored at 4°C. 40 µL of disrupted cells and 90 µL of a diluted 4-MUC solution (1.67x) were transferred separately into a 96-well MTP (flat-bottom, black/clear, BD Falcon, USA), sealed with a clear sealing tape (EN77.1, Roth, Germany) and preheated to 30°C. After the pre-incubation, 60 µL of the 4-MUC solution were mixed with the disrupted cells. Subsequently, the reaction mixture was incubated at 30°C for 20 min in a Synergy 4 Microplate Reader (BioTek, Winooski, VT, USA). The increase in fluorescence was measured at $\lambda_{ex}/\lambda_{em}$ = 365/455 nm in intervals of one minute. For evaluation, a calibration curve, fluorescence versus 4-methylumbelliferone concentration (0.3 - 300 µM), was recorded in the same phosphate buffer and a final volume of 100 µL. Specified activity values for all measured clone variants refer to the volumetric activity within the culture broth.

Chapter 3

Automated HTS platform for recombinant cellulase expression

3.1 Extended RoboLector HTS platform

To meet the demands for an automated HTS of cellulase expression, the original RoboLector system (Huber et al. 2009b) had to be extended. Figure 3-1 A shows the layout of the robotic platform equipped with its different components. The conventional RoboLector system contained the custom-built BioLector online monitoring system (1), a carrier for pipetting tip storage (2), a carrier for the storage of different MTPs (3) with an additional position to park the CO-RE gripping tool (4), and a waste bag for used tips and MTPs (8). With this setup a sufficient upstream process including media preparation, inoculation, cultivation (including online monitoring) as well as automated sampling is possible. But, it lacks possibilities for further sample processing like storage, purification and analysis. Therefore, additional components had to be added to the robotic platform. For tempering tasks, two further tools were integrated. A cooling carrier with five MTP positions (5) connected to a controllable recirculation cooler allows storage of samples and chemicals at low temperatures. With two MTP shakers (6), heat treatment at temperatures up to 110°C can be performed. Furthermore, the RoboLector system was extended by a vacuum filtration module for micro- and ultrafiltration steps in special multiwell filter plates. The filtration module consists of the vacuum chamber (7a), also containing the filtrate receiver plate, and a parking position for the lid of the chamber (7b). The components 2-8 are commercially available from Hamilton Robotics GmbH (Martinsried, Germany).

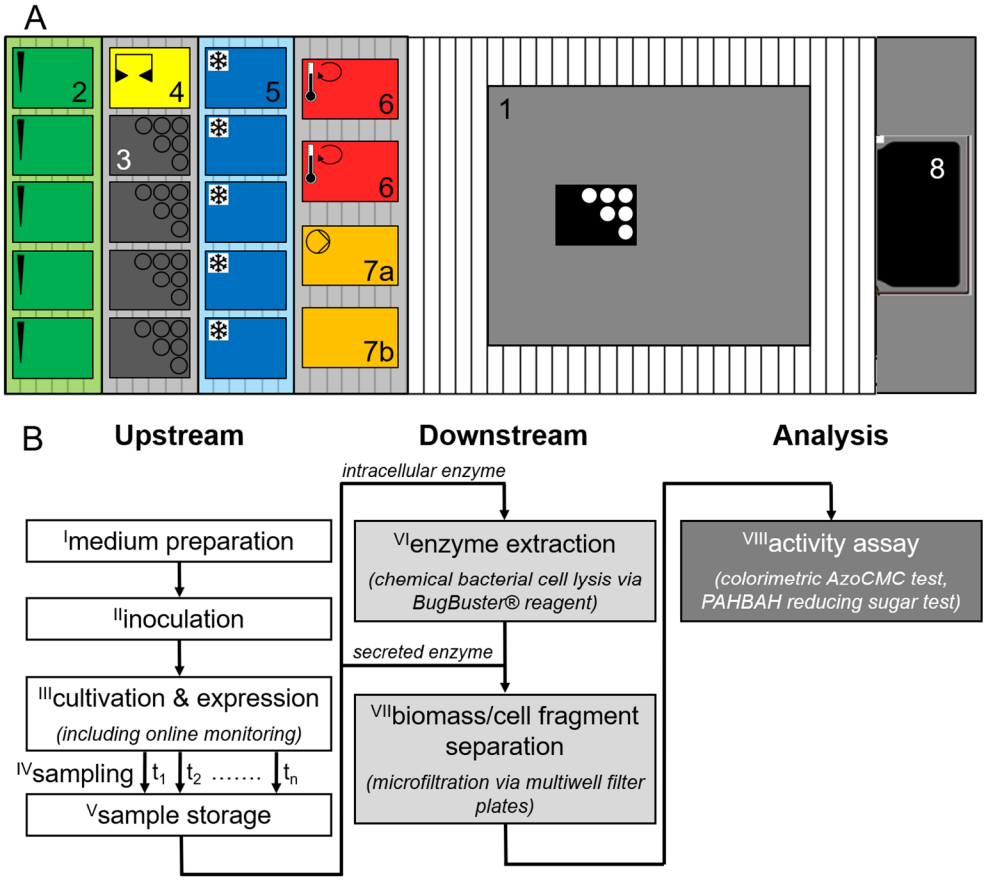

Figure 3-1: Automated HTS of recombinant cellulase expression applying the RoboLector platform. A) Layout of the automated HTS RoboLector platform: 1) Customized BioLector online monitoring device; 2) Pipetting tip carrier for up to 5x 96 tips; 3) Carrier with 4 MTP storage positions; 4) Gripping tool parking position; 5) Cooling carrier for storage of up to 5 MTPs containing samples and/or chemicals; 6) Heater shakers (2x) for MTPs; 7a) Vacuum filtration module for one filter MTP with vacuum chamber, 7b) Lid parking position; and 8) Waste bag. **B)** Schematic protocol for an automated HTS procedure for recombinant cellulase expression with processing steps I-VIII.

Figure 3-1 B shows the schematic protocol for automated HTS experiments with the necessary process steps for cellulase expression, purification and quantification. Depending on the experiment's needs, single steps can, of course, be skipped. The screening process can be classified into three major phases: upstream, downstream, and analysis. The upstream part starts with the preparation of the cultivation medium direct in the cultivation MTP from up to 15 supplied stock solutions stored in DWPs on the cooling carrier (step I). Thereby, the combination of automated medium preparation and cultivation in MTPs allowed to compare different media or to investigate the influence of one or more medium components in short time. Subsequently, the medium is inoculated from a prepared MTP containing the preculture which is shaken on a MTP shaker to ensure a homogeneous suspension (step II). The inoculated cultures are then cultivated under defined conditions in the BioLector system, accompanied by

optical online monitoring of relevant fermentation parameters such as biomass and product formation, DOT and pH (step III, (Samorski et al. 2005; Kensy et al. 2009a)). If necessary, chemicals can be added to the cultures by the pipetting robot at pre-defined times, e.g. inducing chemical compounds to start product formation. At pre-defined time points, samples can fully automatically be taken (step IV) and stored in MTPs on the cooling carrier for further processing (step V). Both, the adding of substances as well as taking samples cause only short interruptions of the cultivation process so that no negative influences are observed.

The upstream phase ends when the cultivation is finished and final samples are taken and stored. The subsequent downstream processing is focused in this work on the elimination of cell material from the cultivation samples. The fact that the target enzyme is either produced intracellular or secreted to the medium dictates which route is taken to gain a cell free cellulase solution. For extracellular enzymes a microfiltration step applying multiwell filter plates with a maximum pore size of 0.2 µm is sufficient to remove all microbial cells and cell fragments (step VII). Afterwards, the corresponding filtrate contains the soluble target enzyme. Intracellular cellulases need a preceding extraction step (step VI). This is done by chemical cell lysis since mechanical procedures or sonification are not applicable for HT processing on a liquid handling robot platform. After the enzyme release by chemical cell lysis, the remaining cell fragments are removed by microfiltration as described earlier for secreted enzymes. It must be considered that the resulting filtrate contains all other soluble components from the cultivation step. But since this work focused on the expression of cellulases and not on their detailed characterization, these impurities are accepted due to the fact that all investigated enzyme candidates are affected in the same way.

The sample analysis aims for the activity measurement of expressed cellulases. Therefore, a method for cellulase activity measurement was adapted for automated HTS. The colorimetric Azo-CMC test quantifies a blue dye which is released during cellulase driven CMC hydrolysis. According to the manufacturer's instructions, this method is most effective for endoglucanases. Additionally, a second assay was applied for cellulase activity determination applying the fluorescent dye releasing substrate 4-MUC. This assay was not performed automatically yet, due to its fast and simple manual procedure. However, a full automation would be easy to realize with a sample amount of less than 48 wells.

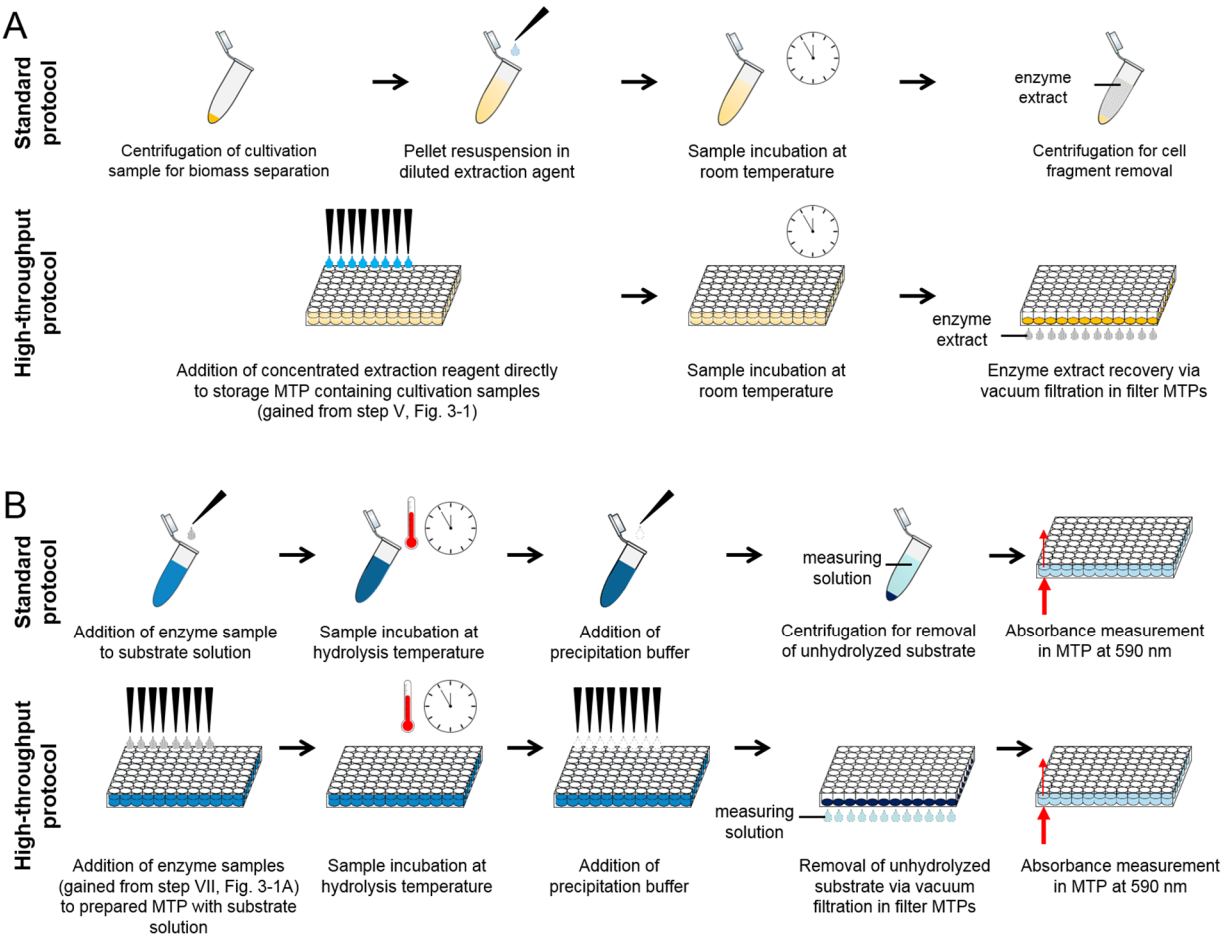

Figure 3-2: Schematic comparison of conventional protocols and modified protocols adapted for HT application in MTPs. A) Extraction of recombinant enzymes/proteins from *E. coli* by chemical cell lysis applying BugBuster reagent. **B)** Colorimetric Azo-CMC assay for cellulase activity measurement.

The control of the robot system is based on a modular structure. Each processing step has its own routine. Depending on the demands of the experiment, all necessary steps can be combined. In this way, the flexible use of the system is ensured and routine programming is simplified. On the other hand, it might be disadvantageous that several steps cannot be operated in parallel, eventually causing increased processing times.

Several process steps from Figure 3-1 B were not yet designed for a liquid handling robot platform, namely enzyme extraction (VI), biomass separation (VII) and the cellulase activity assays (VIII). Consequently, modifications were necessary for down-scaling and automation. Figure 3-2 compares schematically the standard lab protocols with the modified protocols for an application on the extended RoboLector system. They are described in detail in section 3.2.2 and section 3.2.3.

3.2 Development of HT methods

An overview of the developed or extended HT methods is illustrated in Table 3-1. Most of these methods are described in more detail in the next sections: *Automated sampling* in section 3.2.1, *protein extraction* in section 3.2.2, the cellulase activity assay (*Azo-CMC*) in section 3.2.3 and the protein quantification assay (*Bradford*) in section 3.2.4. A combination of the methods *media preparation, protein extraction* and *Azo-CMC* assay is applied for the investigation of cellulases that were expressed in *K. lactis* (section 3.3.1). The methods *biomass specific replication* and *biomass specific induction* were utilized in the clone library screening of *E. coli* strains expressing cellulase mutants in section 3.3.2. The method *induction profiling* is intensively applied in chapter 4.

Table 3-1: Overview of developed or extended HT methods.

Method name	Description
Media preparation	Pipetting of media out of different stock solutions a) Out of 3 sources (in particular for auto-induction experiments) b) Out of 12 sources within 48- and 96-well plates (optional HEPA-hood)
Detection of MTP filling volume	Capacitive detection of filling volume via conductive graphite containing Hamilton tips within all wells of a 48- or 96-well plate (specification of volume requires calibration curve, otherwise only the filling height is recorded)
Automated sampling	Individual time dependent sampling from 48-well or 96-well plates during a BioLector cultivation. Cool down of samples possible on the cooling carrier.
Protein extraction	Combines time dependent individual sampling from BioLector and subsequent vacuum filtration (optional cell lysis step)

Method name	**Description**
Azo-CMC assay	Cellulolytic enzyme activity assay (includes heating, incubation and precipitation of samples as well as final vacuum filtration and preparation of absorption measurement plate)
Bradford assay	Total protein quantification (includes preparation of BSA calibration curve and sample dilution and Bradford incubation step)
Biomass specific replication	Preculture synchronization: Equalization of biomass concentration considering reference values a) Two precultures within one 96-well plate (32 samples) b) One preculture within one 96-well plate (48 samples)
Biomass specific induction	Automated induction of a 96-well plate at a user-defined trigger point (specific reached value of ScL or any other BioLector filter value considering reference values) a) Individual induction of wells when individual trigger point is reached b) Induction of whole plate after last well has reached trigger point
Induction profiling	Time dependent induction of a 48-well or 96-well plate a) Individually for each well b) Column by column
Tip cleaning	Automated cleaning of used pipetting tips (variable amount of cleaning solutions and cleaning cycles)

3.2.1 Automated sampling from a microtiter plate

Many cultivation parameters are already accessible using online detection systems within small-scale reactors. Nevertheless, some parameters still need to be analyzed using offline samples. This is usually linked to time-consuming procedures. Simplification of the process is obtained when sampling is automated. To keep a sterile atmosphere and reduce water evaporation within microtiter plate cultivations, gas permeable sealing tapes are usually used to cover the plates (Sieben et al. 2016). There are a few sealing tapes which are produced in particular for robotic applications. One of them is the sandwich membrane manufactured by m2p-labs (F-GPRS48-10, Baesweiler, Germany). The sealing tape is manufactured for 48-well plates and consists of three layers. The 2 mm thick silicone top layer includes venting holes and pre-cut slits for each well. Liquid handling systems can automatically add substances into a microtiter plate cultivation by piercing through the pre-cut slit and the two lower layers. For this action, the shaking process has to stop shortly. Depending on the liquid handling system and the diameter of the used pipette tips, the piercing depth can be restricted by the narrow slit. Typical filling volumes in 48-well plates are in between of 800 µL - 1000µL. Very thin pipette needles allow full aspiration of the whole volume while the here applied single-use tips get already stuck above the liquid level. Since there is no need for a sterile well after removal of the whole filling volume, the venting hole is pierced and used to aspirate the culture broth with single-use tips.

The programmed method can be applied for 96-well and 48-well plates. The sampling wells, the sampling volume and times can individually be selected and defined in an Excel-template, which is automatically imported when the method is started. The strain *E. coli* Tuner(DE3) FbFP was used as model organism. Half of a 48-well Flowerplate was induced with 0.05 mM IPTG at the beginning of the cultivation. The liquid handling robot transferred every hour, one induced and one non-induced sample into a microtiter plate standing on the cooling carrier. Samples were cooled down to 4°C leading to a rapid stop of cell proliferation. At the end of the cultivation, samples were sterile filtered and used for analysis of glucose and acetate via HPLC as well as pH and osmolality measurements (see Figure A- 2).

3.2.2 Recombinant protein extraction

For the extraction of recombinant proteins from *E. coli* cells, chemical cell lysis was chosen applying the BugBuster reagent kit. In Figure 3-2 A the standard protocol according to the

operator's manual is compared with the modified HT protocol for automated handling. The conventional procedure applying 1.5 mL tubes started with a centrifugation step of cell suspension gained from a cultivation sample to separate biomass from the fermentation medium. After removal of the supernatant the cell pellet was resuspended applying the extraction reagent. Therefore, the supplier is offering a 10-fold concentrated solution which was appropriately diluted. After incubation at RT the mix was centrifuged again to remove solid components such as cell fragments. The resulting supernatant contained the target protein in soluble form. In contrary, the HT protocol was performed in 96-well MTPs. Since centrifugation was not possible on the RoboLector platform, the respective steps had to be replaced. An alternative is microfiltration applying multiwell filter plates. In this way, whole cells and cell fragments can be sufficiently removed from liquid media. But as it turned out, complete resuspension of cell pellets after the filtration was not possible due to a resistant filter cake. Consequently, the first two steps of the conventional protocol, namely biomass separation and resuspension, were replaced by a single step. Therefore, the 10-fold concentrated extraction reagent solution was not diluted but given directly to the cultivation sample including biomass and liquid medium. Nevertheless, the final reagent concentration before incubation was equal to the conventional protocol since the fermentation medium served as solvent. After sample incubation on a heater shaker (Figure 3-1 A, no. 6) at RT all solid components were removed by microfiltration applying 96-well filter plates equipped with a membrane of 0.2 µm pore size on the vacuum filtration module (Figure 3-1 A, no. 7a). The resulting filtrate in the receiver plate contained the target protein in soluble form. To simplify the process and save material and time, all steps were performed directly in the filter plate. Consequently, in this case the filter plate served for sample storage, the extraction reaction and, finally, for cell fragment separation.

To validate the modified HT protocol, samples from a cultivation of *E. coli* expressing the fluorescent protein FbFP were treated with both protocols and the extraction results were determined by fluorescence measurement and SDS-PAGE analysis (Figure 3-3). For fluorescence measurement, the fluorescence intensity of the original cell suspension was used as a reference so that the first column in Figure 3-3 A shows a relative FbFP fluorescence of 100 %. In the corresponding lane of the SDS-PAGE gel in Figure 3-3 B a prominent band (framed) can be seen, indicating the target protein.

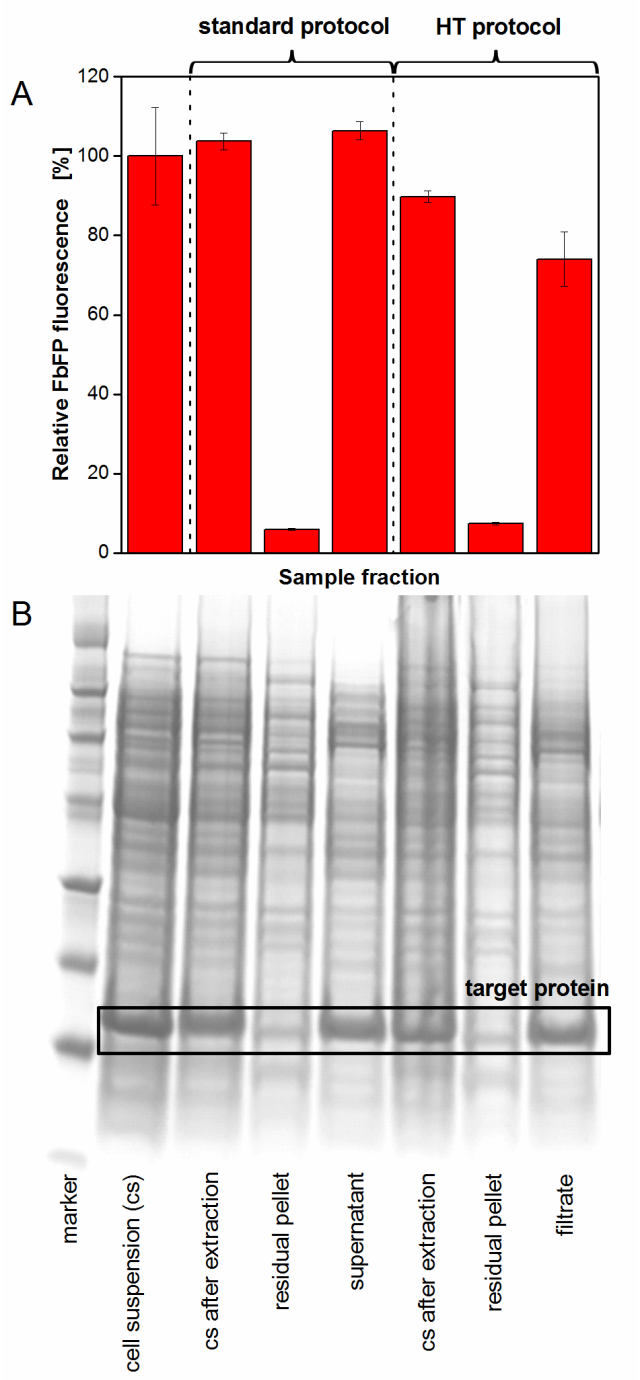

Figure 3-3: Extraction of the fluorescent model protein FbFP from *E. coli* BL21(DE3) pRhotHi-2 comparing the standard and HT protocol (according to Figure 3-2 A). **A)** Fluorescence measurement of different fractions occurring during the extraction procedure applying the BioLector technique. Error bars indicate standard deviation of three simultaneously performed extraction experiments. **B)** SDS-PAGE analysis of different fractions occurring during the extraction procedure. Target protein FbFP is framed. Conditions: Cultivation in 10 mL OnEx auto-induction medium, 250 mL shake flask, n = 350 rpm, d_0 = 50 mm, 37ºC. Extraction with BugBuster 10x Protein Extraction Reagent.

For the comparison of the standard and the HT protocol, three fractions which occur during the extraction process were analyzed: the cell suspension after the incubation with the extraction reagent, the pellet after cell fragment removal and the supernatant or filtrate, respectively, after cell fragment removal. For the standard protocol it can be seen that both, cell suspension after the extraction and supernatant after biomass removal, show relative fluorescence intensities around 100 %. The SDS-PAGE gel confirms these measurements, showing strong bands for the target protein (framed) in both fractions. Almost no fluorescent target protein was found in the residual pellet. This means that the standard protocol works properly. The HT protocol shows similar results. The cell suspension after extraction gives a fluorescence intensity of 90 %, the filtrate after cell fragment removal 74 %, and the retained cell fragments a very low value of 7 %. The SDS-PAGE gel is in good agreement with these values.

Even though, the measured values, especially those for the fraction containing the target protein, are lower for the HT protocol, the applicability for the RoboLector system could be shown since the majority of the target protein was found in the filtrate. It must be considered, that fluorescence measurement depends on many factors such as pH and ion concentrations (Sarder et al. 2015). After the extraction from the protecting cells, the FbFP was exposed to the respective environment. Since the medium composition slightly differed in the standard and HT protocol, the fluorescence of the protein might be affected leading to inaccurate results. The SDS-PAGE gel, on the other hand, shows very similar bands for the target protein for both protocols.

3.2.3 Colorimetric Azo-CMC assay

Assays applying dyed substrates are a convenient way to quantify enzymatic activity. For cellulases, Azo-CMC is a well-established substrate which releases a blue dye during hydrolysis. Subsequently, cellulase activity can be easily determined via absorbance measurement. However, this assay was not yet applied for automated HTS. One reason for this might be the difficult handling with a pipetting robot. Figure 3-2 B shows the manually performed standard protocol as well as the modifications of the assay procedure to adapt it for the application on the RoboLector platform. For comparison, starting point was the addition of an enzyme sample to the ready prepared and pre-heated Azo-CMC substrate solution. The standard protocol was performed in 5 mL tubes. For incubation, the filled tubes containing preheated enzyme sample and preheated substrate solution were shaken on a tube shaker at

hydrolysis temperature. Subsequently, the reaction was stopped by adding precipitation buffer. To remove the precipitated non-hydrolyzed substrate, samples were centrifuged and part of the supernatant (measuring solution) was transferred to a MTP for absorbance measurement. Thereby, it was critical to leave the unstable pellet unaffected since dispersed particles falsify the measurements. For the HT application, the assay was adapted to 96-well DWPs. After addition of enzyme samples to the DWP placed on the heater shaker containing pre-heated Azo-CMC solution, the plate was shaken and incubated at hydrolysis temperature. By adding precipitation buffer, the hydrolysis reaction was stopped. At this point, it was challenging to remove the precipitated substrate. On the one hand, the RoboLector is lacking a centrifuge. On the other hand, the reduction of the reaction volume due to the assay adapted to DWPs made it very difficult for the pipetting robot to remove a sufficient volume of supernatant without affecting the pellet. Considering the available hardware, a promising approach was microfiltration applying multiwell filter plates. It turned out that a membrane with a pore size of 0.2 µm was sufficient to retain the precipitated substrate particles (data not shown). After the filtration, part of the filtrate was transferred from the receiver plate to the final MTP for absorbance measurement in a MTP reader. It should be noticed that the MTP reader is not yet integrated into the RoboLector platform. Transport and measuring were done manually. Nonetheless, these steps could be automated in the foreseeable future.

To validate the modified HT protocol, calibration curves were determined with a commercially available endoglucanase. The relationship between enzyme activity and measured absorbance is shown in Figure 3-4, comparing the manual standard protocol and the HT protocol at varied incubation times. It becomes obvious that the standard protocol (triangles) gives consequently higher values than the HT protocols. Better mixing conditions in the 5 mL tubes and, consequently, an improved substrate access for the enzyme might be the explanation. Nevertheless, a linear relationship is ensured for enzyme activities up to only 400 mU/mL, before the curve runs into saturation. On the contrary, the HT protocol with 10 min incubation (circles) shows a linear trend up to 1000 mU/mL. However, the narrow measuring range for the absorbance is rather disadvantageous. To face this problem, the incubation time was increased to 20 min (squares). In this way, the measuring range was more than doubled and measurements of high cellulase activities up to 1000 mU/mL were still possible. By looking at the respective standard deviations it must be stated that the accuracy of the HT protocols was much better compared to the manual standard protocol. This fact was ascribed to the filtration process which is much more efficient for the separation of the precipitated non-hydrolyzed Azo-CMC than

centrifugation. Therefore, it was possible to adapt the colorimetric Azo-CMC assay for application on the RoboLector platform by modifying the assay procedure and optimizing the process parameters.

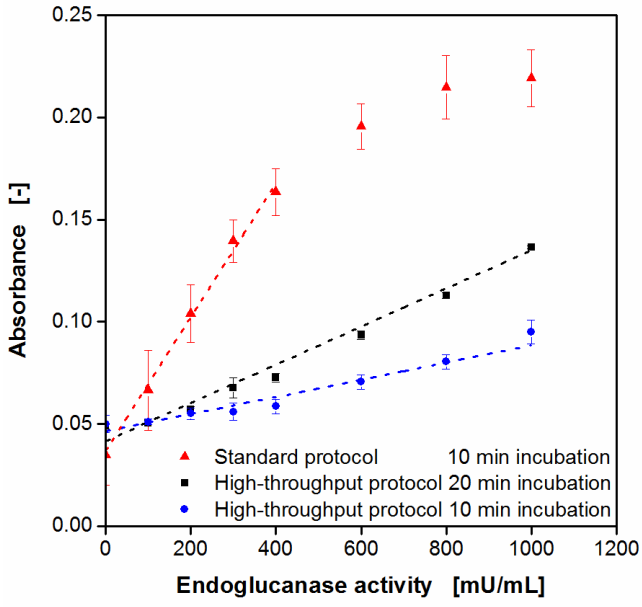

Figure 3-4: Calibration curves for the Azo-CMC cellulase activity assay comparing the standard protocol and HT protocol at varied incubation times (according to Figure 3-2 B). Error bars indicate standard deviation of three simultaneously performed assays. Assay conditions: incubation for 10 min in 5 mL tubes, V_L = 1 mL, n = 900 rpm, d_0 = 3 mm (standard protocol). Incubation for 10 / 20 min in 96-well DWP, V_L = 400 µL, n = 900 rpm, d_0 = 3 mm (HT protocol). 0.2 g/L Azo-CMC in 0.1 M acetate buffer (pH = 4.8), endoglucanase (EGII) from *Trichoderma longibrachiatum*, 50°C, absorbance measurement at 590 nm.

3.2.4 Bradford protein quantification assay

The Bradford assay is a colorimetric detection method for the quantification of total protein content. A coomassie dye binds to proteins in an acidic medium and shifts the absorption maximum from 465 nm to 495 nm. This leads to a color change from brown to blue (Bradford 1976). Typically, bovine serum albumin (BSA) serves as a reference to create a calibration curve and estimate the protein concentration for unknown samples. A series of standard protein solutions has to be prepared for each assay. This is the most time-consuming step within the manual approach.

The aim of the automated process was to reduce the workload for the laboratory assistant. The new method only requires the starting reagents on the RoboLector deck. The plate set-up at the beginning of the experiment is illustrated in Figure 3-5. It is in accordance with the general RoboLector set-up which was already described in section 3.1.

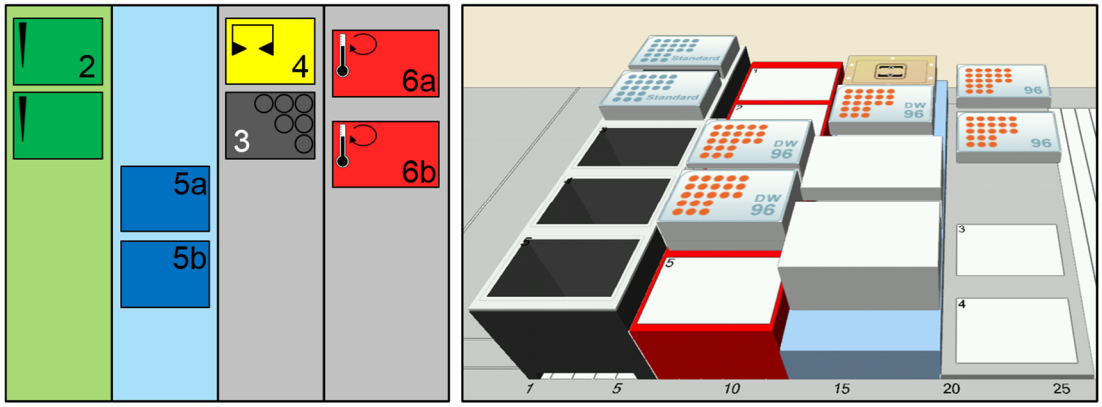

Figure 3-5: Set-up for the automated Bradford-assay on the RoboLector platform. Illustration according to Figure 3-1 (left). 2) Pipetting tip carrier with 2x96 tips; 3) 96-deep well MTP on a storage positon; 4) Gripping tool parking position; 5) Reservoir tank with BSA stock solution (5a) and a deep well plate with Bradford reagent (5b), both on storage positions of the cooling carrier (different position than in Figure 3-1); 6) 96-well sample MTP (5a) and 96-well target MTP for absorbance measurement (5b) standing on two heater shakers; Associated 3D-view in the Hamilton Venus Software (right).

The pipetting was conducted with tips arranged on the tip carrier (2). The BSA stock-solution and water were stored within deep well (DW) reservoir plates (single cavity, polypropylene, Agilent, CA, USA) at position 5a and 3. There is no active cooling necessary, for this experiment. The commercially available Bradford reagent was provided within the first three columns of a deep well reservoir plate (12 column, polypropylene, Agilent, CA, USA) at position 5b. The samples and the final measurement solutions were stored within standard 96-well plates (6a, 6b).

The method can handle up to 23 samples. If needed, a single or serial dilution can be selected for each sample. Moreover, the dilutions for the calibration curve are created automatically in triplicates within the sample plate. For this purpose, 9x3 wells are occupied. All the adjustments were handled within an Excel-template. When the RoboLector method is started, a user output allows the selection of further properties like mixing time in between dilution steps, shaking speed and time for the Bradford incubation step. After the whole process is finished, the user can transfer the final 96-well plate into a microplate reader. As an example, an automatically produced calibration curve with BSA is illustrated in Figure A- 1**.** A very low standard deviation of 0.4 - 2.6% was obtained.

3.3 Application of HT methods

3.3.1 Expression study of *K. lactis* for cellulase production

For the first example, the behavior of the yeast *K. lactis* for the extracellular expression of recombinant endoglucanase cel5A from *T. reesei* was investigated. Therefore, the complex YP medium was automatically supplemented with different concentrations of galactose, which serves as substrate and at the same time as inducer. Subsequently, the media were transferred to a 48-well Flowerplate and inoculated from the provided preculture. All these actions were performed via the pipetting robot. After sealing the plate and transporting it to the climate chamber of the BioLector, the cultivation was started. Up to now, automated plate sealing is not possible. But, it could be performed with the integration of the necessary equipment, which is commercially available, into the RoboLector system. Another task which requires manual intervention is the positioning of MTPs in the BioLector. The very tight holding mechanism cannot be handled with the robotic gripping tool. Hence, the development of a new mechanism controllable by the RoboLector software would be advantageous for further automation. Via optical online monitoring, microbial growth (ScL) and DOT were determined over time, shown in Figure 3-6 A and B, respectively. It can be seen that all cultures started growing exponentially after a *lag* phase of 5 - 6 h, thereby showing almost identical growth rates until 12 h of cultivation. This is accompanied by an inverse decrease of the DOT signals. After 14 h, the culture with 10 g/L galactose reached the stationary phase, whereas it took 16 h and 19 h for the cultures with 25 g/L and 50 g/L galactose, respectively. The simultaneous increase of the DOT signal indicates the complete consumption of the primary substrate galactose. The three curves show no distinct signs of limitation. This is confirmed by the DOT signals which show minimum values of 63 and 16 % for 10 and 25 g/L galactose, and only a short period of oxygen limitation for 50 g L^{-1}. Also inhibitions, e.g. caused by osmotic stress or recombinant protein productions, seem not to be apparent. Contrary to that, the culture with 100 g/L galactose showed a first decrease in the growth rate after 12 h. The reason for this is not yet clear. Oxygen limitation can be excluded since the DOT at this time was still higher than 50 %. Nevertheless, a short interruption in the DOT decrease could be observed at this time, too. In the following, microbial growth slightly recovered before becoming linear after 17.5 h due to an oxygen limitation. After 21 h, the DOT signal started increasing before another drop at 22 h accompanied by a further increase of the biomass signal, albeit with decreased growth rate. *K. lactis* is known to produce ethanol under oxygen limitation or as a product of overflow

metabolism. Consequently, the second decrease of the DOT signal is due to the utilization of ethanol which was formed from galactose in the earlier stages of the cultivation. This phenomenon was described before (Wewetzer et al. 2015). After 25 h, the culture enters the stationary phase and the DOT recovers again.

For the quantification of cellulase production, samples were taken automatically, starting after 8 h of cultivation when the cultures had already entered the exponential growth phase. For sampling, whole wells of the cultivation plate in the BioLector were sacrificed and the cell suspension was transferred to the storage plate on the cooling carrier. In this case, a multiwell plate for microfiltration served for storage at 4°C. After the final samples were taken, the filter plate with the samples was transported to the vacuum station, filtration was done, and the cell-free permeate was collected in a receiver DWP for subsequent analysis via Azo-CMC assay. Since the enzyme is secreted from the host cells, no further extraction step was necessary. The results in Figure 3-6 C show that all cultures had a strongly growth related cellulase production behavior. With the beginning of exponential growth, cellulase activity started increasing in the same way, reaching higher final activity values with higher initial galactose concentrations. However, an increase to 100 g/L galactose didn't result in further improvement. Interestingly, cellulase production did not stop with biomass formation, but it continued until the DOT signal was fully recovered. Consequently, *K. lactis* had the ability for recombinant protein expression, even though the inducing component in the medium was depleted. Earlier reported carbon storage mechanisms might be the explanation for this phenomenon (Dalibor Mijaljica et al. 2007).

For comparing the biomass and product formation under consideration of the used substrate, the respective yields were calculated and listed in Table 3-2, thereby taking the culture with 10 g/L galactose as reference. It can be seen that an increase of the substrate concentration leads to a decrease of the yields for biomass and product formation. Even though, the maximum space time yield (STY) for cellulase production is found for all cultures after 20 h, it was highest with 50 g/L galactose. Consequently, for a later application of the *K. lactis* expression system for endoglucanase production, priorities need to be defined in order to choose the optimal substrate concentration, thereby considering the factors time, substrate costs, and desired product concentration. Therefore, the RoboLector system with its novel tools can deliver a good data base for decision.

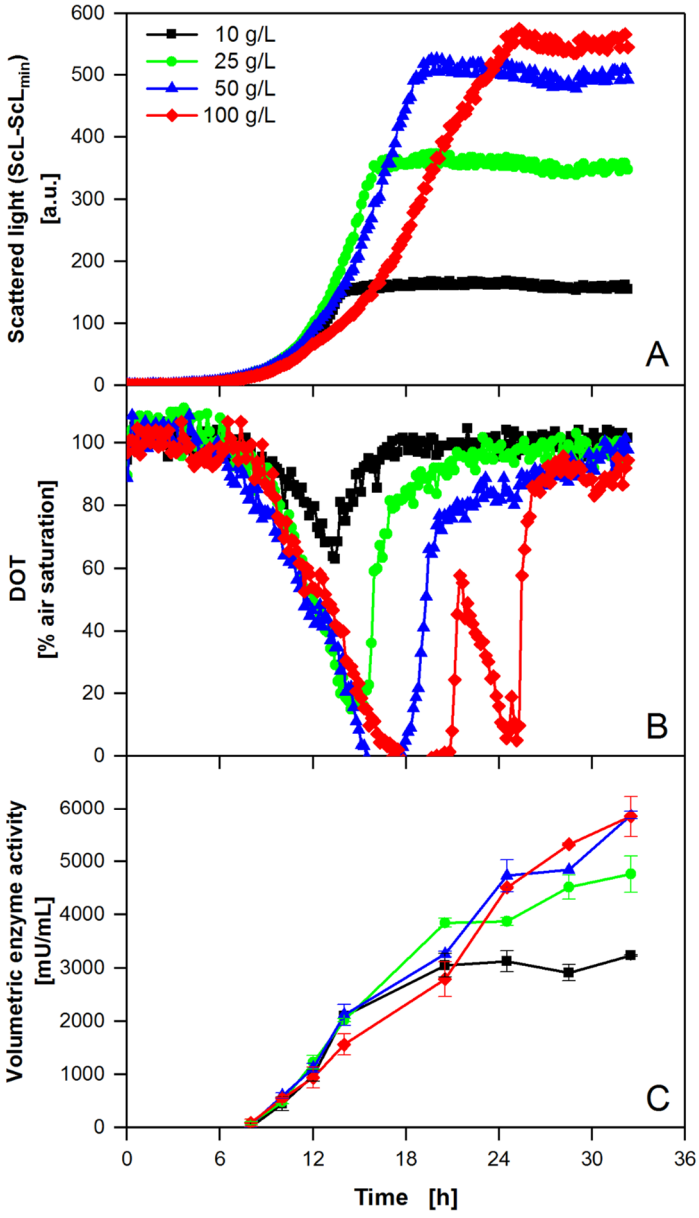

Figure 3-6: Expression study of *K. lactis* expressing recombinant endoglucanase cel5A from *Trichoderma reesei* at varied medium composition applying the RoboLector system. Cultivation and online monitoring of microbial growth (via ScL, **A)** and DOT **B)**) at varied galactose concentrations. The data were derived from representative single experiments. They are in very good agreement with preliminary, non-automated characterization experiments focusing on growth kinetics and final product yield (data not shown). **C)** Automated offline analysis of volumetric cellulase activity applying the Azo-CMC assay. Error bars indicate standard deviation of three simultaneously performed assays. Cultivation conditions: 48-well Flowerplate, YP medium containing galactose as carbon source, V_L = 1 mL, n = 1500 rpm, d_0 = 3 mm, 30°C. Activity assay conditions: incubation in 96-well DWP, 0.2 g/L Azo-CMC in 0.1 M acetate buffer (pH=4.8), V_L=400 µL, n=900 rpm, d_0=3 mm, 50 °C, absorbance measurement at 590 nm.

Table 3-2: Product, biomass and space time yield (STY) of *K. lactis* in dependency on the utilized galactose concentration in YP medium.

Galactose conc. [g/L]	Relative $Y_{X/S}$ [%]	Relative $Y_{P/S}$ [%]	Relative max. product STY [%]
10	100	100	100 (after 20 h)
25	89	59	124 (after 20 h)
50	63	36	152 (after 20 h)
100	34	18	145 (after 20 h)

3.3.2 Automated HTS of recombinant cellulases

A more complex example is depicted in Figure 3-7. The data was generated during a primary clone bank screening for the expression of 46 variants of endoglucanase celA2 in *E. coli*. The enzyme variants were created by directed evolution applying a triple site-saturation mutagenesis (Wang and Malcolm 1999; Lan Tee and Schwaneberg 2007; Lehmann et al. 2012). This screening protocol consisted of a two-step cultivation including one pre-cultivation and a main cultivation with automated biomass specific induction. To enable a complete automated cultivation, the first six columns of the plate were used for the preculture and the last six columns for the main culture. This avoided the manual transport of MTPs out of the BioLector. For reference, one well in each step of the cultivation was filled with plain medium. Moreover, the strain expressing the wildtype enzyme was present two times in both cultivation steps. One served as a non-induced reference.

At the end of the cultivation, the cultures were harvested and used for cell lysis. The already published method to determine celA2 activity in MTP format is the 4-MUC assay (Lehmann et al. 2012). The volumetric activity was calculated from a kinetic measurement of the increase in released fluorescent 4-MU. Therefore, a quick measurement of all micro-wells was necessary.

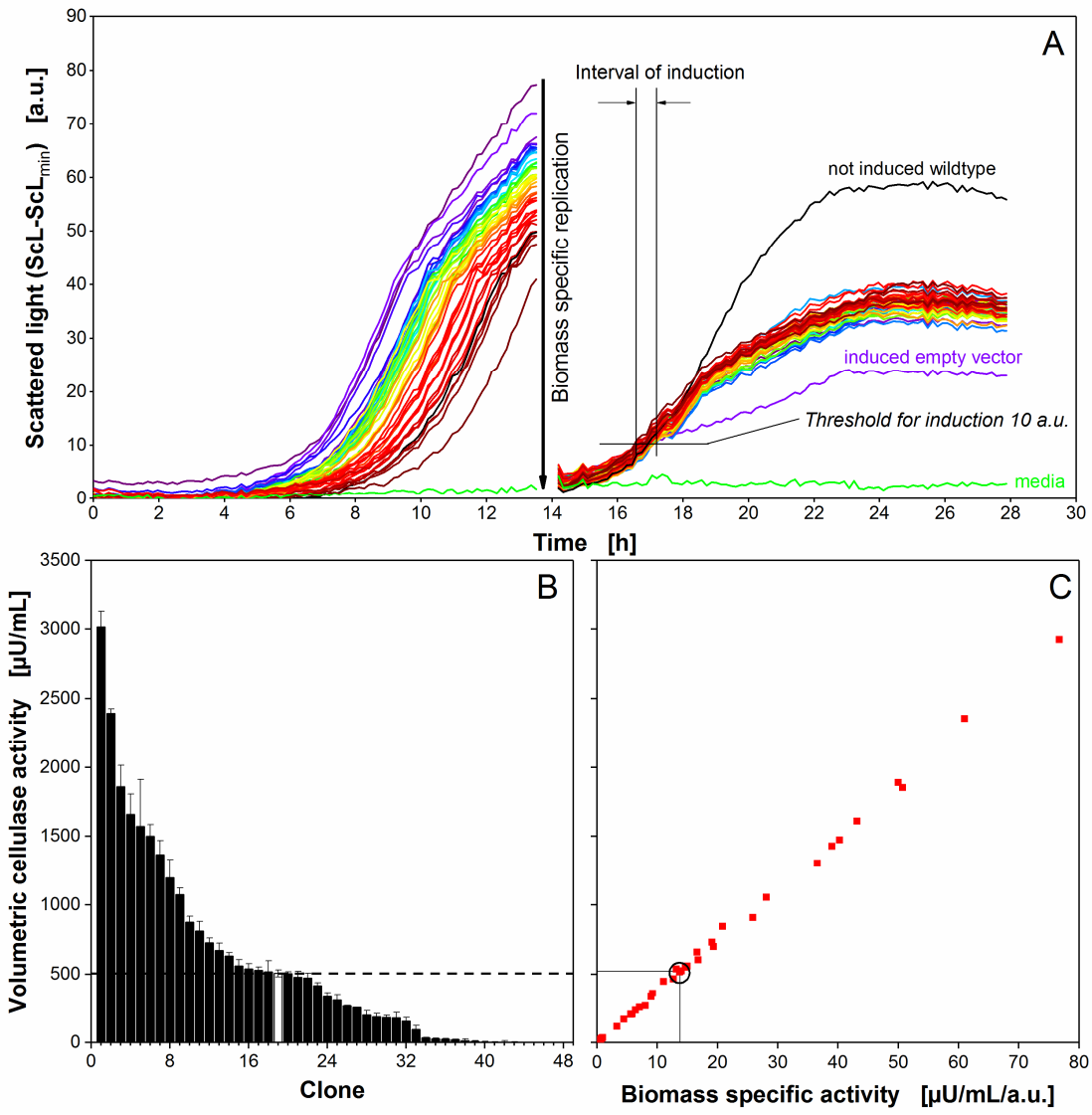

Figure 3-7: Primary screening of an *E. coli* clone library expressing variants of endoglucanase celA2 applying the RoboLector system. A) Online biomass signal (monitored via ScL) for a two-step cultivation of 46 *E. coli* clones consisting of one non-induced pre-cultivation and an induced main cultivation. Additionally, a non-induced wildtype and plain media served as references. The main cultivation was automatically inoculated from the previous cultivation step. **B)** Volumetric cellulase activity (via 4-MUC assay) of the supernatant after cellulase extraction from *E. coli* cells including standard deviations of three independent main cultivations. Reference activity of the clone expressing the original enzyme indicated by dashed line and white bar. Not induced wildtype and media are depicted as clone no. 47 and 48. **C)** Parity plot comparing volumetric and biomass-specific cellulase activities of the supernatants after cellulase extraction from *E. coli* cells of the main cultivation. For calculation of biomass specific activities, the final ScL values of the main cultivation were used. The strain expressing the wildtype enzyme is indicated by a circle. Cultivation conditions: 96-well MTP, V_L = 150 µL, n = 995 rpm, d_0 = 3 mm, pre-cultivation and main cultivation in Wilms-MOPS medium containing 15 g/L glucose, cellulase expression automatically induced by adding 0.1 mM IPTG after reaching the ScL threshold of 10 a.u.. Activity assay conditions: incubation in 96-well MTP, 0.05 mM 4-MUC solution in potassium phosphate buffer (pH = 6.5), V_L = 150 µL, 30 °C, fluorescence measurement at 365/455 nm.

This was not possible within the BioLector since it takes about four minutes to measure 96 wells. Therefore, a manual offline activity assay using a Synergy 4 Microplate reader was chosen for the evaluation of this clone library. However, it is important to consider, that the final assay only measures the volumetric activity. As described in Eq. (3-1) a change in volumetric activity can originate from a difference in the enzymatic specific activity (term 1), from a difference in the biomass specific activity (term 2), or from a difference in the biomass concentration (term 3).

$$\frac{U}{mL} = \frac{U}{g_{enzyme}} \cdot \frac{g_{enzyme}}{g_{biomass}} \cdot \frac{g_{biomass}}{mL} \tag{3-1}$$

Since the volumetric activity is dependent on these three parameters and only the last term describing the biomass concentration is known from ScL measurements, it is in most cases not possible to distinguish whether the differences are caused by the first or second term. Even a concurrent effect of all three terms cannot be excluded. Dependent on the purpose of a library screening, a subsequent enzyme quantification would be necessary to yield the enzyme specific activities. HT affinity chromatography in MTP-format are commercially available for this task, however this leads in most cases to an undesired increase of investment. An easy solution for this problem would be to label the target proteins with fluorescent tags. Term 2 and 3 from Eq. (3-1) would then be known and the enzymatic specific activity could be calculated. However, tags with high molecular weight may stress the host cell metabolism and thus change the target protein expression efficiency or even the enzyme activity. Using smaller tags like tryptophan tags (Siepert et al. 2012) or splitted tags such as the Split-GFP technology (Santos-Aberturas et al. 2015) could be the method of choice.

The ScL curves of all clones in Figure 3-7 A show different *lag* phases within the preculture. A time shift of up to four hours within the exponential growth phase was observed when comparing the variants. This is most likely due to fluctuations in the initial cell concentration which are commonly present in cryo cultures of clone libraries. These differences are then transferred into the culture plate. Moreover, the replication tool which was used to transfer the cells from the cryo plate to the culture plate plays an important role, as described elsewhere (Huber et al. 2010). The asynchronous growth was eliminated after operating the automated biomass specific normalization step shortly after 13 hours. Nevertheless, an automated biomass specific induction was followed which ensures identical induction conditions. As soon as the

ScL exceeded the preset threshold of 10 a. u. the robot induces these specific wells with 10 µL of IPTG, resulting in a final concentration of 0.1 mM. Interestingly, all variants behave the same way after induction and end up with the same biomass concentration at the end of the cultivation. Consequently, similar metabolic burden and similar protein production can be assumed. Integration of this assumption into Eq. (3-1) lead to a direct proportionality of volumetric activity and enzyme specific activity. Thus, an elaborate quantification of the celA2 protein content is not necessary.

After about 14 h of main culture, the cell suspensions were harvested and cell pellets were lysed using BugBuster. The volumetric activity of received crude extract was determined by the fluorescence-based 4-MUC assay. The final clone ranking is depicted in Figure 3-7 B. Mean values of cellulase activity and error bars coming from three independently conducted HTS are shown. This includes the experiment depicted in Figure 3-7 A and two more experiments whereof no ScL curves are shown here. The volumetric activity of the induced wildtype is illustrated as white bar. A six times higher activity was obtained by the best variant when compared to the wildtype. A very small relative standard deviation (c_v) is observed (wildtype, 5.1 %; best clone, 4.0 %). This confirms a very high reproducibility of the screening method using the automated preculture synchronization and the biomass specific induction. Furthermore, it gives a maximum of standardization accompanied by an online monitoring signal to control it. Considering the final ScL values of the cultures, biomass specific cellulase activities can be determined. Figure 3-7 C describes the dependency of volumetric activity and biomass specific enzyme activity. Since the biomass concentration was similar for all clones, a completely linear trend was observed.

3.4 Conclusion

The RoboLector platform was successfully extended by a cooling carrier, a MTP shaker for heat treatment and a vacuum filtration module. This enables the robot to perform a cellulase screening experiment consisting of upstream, downstream and analysis steps. Some downstream and analysis protocols were adapted from manual handling to a HT protocol suitable for automated handling. This comprises enzyme extraction, protein quantification and the Azo-CMC cellulase activity assay.

The established methods were successfully applied to investigate the expression of cellulase cel5a in *K. lactis*. The results showed how the RoboLector system can conveniently be used to optimize media compositions and analyze the outcome without manual intervention.

The automated HTS of the *E. coli* celA2 library showed the advantage of a biomass specific replication step, to achieve synchronized cultures. A highly parallel biomass growth could be achieved and via biomass specific induction a comparable expression of target protein was secured. The reliability of the final ranking was confirmed by very low relative standard deviations of ~5% amongst three independent clone screenings. This underlines the reproducibility of the RoboLector method. The ranking revealed a six times higher activity of the best variant, compared to the wildtype.

It was demonstrated that a large variety of methods could successfully be automated on the extended RoboLector platform. The device allows a strongly increased information content compared to screening systems reported so far. The results confirm the feasibility of a reliable and automated HTS on the robotic platform. Up to now, only a small clone library consisting of 46 different variants was screened. The future strategy will be the automation of the whole cellulase screening system with emphasis on the linkages between the already described automated modules and finally screen a large clone library. A comparison of the manual and automated screening is certainly of great interest and will be part of upcoming experiments.

Chapter 4

Induction profiling at different temperatures

4.1 Comparable oxygen supply in microtiter plates and shake flasks

Comparable cultivation conditions for *E. coli* in microtiter plates and shake flasks can be obtained when oxygen supply is identical in both fermentation systems (Marques et al. 2010; Wewetzer et al. 2015). To avoid production of anaerobic side products and to increase the recombinant protein yield, oxygen unlimited conditions are favored. The filling volume and shaking frequency can serve as parameters to adjust the maximum oxygen transfer capacity (OTR_{max}) (Maier and Büchs 2001). The upper limit of shaking frequency for shake flasks on a conventional shaker is typically 300 -350 rpm at a shaking diameter of 50 mm. Furthermore, low filling volumes are associated with an increased ratio of evaporated water per applied culture volume. Therefore, the shaking frequency and the filling volume were set to 1400 rpm / 350 rpm and 800 µl / 8 mL for microtiter plates and shake flasks, respectively. To verify the comparability of both systems with these settings, *E. coli* Tuner(DE3) was cultured exemplarily under non-induced and induced cultivation conditions. The OTRs were measured within a RAMOS device and dissolved oxygen tensions (DOT) were measured in a 48-well Flowerplate featuring optodes (MTP-48-BO, m2p-labs, Baesweiler, Germany) using the BioLector device (m2p-labs, Baesweiler, Germany). The comparison of the OTR and DOT during the cultivation of *E. coli* Tuner(DE3) EcFbFP is shown in Figure 4-1. The progress of OTR over time in the shake flask for the non-induced culture is characteristic for *E. coli* and well known from previous studies (Huber et al. 2011; Wewetzer et al. 2015). The two peaks reflect increased respiration due to glucose consumption during the first 11 hours of cultivation, followed by

acetate consumption at around 11-14 hours. The DOT in the microtiter plate runs entirely inverse to the OTR, leading to two local minima. The DOT describes the same phenomenon as the OTR since decreasing dissolved oxygen availability in the surrounding media is the consequence of high oxygen consumption of the organism. This demonstrates the comparability of microtiter plate and shake flask cultivations under the chosen cultivation conditions. The measurement interval of DOT (15 min) is shorter than for the OTR (30 min), leading to a higher data density. A short oxygen limitation of around 1 hour can be detected, shortly before the OTR drops and the DOT rises. Although DOT does not reach 0%, this is clearly an oxygen limitation. Low oxygen tensions cannot sufficiently be resolved with the used optical sensor spot (accuracy according to manufacturer +/- 5%). The maximum reached OTR lies at 76 mmol/L/h. This agrees with the calculated OTR_{max} according to Meier et al. 2016. The osmolality, which is required to calculate the OTR_{max}, was determined in an additional experiment (Figure A- 2), where samples were taken automatically every hour. The osmolality decreased from 0.69 Osmol/kg at the beginning of the cultivation to 0.52 Osmol/kg at the end of the cultivation. During the critical time at around 9 to 11 h, the osmolality reached a value of around 0.62 Osmol/kg leading to the calculated OTR_{max} value. This is the first hint of a short oxygen limitation and it is confirmed when looking at the slope of the OTR curve. It is clearly visible, that a higher OTR would have been reached when the increase in OTR would not be limited by the maximum oxygen transfer capacity of the shake flask under these cultivation conditions. Hence, a short oxygen limitation is present for both cultivation systems. This was accepted since induced cultures typically do not reach such high OTR values. This was proven for the culture which was induced after 7 h with 0.1 mM IPTG. The OTR and DOT differ quite much from the non-induced culture. The oxygen consumption decreases more or less directly after induction and remains afterwards at a low plateau. At the end of the cultivation the OTR increases again, but throughout the cultivation no oxygen limitation occurred. This can be confirmed by the progress of DOT as the curve never falls below 40 % of air saturation.

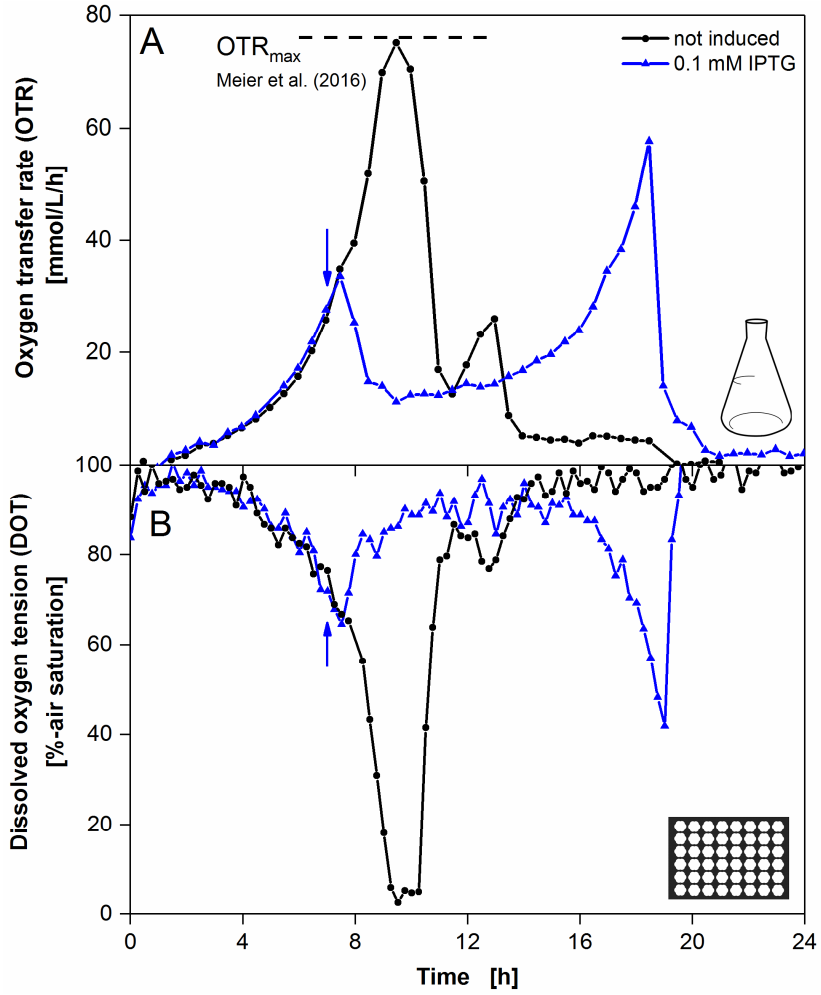

Figure 4-1: Comparison of oxygen transfer rate (OTR, measured in shake flasks) and dissolved oxygen tension (DOT, measured in microtiter plates) measured by a RAMOS and a BioLector device, respectively. A mastermix of medium and cells was used to start the experiment in both systems simultaneously. The non-induced cultures served as references. The induction for the induced cultures took place after 7 h (blue arrows) by the addition of IPTG (0.1 mM final concentration in cultures). The maximum oxygen transfer capacity (OTR_{max}) was calculated after Meier et al. (Meier et al. 2016) (dashed line). Cultivation conditions for *E. coli* Tuner(DE3)/pRhotHi-2-EcFbFP in RAMOS device **(A)**: Wilms-MOPS mineral medium, 250 mL flask, V_L = 8 mL n = 350 rpm, d_0 = 50 mm. Cultivation in the BioLector device **(B)**: Wilms-MOPS mineral medium, 48-well Flowerplate with DOT optodes, sandwich membrane (m2p-labs), V_L = 800 µL, n = 1400 rpm, d_0 = 3 mm, 37°C.

4.2 Induction profiling covering conventional conditions

The induction profile of *E. coli* Tuner(DE3) EcFbFP at 37°C in a 48-well Flowerplate is illustrated in Figure 4-2**.** During the whole cultivation process, scattered light and FbFP-fluorescence was measured. The maximal achieved recombinant protein content in terms of fluorescence intensity is shown in dependency of the inducer concentration and time of

induction. Since many manuals recommend to use 1 mM IPTG by default (Donovan et al. 1996), the utilized IPTG gradient ranges from 0 - 1 mM. As described in the methods section, this IPTG-gradient is automatically added by the RoboLector into the 48-well Flowerplate. Thereby, the shaking process of the Flowerplate inside the BioLector device stopped shortly at the distinct induction times ranging from 1 h to 10 h after start of the main culture.

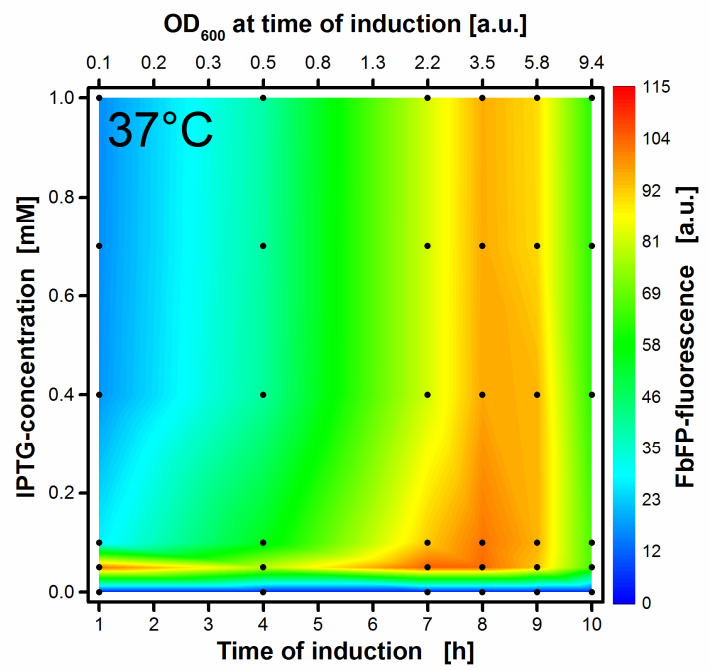

Figure 4-2: Induction profile with automated addition of 0-1 mM IPTG solution after 1–10 h of cultivation time. Colors from blue to red indicate maximal FbFP intensities reached at the end of each culture. Black dots indicate the 36 individual cultivations. The upper x-axis reflects the corresponding optical density of the cultures at the time of induction. It is calculated from the mean scattered light values of the cultures that have not been induced until the respective induction time and a calibration curve that was previously prepared (see Figure A- 7). Cultivation conditions for *E. coli* Tuner(DE3)/pRhotHi-2-EcFbFP: Wilms-MOPS mineral medium, 48-well Flowerplate, sandwich membrane (m2p-labs), V_L = 800 µL, n = 1400 rpm, d_0 = 3 mm, 37°C.

A characteristic optimum consisting of a horizontal and a vertical part forming a reversed “L” is indicated by red color coding in the graph. When induction takes place within the small time slot of 8 to 9 h of cultivation, high fluorescence intensities are reached independently of IPTG concentration. When induction occurs within the first 9 hours of cultivation a specific low inducer concentration of 0.05 mM IPTG has to be used.

The biomass concentration has to reach a distinct threshold to withstand the metabolic burden induced by higher IPTG concentrations. The higher the biomass concentration the lower the IPTG to cell ratio. Involving the optical density OD_{600} (Figure 4-2, upper x-axis) the threshold lies in this case at a value around 3.5. However, a very late induction is also counterproductive

since most of the resources are then already converted to biomass instead of recombinant proteins. For practical and economic reasons, it is worthwhile to utilize low inducer concentrations (0.05 mM IPTG at 37°C). This saves expensive chemicals and no mandatory online monitoring is necessary since induction time has a low impact. Since the temperature is reduced in the next section, the large experimental space up to 1 mM IPTG was also checked for 30°C (see Figure A- 3). Just as for 37°C, no improvement of product formation was observed for IPTG concentrations above 0.4 mM. To optimize the experimental search space, the maximum applied inducer concentration was therefore reduced to 0.4 mM IPTG. Consequently, a higher information density is achieved within the inducer concentration range from 0 – 0.4 mM.

4.3 Comparison of selected induction conditions at 28°C and 37°C

A comparison of OTR, biomass and product formation at 28°C and 37°C is given in Figure 4-3**.** 37°C represents the standard cultivation temperature of *E. coli*. In contrast to that, 28°C is a temperature far away from the optimal growth temperature. However, it is often used to obtain soluble recombinant protein production and to avoid inclusion body formation (Schein and Noteborn 1988; Dragosits et al. 2011). The results are obtained from two parallel RAMOS and BioLector cultivations, respectively. The same data is also available for 30°C and 34°C in Figure A- 5. The cultivation at 37°C is conducted under the same cultivation conditions as for Figure 4-2, besides a smaller IPTG range.

Induction was manually performed in shake flask cultivations and automatically in microtiter plate cultivations after 7 h (indicated by arrows). This time was chosen in advance. It was intended to achieve the most diverse OTR courses and product formations for different inducer concentrations at one induction time. Because of one failed automated induction in the microtiter plate, the curves for 0.4 mM IPTG at 28°C (Figure 4-3 C, E) are missing.

The non-induced culture reached the maximum OTR within 16 h at 28°C (Figure 4-3 A) whereas it took only 9 h at 37°C (Figure 4-3 B). This clearly indicates, as expected, a higher growth rate at a higher temperature.

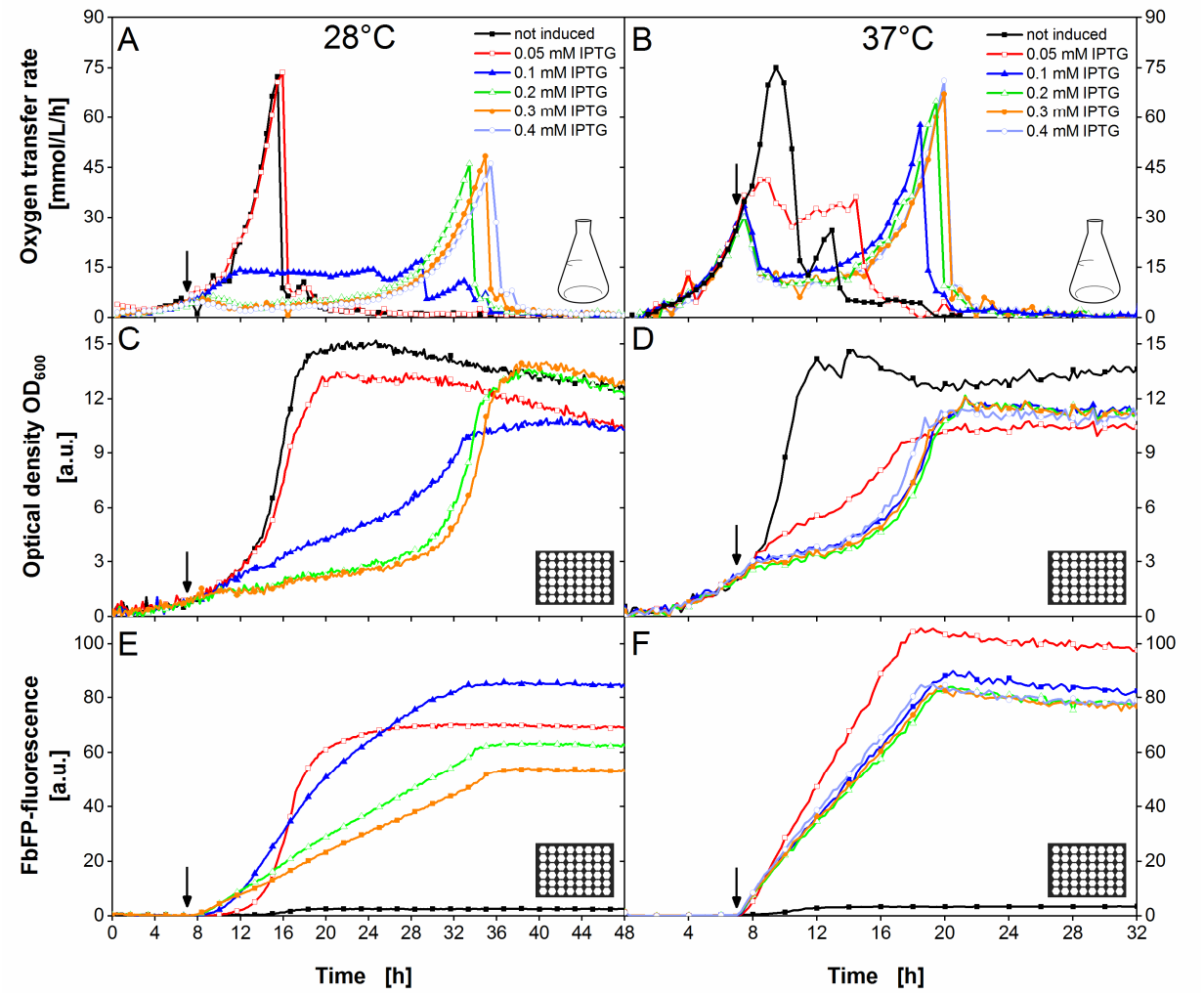

Figure 4-3: Comparison of selected induction conditions at 28°C and 37°C measured in a RAMOS and a BioLector device. Manual induction (shake flask) and automated induction (MTP) after 7 h with 0-0.4 mM IPTG (indicated by black arrow). Cultivation temperature was 28°C for the graphs in the left column and 37°C for the graphs in the right column. RAMOS and BioLector cultivations were conducted for each temperature in parallel using the same *mastermix* (medium plus microorganisms). **A), B)** Oxygen-transfer rate of RAMOS cultivations in 250 mL shake flasks, **C), D)** Scattered light signal from BioLector cultivations, **E), F)** FbFP-fluorescence from BioLector cultivations. Cultivation conditions for *E. coli* Tuner(DE3)/pRhotHi-2-EcFbFP in RAMOS device: Wilms-MOPS mineral medium, 250 mL flask, V_L = 8 mL n = 350 rpm, d_0 = 50 mm. In BioLector device: Wilms-MOPS mineral medium, 48-well Flowerplate, sandwich membrane (m2p-labs), V_L = 800 µL, n = 1400 rpm, d_0 = 3 mm.

For the induced cultures, the induction took place after 7 h for both temperatures. Therefore, the culture at 28°C was induced at lower cell densities than the one at 37°C. A direct comparison of the effect of induction at the same biomass concentration is provided in Figure A- 6.

Surprisingly, an induction with 0.05 mM IPTG at 28°C did hardly affect the respiration of *E. coli*. Whereas at 37°C, the OTR stagnated at a more or less constant level in between 30 and 40 mmol/L/h until all of the carbon source is depleted and the OTR drops down. This

phenomenon is also reflected in the optical density (Figure 4-3 C, D). The induced growth curve (0.05 mM IPTG) at 28°C has only low deviations compared to the non-induced culture. The deviation becomes apparent at the end of the cultivation when an optical density of only 13 instead of 15 is reached. Thereby, some of the glucose is consumed to form the product instead of biomass. However, at 37°C the biomass growth is strongly disturbed after induction with 0.05 mM IPTG and only a very low final optical density of around 10 is reached. The cells obviously redirected key metabolites into production of FbFP. This becomes clearly apparent in Figure 4-3 E, F. The induced culture (0.05 mM IPTG) at 37°C resulted in higher fluorescent intensities than the one at 28°C. Moreover, the product formation seemed to be linear at 37°C and S-shaped at 28°C. Generally, the production of FbFP stopped for all cultivations as soon as the stationary phase was reached. Although the biomass concentration during induction was higher at 37°C (lower inducer per biomass ratio), the metabolic burden was higher than for 28°C.

Doubling the inducer concentration to 0.1 mM IPTG increased the metabolic burden significantly for both temperatures. The OTR curve for 28°C also revealed a plateau but at a lower level of around 13 mmol/L/h. The optical density progression looks similar to the cultivation with 0.05 mM IPTG at 37°C, resulting for both in the highest production among the investigated induction conditions in Figure 4-3. The induction with 0.1-0.4 mM IPTG at 37°C led to the following analogous trends. Directly after induction, the respiration was strongly reduced and recovers after a few hours ending with a final relatively high OTR peak. This is consistent with the biomass growth, which was slower compared to 0.05 mM IPTG. The final product concentration attained only a value of 80 a.u.. Increasing the IPTG concentration to 0.2 mM or higher at 28°C, did result in similar trends. The OTR stayed at a very low level below 4 mmol/L/h after induction, the optical density barely increased for a long time and only low final product concentrations were achieved. However, the biomass growth recovers after 28 h and high final ODs were reached, thus, marginal energy was spent for recombinant protein production. Consequently, the metabolic burden was too high at the time of induction.

The results are in good agreement with earlier published observations. Kunze et al. 2012 noticed a correlation of OTR and product formation. Phases of low OTR were identified as production phases whereas phases of high OTR were related to low productivity and undisturbed cell growth. There is one extension, which has to be made. Phases of low OTR are only related to

high productivity, if a specific threshold is exceeded. A respiration rate of about 10 mmol/L/h should still be present.

4.4 Comparison of induction profiles at four temperatures

So far, a strong influence of temperature on the metabolism of *E. coli* was presented in the previous section. The results were shown for selected induction conditions as temporal progress. Figure 4-4 shows the overall formed product at four temperatures (28, 30, 34 and 37°C) at a broad range of induction conditions. The corresponding induction profiles are illustrated in Figure 4-4 A-D. Vertical black boxes symbolize the induction conditions from parallel shake flask cultivations. Thereby, Figure 4-4 A + D refer to Figure 4-3 and Figure 4-4 B + C refer to the Figure A- 5.

The induction profile at 37°C (Figure 4-4 D) is a replication of Figure 4-2 at lower IPTG concentrations. The area for optimal induction concurs quite well for both experiments. The ideal inducer concentration of 0.05 mM IPTG is identical as well as the best time-point for induction at 8 h or accordingly an optical density of 3.5.

With reduction of temperature, the optimal induction zone is shifted and altered (Figure 4-4 A-D). Firstly, the absolute measured product concentration varied with the temperature. The horizontal optimum at 34°C (0.05 mM IPTG, 1-6 h) was even out of the applied fluorescence scale. Since the FbFP fluorescence is not temperature sensitive within the investigated temperature range and no inclusion body formation at 37°C could be detected via SDS-PAGE (data not shown), the highest product concentration was achieved at 34°C. These findings are in contradiction with the common approach to reduce temperature for increased productivity (Dragosits et al. 2011) but they are consistent to some other studies (Baumann et al. 2015; Ladd Effio et al. 2016).

Secondly, the vertical optimum strongly changes. While the vertical optimal zone is present at 37°C and 34°C, it fades out at 30°C and disappears at 28°C. Thus, a defined low inducer concentration is all the more important at lower temperatures. There was the assumption of a later vertical optimum (induction after 11 h and later) for 28°C and 30°C but it was rebutted by the trend of lower optimal optical densities at lower temperatures. While the best optical density for induction is 3.5 (x-axis at the top of the graph) at 37°C it decreases to 2.6 at 34°C. It is less clear at 30°C, but there is a light green-yellow area above the optimum in particular at 9 h. This

less pronounced vertical area corresponds to an optical density of 2.1, which is again lower compared to higher temperatures. Therefore, a further optimum after 11 hours at 28°C is rather unlikely.

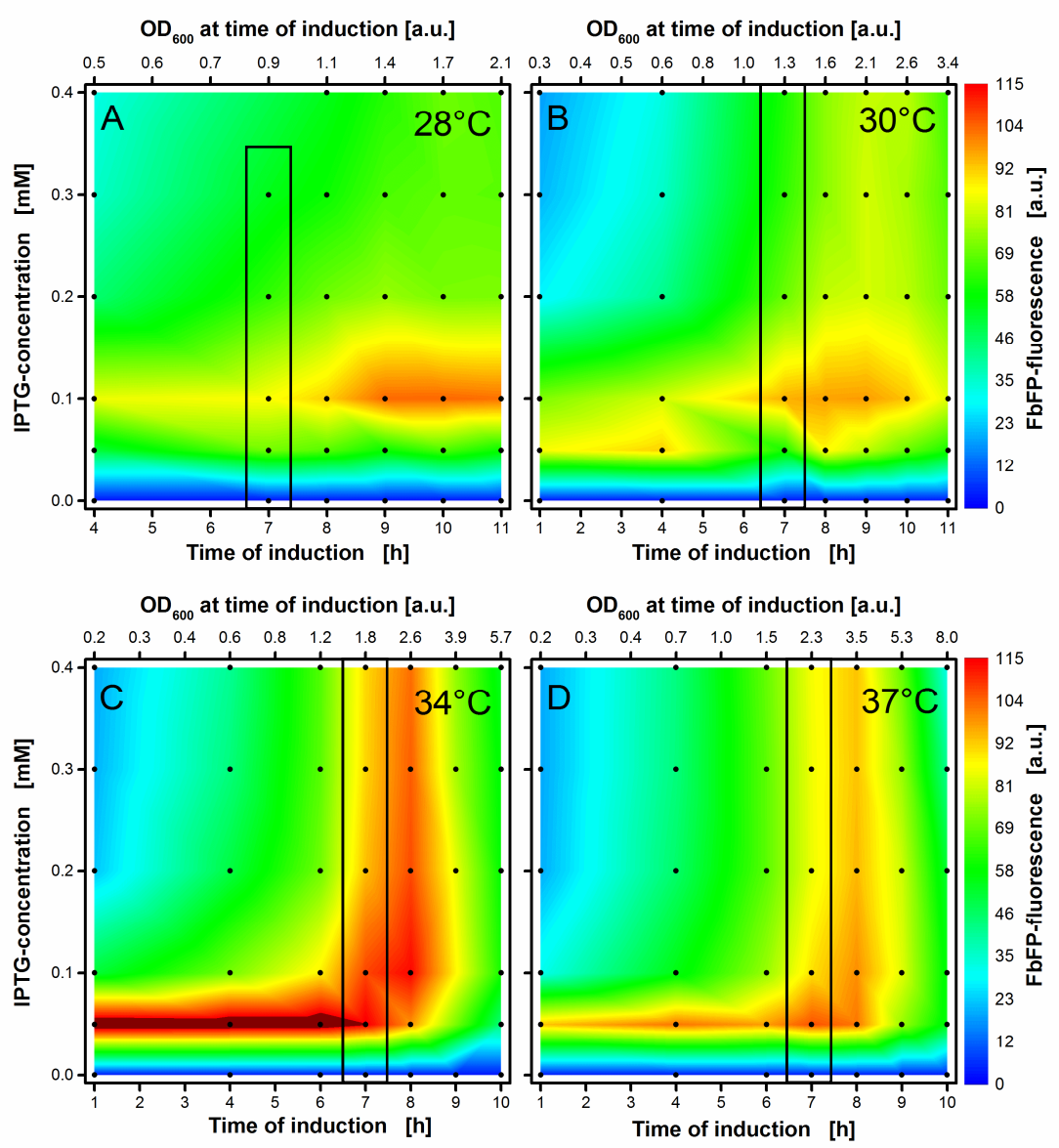

Figure 4-4: Induction profiles with automated addition of 0-0.4 mM IPTG at different temperatures. Colors from blue to red indicate maximal FbFP intensities reached at the end of each culture. Black dots indicate the 35-42 individual cultivations for each temperature. The upper x-axes reflect the corresponding optical density of the cultures at the time of induction. It is calculated from the mean scattered light values of cultures that have not been induced until the respective induction time and a calibration curve that was previously prepared (see Figure A- 7). Black boxes indicate conditions of parallel RAMOS cultivations. **A)** 28°C, induction after 4-11 h, **B)** 30°C, induction after 1–11 h, **C)** 34°C, induction after 1-10 h, **D)** 37°C, induction after 1-10 h. Cultivation conditions for *E. coli* Tuner(DE3)/pRhotHi-2-EcFbFP: Wilms-MOPS mineral medium, 48-well Flowerplate, sandwich membrane (m2p-labs), V_L = 800 µL, n = 1400 rpm, d_0 = 3 mm.

Thirdly, the optimal inducer concentration decreases with higher temperatures. This effect was already identified above (see Figure 4-3). Thus, the trend is valid for a broad range of induction conditions. While the optimal inducer concentration is 0.1 mM IPTG at 28°C, it decreases at 34°C and 37°C to 0.05 mM IPTG. A transition area is visible at 30°C, where 0.05 mM IPTG is preferable for early induction and 0.1 mM IPTG is better for later induction. The optimal inducer concentration seems to lie in between these both concentrations. Thus, this area is investigated in more detail in the next section.

Interestingly, the induction profiles are in good accordance with experiments conducted in 96-well plates (see Figure A- 4). Same trends can be identified for 30°C and 37°C. Additionally, the latter discussed effect of alternating optimal IPTG concentration is visible in the induction profile at 30°C (Figure A- 4 C). However, the absolute FbFP fluorescence intensities cannot be compared since completely different well geometries and filling volumes were used in 96-well plates.

4.5 Induction profile with low inducer concentrations

In the previous section, a switch in the optimal inducer concentration from 0.05 to 0.1 mM was detected at 30°C. It was assumed, that the real optimal inducer concentration is to be found in between those concentrations. In order to examine the optimal induction conditions at 30°C more closely, a detailed analysis of smaller inducer concentrations ranging from 0 – 0.09 mM IPTG was conducted. The results are presented in Figure 4-5.

To highlight the best induction conditions, the scale indicating the FbFP fluorescence is modified in this plot. The highest FbFP fluorescence intensity of 120 a.u. was reached by induction with 0.07 mM IPTG within the first 8 h. The best inducer concentration of 0.05 and 0.1 mM found in the upper section (see Figure 4-4 B) resulted only in a maximal fluorescence intensity of 100 a.u. Thus, already very small changes of IPTG concentration can alter the outcome, which is why the overall product formation could be further enhanced by a fine-tuning of the inducer concentration. The highest FbFP fluorescence of 125 a.u. identified in the previous section at 34°C (0.05 mM IPTG – Figure 4-4 C) can now be explained differently. Since, the product concentration is in the same range as for the improved protocol at 30°C, the assumption is obvious, that coincidently the ideal inducer concentration was met at 34°C. Probably, equal high product formation can be achieved at all temperatures in between 28°C

and 37°C when the exact individual inducer concentration in between 0 - 0.1 mM IPTG is applied.

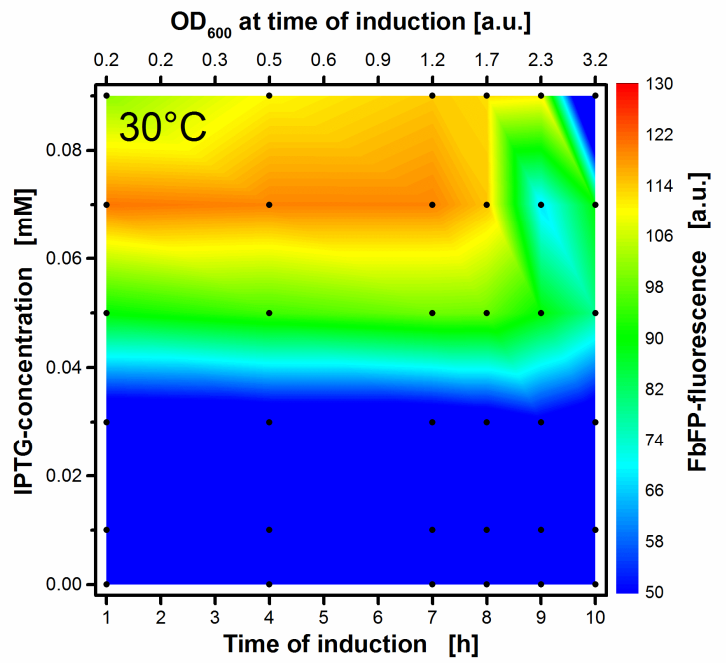

Figure 4-5: Induction profile with automated addition of 0-0.09 mM IPTG solution after 1–10 h of cultivation time. Colors from blue to red indicate maximal FbFP intensities reached at the end of each culture. Black dots indicate the 36 individual cultivations. The upper x-axis reflects the corresponding optical density of the cultures at the time of induction. It is calculated from the mean scattered light values of cultures that have not been induced until the respective induction time and a calibration curve that was previously prepared (see Figure A- 7). Cultivation conditions for *E. coli* Tuner(DE3)/pRhotHi-2-EcFbFP: Wilms-MOPS mineral medium, 48-well Flowerplate, sandwich membrane (m2p-labs), V_L = 800 µL, n = 1400 rpm, d_0 = 3 mm, 30°C.

4.6 Conclusion

Within this chapter, the ideal induction conditions for the expression of recombinant proteins as function of temperature was comprehensively investigated. Thereby, the strain *E. coli* Tuner(DE3) expressing the fluorescent protein FbFP was used as model organism. Automated induction profiles at 28°C, 30°C, 34°C and 37°C were prepared in non-oxygen limited cultures in 48-well Flowerplates using a robotic platform. The obtained results clearly illustrate major changes in induction optima at different temperatures.

In general, the following trends could be determined:

- Optimal inducer concentrations for the investigated strain are far below the conventional recommended inducer concentration of 1 mM IPTG. Best results were obtained with an IPTG concentration in between 0.05 mM – 0.1 mM for all investigated temperatures.
- The higher the temperature, the lower the optimal IPTG-concentration.
- The lower the temperature, the smaller the scope for the inducer concentration. At higher temperatures, the area for optimal induction forms a reversed "L", meaning a horizontal optimum at different induction times and a vertical optimum at different inducer concentrations. At lower temperatures, only the horizontal optimum is left. While IPTG concentrations from 0.05 to 1 mM IPTG at distinct induction times result in high product formation at 37°C, it is restricted to 0.1 mM at 28°C.

For selected induction conditions, parallel shake flask cultivations were conducted to evaluate the OTR courses. Comparable cultivation conditions in microtiter plate and shake flask were guaranteed by retaining the maximum oxygen transfer capacity (OTR_{max}) constant. Highest product formation was obtained, when the metabolic burden led to a reduced and relatively constant low breathing activity. Furthermore, this was related to a linear growth behavior (Ladner et al. 2017). When induction took place at the same biomass concentration, lower inducer concentrations resulted in similar metabolic burden, at higher temperature than higher inducer concentrations at lower temperature.

These results confirm the imperative of induction profiling. Without precise investigation of induction conditions, it is hardly possible to find optimal cultivation conditions to express high amounts of recombinant proteins. Certainly, another *E. coli* strain or another target protein can lead to completely different induction profiles, but the effect of temperature should always be considered. When comparing expression efficiencies at different temperatures, the respective optimal induction conditions have always to be used. Otherwise, the comparison is misleading.

Chapter 5

Proportionality of OTR and dScL/dt over time for *E. coli*

5.1 Transformation of scattered light curves

The cell growth of microorganisms in a batch process is described by the following differential equation:

$$\frac{dX}{dt} = \mu \cdot X \tag{5-1}$$

$\frac{dX}{dt}$ is the change in biomass (X) over time and μ is the specific growth rate. With increasing biomass during an aerobic microbial fermentation, more oxygen is consumed and, consequently, the dissolved oxygen concentration in the media declines. Simultaneously, the continuous transfer of oxygen (OTR) rises as a result of an increased oxygen concentration gradient from the gaseous ($c_{O_2}{}^*$) into the liquid phase (c_{O_2}). At typical cultivation conditions for *E. coli* (37°C, atmosphere pressure) the maximal oxygen solubility in water is 0.22 mmol/L (Wilhelm et al. 1976) (and even lower in media including salts and other dissolved ingredients). Depending on the media composition, *E. coli* reaches OUR values higher than 70 mmol/L/h (chapter 4 and Diederichs et al. 2014). Therefore, high k_La values are necessary, to supply the organisms with enough oxygen. The relation of OTR and OUR is expressed in Eq. (5-2):

$$\frac{d_{c_{O_2}}}{dt} = k_L a \cdot \left(c_{O_2}{}^* - c_{O_2}\right) - q_{O_2} \cdot X = OTR - OUR \approx 0 \tag{5-2}$$

Where $\frac{d_{c_{O_2}}}{dt}$ is the change in dissolved oxygen concentration in the culture medium, $k_L a$ the volumetric mass transfer coefficient and q_{O_2} the specific oxygen uptake rate. Within a normal

batch process, the change in dissolved oxygen is in comparison to the high OTR and OUR values negligibly low (on average for *E. coli* at 37°C ~0.02 mmol/L/h, refer to Eq. (A1-A2). Consequently, the OTR can be assumed equal to the OUR.

When assuming a culture without product formation and neglecting the cell maintenance, the OUR can also be described by the yield coefficient of biomass on oxygen (Y_{X/O_2}) (Garcia-Ochoa et al. 2010). Involving Eq. (5-2), the following equation is obtained:

$$OTR = OUR = \frac{1}{Y_{X/O_2}} \cdot \mu \cdot X \tag{5-3}$$

Eq. (5-1) can be used to replace the term $\mu \cdot X$ in Eq.(5-3). Since ScL signals derived from BioLector cultivations are proportional to the biomass concentration for *E. coli* (Kensy et al. 2009b), dX/dt is proportional to the first derivative of ScL. Therefore, it can be concluded that the OTR is proportional to the ScL derivative ($\frac{dScL}{dt}$):

$$OTR = \frac{1}{Y_{X/O_2}} \cdot \frac{dScL}{dt} \tag{5-4}$$

When assuming a constant yield coefficient Y_{X/O_2} during a cultivation, a plot of all OTR values versus dScL/dt should demonstrate a linear relationship of both parameters. Consequently, OTR and dScL/dt should change over time with a similar pattern.

For validation, simultaneous cultivations of a non-induced *E. coli* Tuner(DE3) strain in a shake flask and a 48-well Flowerplate were conducted. The OTR values were obtained by a RAMOS-device and ScL values were received from BioLector measurements (see Figure 5-1 A,B). A typical exponential increase in OTR is visible within the first 13 hours of cultivation. The supplied glucose is consumed and primarily converted into biomass. The exponential growth phase is also apparent when looking at the biomass (ScL) growth curve. As soon as the glucose is depleted (~15 h), the overflow metabolite acetate, which was formed before, is consumed (indicated by the symbol *).

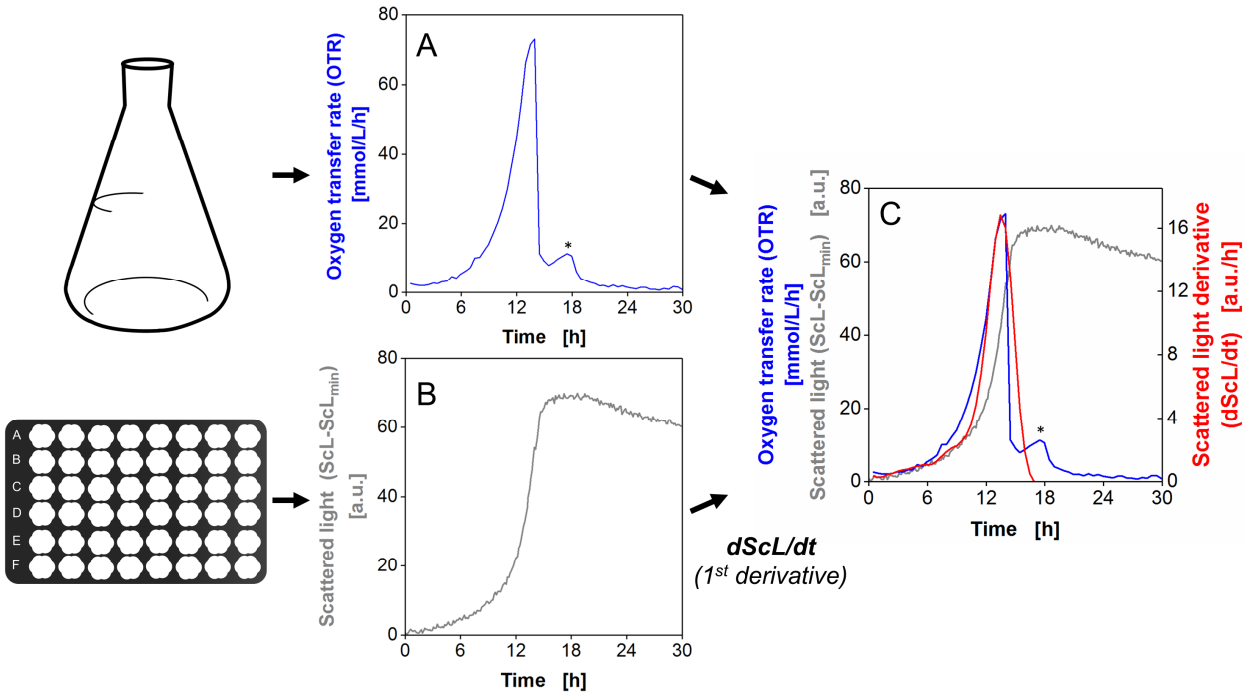

Figure 5-1: Schematic illustration of the transformation procedure of the ScL signal into its first derivative and comparison with the OTRs. OTRs (blue) were obtained from a RAMOS cultivation in a shake flask and serve as a reference (**A**). The ScL values (grey) were received from a simultaneous BioLector cultivation in a MTP (**B**). A smoothing spline of the ScL curve was produced with MATLAB and subsequently the first derivative was taken (dScL/dt, red) (**C**). The *E. coli* Tuner(DE3) FbFP cultures were derived from one *mastermix* and were started simultaneously in shake flask and MTP at 37°C in WilmsMOPS medium (20 g/L glucose) The second OTR peak describes the acetate consumption (*). Cultivation conditions for shake flasks: 250 mL flask, V_L = 8 mL n = 350 rpm, d_0 = 50 mm. Cultivation conditions for MTPs: 48-well Flowerplate, sandwich membrane (m2p-labs), V_L = 800 µL, n = 1400 rpm, d_0 = 3 mm.

The raw ScL curve was pre-processed by subtraction of the lowest intensity value at the beginning of the culture (ScL_{min}). Afterwards, a smoothing spline was created (smoothing parameter p = 0.464) and the first derivative was taken, both with a programmed tool in MATLAB (vR2016a) (screenshot of the program is illustrated in Figure A- 24). As Figure 5-1 C illustrates, the measured OTR curve is in good agreement with the scattered light derivative (dScL/dt). The inflection point of the ScL curve becomes the maximum of the dScL/dt curve after taking the derivative. The second little OTR peak coming from acetate consumption cannot be resolved with the dScL/dt curve. The acetate metabolism has low impact on biomass growth. This has already been shown in numerous investigations (Losen et al. 2004; Kunze et al. 2012; Wewetzer et al. 2015). Thus, the dScL/dt course cannot visualize any effect of acetate. However, the rising part of the large OTR peak and of the dScL/dt peak lie nearly perfectly on top of each other.

5.2 Validity of proportionality between OTR and dScL/dt also for product forming cells

Up to here, only a non-induced culture was shown to compare the OTR curve with the dScL/dt curve. Now, product formation will be considered. Consequently, Eq. (5-4) has to be extended to:

$$OTR \sim \frac{1}{Y_{X/O_2}} \cdot \frac{dScL}{dt} + \frac{1}{Y_{P/O_2}} \cdot \frac{dP}{dt} \tag{5-5}$$

The differential equation of the product formation is defined as follows:

$$\frac{dP}{dt} = q_p \cdot X \tag{5-6}$$

Where q_p is the product formation rate. The biomass concentration is replaced by Eq. (5-1), and integrated into Eq. (5-5):

$$OTR \sim \frac{dScL}{dt}\left(\frac{1}{Y_{X/O_2}} + \frac{1}{Y_{P/O_2}} \cdot \frac{q_p}{\mu}\right) \tag{5-7}$$

Assuming more or less constant yield coefficients and a constant relation of q_p and µ during the cultivation, again a proportionality between OTR and dScL/dt is obtained. However, the proportionality factor, which is represented by the terms in brackets in Eq. (5-7), will be different for altered cultivation temperature and induction conditions. This hypothesis is supported by experiments with the strain *E. coli* BL21(DE3) pET-28a(+) which expresses the cellulase celA2 after induction with IPTG. The simultaneous main cultures in shake flasks and in a 48-well Flowerplate were inoculated from an identical second preculture and were online monitored. The induction took place with different IPTG concentrations after 7 h (indicated by black arrow in Figure 5-2). As already described in chapter 4 and in by previous studies, the OTR and ScL pattern changes with increasing inducer concentration (Wandrey et al. 2016; Ladner et al. 2017). The OTR and ScL curves as well as the dScL/dt curves are plotted in Figure 5-2.

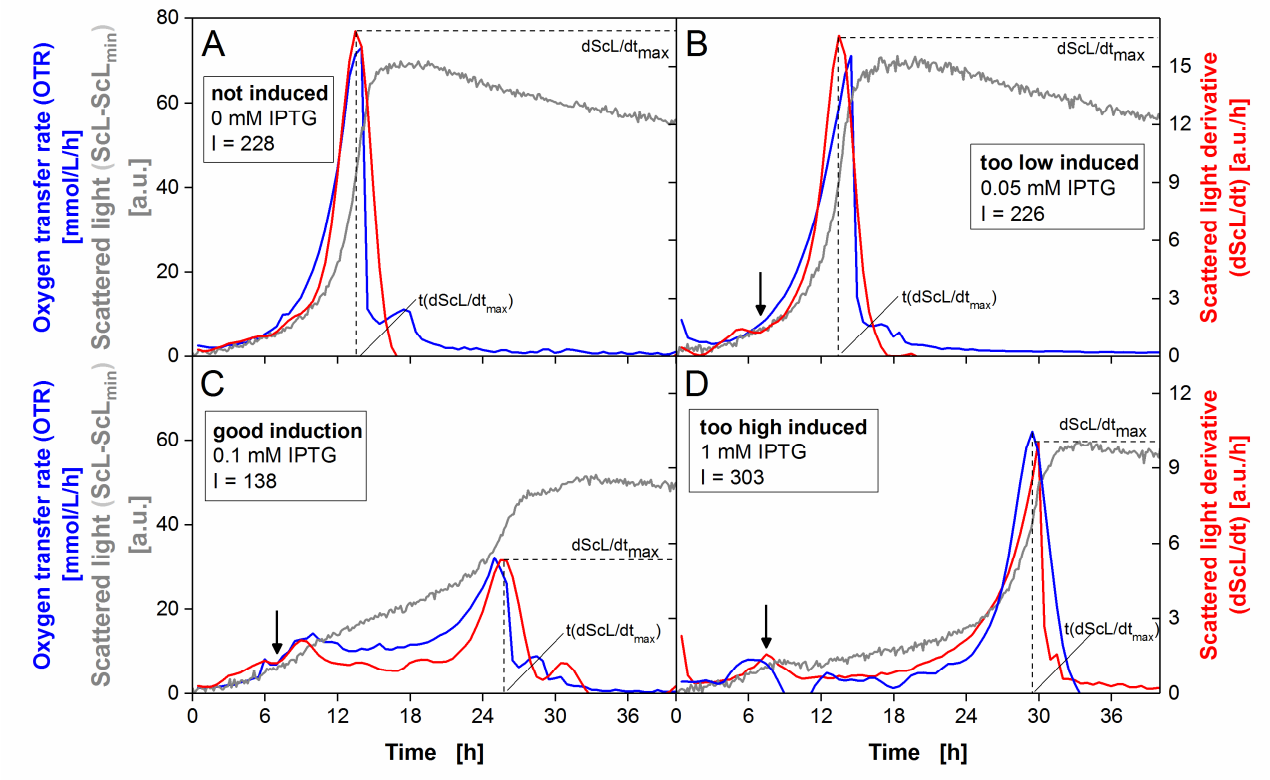

Figure 5-2: Categorization of cultures depending on OTR, ScL and dScL/dt patterns. The *E. coli* Tuner(DE3) FbFP cultures were prepared from one *mastermix* and were started simultaneously in a RAMOS and a BioLector device at 37°C in WilmsMOPS medium (20 g/L glucose). The induction with IPTG was manually performed in shake flasks and automatically with a liquid handling robot in the MTP at 7 h (black arrows). Smoothing splines of the ScL curves were produced with MATLAB and subsequently the first derivatives were taken (dScL/dt, red). The indicator values (I) were calculated according to Eq.(6-1) described later. **A)** Not induced culture, **B)** too low induced culture (0.05 mM IPTG), **C)** culture with good induction (0.1 mM IPTG), **D)** too high induced culture (1 mM IPTG). Cultivation conditions for shake flasks: 250 mL flask, V_L = 8 mL n = 350 rpm, d_0 = 50 mm. Cultivation conditions for MTPs: 48-well Flowerplate, sandwich membrane (m2p-labs), V_L = 800 µL, n = 1400 rpm, d_0 = 3 mm.

While the data of Figure 5-2 A are identical to Figure 5-1 C showing a non-induced reference, Figure 5-2 B-D represent induced cultures. At the lowest employed IPTG concentration of 0.05 mM (Figure 5-2 B) no significant change in growth rate or oxygen consumption is observed. An early high OTR and dScL/dt peak is visible, associated with an exponential biomass growth. The metabolism obviously is not impaired. It is known from previous studies, that higher growth rates are related to lower product formation (Jensen and Carlsen 1990; Bienick et al. 2014; Basan et al. 2015). Therefore, this culture is labeled as “too low induced”.

Doubling the inducer concentration to 0.1 mM IPTG (Figure 5-2 C) resulted in a complete different OTR pattern. Accordingly, the ScL curve reveals a disturbed biomass growth after induction with a long phase of linear increase (~12-20 h). This was already described as

indicative for high product formation (Ladner et al. 2017). As it is difficult for humans to quantitatively interpret variations in slopes within graphs, it is easier to have a look on the ScL derivative. Here, linear growth is depicted as a plateau. The dScL/dt curve again fits quite good to the OTR curve recorded in shake flasks. Also for a very high IPTG concentration of 1 mM (Figure 5-2 D) the dScL/dt curve matches nearly perfectly, although the pattern has changed to a single late OTR peak. The metabolism is strongly disturbed within the first 24 h of cultivation. During this time, virtually no biomass growth and OTR values below 10 mmol/L/h are detectable. Such low OTR values after induction are already described as unfavorable for product formation in chapter 4. This culture was consequently too highly induced. To obtain an impression of the change in dScL/dt courses for a whole induction profile, they are illustrated in a 3D-plot as a function of the formed product in Figure A- 10.

As mentioned in the beginning of this section, the protein formation of induced cultures exerts an additional load on metabolism of the cells. Therefore, the proportionality factor of OTR and dScL/dt changes. Thus, the y-axes of dScL/dt in Figure 5-2 A and B have a different scale than in Figure 5-2 C and D. Since the progression of OTR and dScL/dt over time are in good agreement, the proportionality factor cannot change much during the cultivation time.

The proportionality of OTR and dScL/dt was validated in many other cultivations of different *E. coli* strains. In all cases (different promoter, target protein or temperature), the proportionality was functional. An excerpt is accessible in Figure A- 8, Figure A- 9, Figure A- 12 and Figure A- 14. Furthermore, cultivations of *E. coli* Tuner expressing the FbFP protein were conducted in a BioLector device, which is combined with a µRAMOS device. This allowed the simultaneous measurement of OTR and ScL values within one microtiter plate. The µRAMOS device is constructed for 48-roundwell MTPs without baffles. To avoid oxygen limitations during the cultivation, the medium composition had to be adapted. Therefore, the glucose concentration in the Wilms-MOPS medium for the main culture was reduced to 10 g/L. The induction was performed manually after 1 or 7 h and the IPTG concentration ranged from 0 - 1 mM. Although a different device was used than for the experiments described above, which leads to completely different absolute ScL intensities, and the C-source concentration was reduced, the OTR and the first derivative of ScL still agree very well. The results of all 48 cultivations are presented in Figure A- 16.

5.3 Conclusion

The mathematical relation of OTR and the biomass during a batch cultivation was presented in this chapter. This relation was successfully applied to convert online monitored ScL signals derived from BioLector measurements (proportional to biomass concentrations) into dScL/dt for different *E. coli* BL21 variants and an *E. coli* Tuner strain. This transformation is based on taking the first derivative of ScL data. All cultivations were conducted in 48-well Flowerplates or 48-roundwell plates using Wilms-MOPS mineral medium at temperatures ranging from 28-37°C. Different dScL/dt patterns were obtained through the variation of induction conditions for all *E. coli* variants expressing either the cellulase celA2 wildtype, a celA2 mutant or the fluorescent protein FbFP. Several cultivation conditions were validated with data from shake flasks obtained from a RAMOS device. Additionally, a µRAMOS-BioLector device was used for the direct comparison of OTR values and transformed ScL values originating from the same MTP cultivation. For all investigated conditions, the proportionality between OTR and dScL/dt was proven. This allows an easy access to the physiological state of investigated microorganism solely by measurement of the biomass-related ScL signal.

Chapter 6

Prediction of the expression performance for *E. coli*

6.1 Categorization of OTR and dScL/dt curves and prediction of production performance

In the previous section, the OTR and dScL/dt curves were categorized in four groups: non-induced, too low induced, good induction and too high induced (Figure 5-2). The first two of them cannot be distinguished due to similar OTR patterns. Therefore, both groups were combined for further evaluations. The experiments illustrated in Figure 6-1 are gained from a whole induction profiling experiment including 45 cultivations of the strain *E. coli* BL21(DE3) pET-28a(+) expressing the wildtype cellulase celA2 after induction with IPTG in a 48-well Flowerplate. They differ in induction time (1-11 h) and inducer concentration (0-1 mM). The ScL derivative was created for all cultivations and could subsequently be categorized into the three described groups of OTR patterns (Figure 6-1 A**)**. The non-induced and too low induced cultures have no sign of metabolic burden, therefore, only one early dScL/dt peak is observed. The good induced cultures reveal two smaller dScL/dt peaks or a low dScL/dt plateau, thus, metabolic burden is apparent. For the too highly induced cultures, only a very late dScL/dt peak is detectable, implying a seriously affected metabolism. To be able to quantify the different cases and also predict the recombinant protein production performance, two parameters according to Ladner et al. were used (Ladner et al. 2017). While Ladner et al. categorized the expression performance according to a standardized slope at the inflection point of the ScL signal and the standardized time when the inflection point appears, in this work the dScL/dt curves were used, since the inflection point of ScL curves equals the maximum of the ScL derivative. Moreover, for simplification, no standardization procedure was used in this case.

Therefore, a product out of the dScL/dt-maximum and the time at this maximum was formed (see Eq.(6-1)). It serves as an indicator for each culture to predict the relative recombinant protein production. Both parameters are exemplarily marked in all four cases of Figure 5-2, chapter 5.

$$I = (dScL/dt)_{max} \cdot t[(dScL/dt)_{max}] \qquad (6\text{-}1)$$

The indicator value (I) was calculated for each of the 45 induction profiling experiments shown in Figure 6-1 A and was plotted against the offline determined volumetric enzyme activity of the produced cellulase celA2 in Figure 6-1 B.

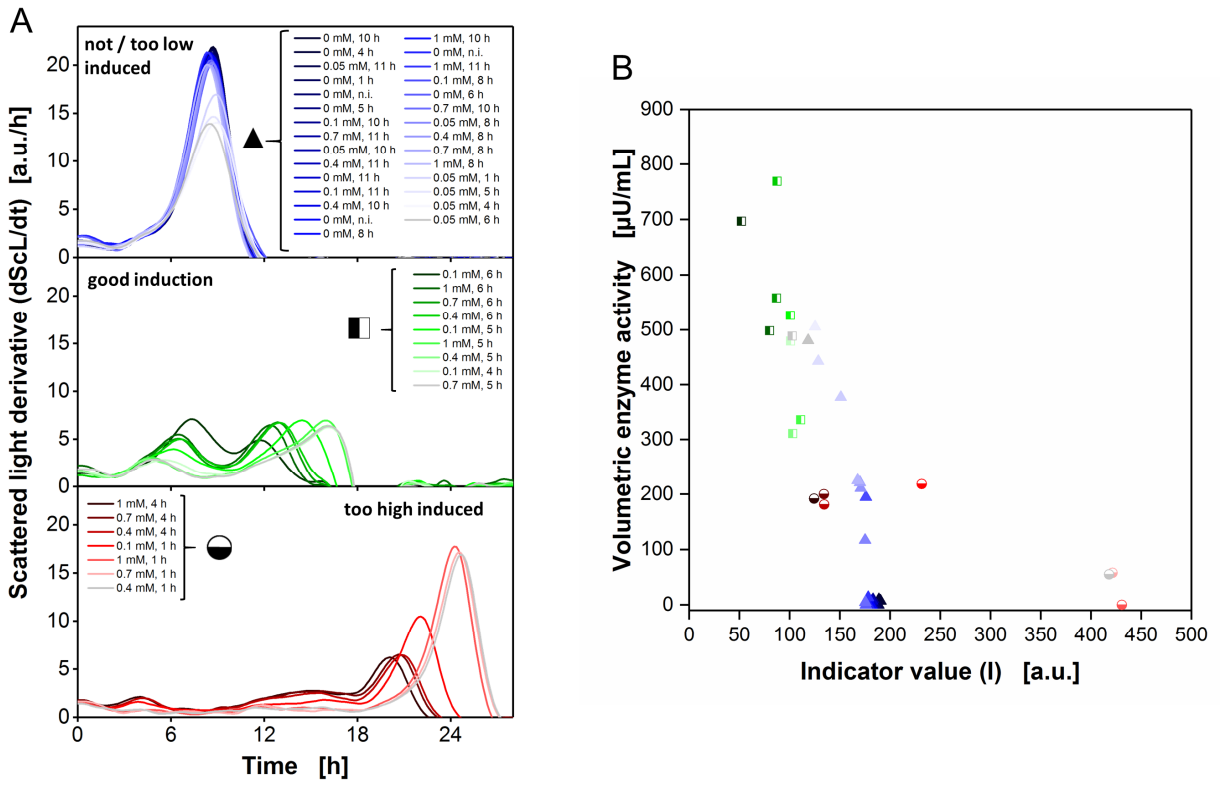

Figure 6-1: Relation of the progresses of dScL/dt over time and recombinant protein production. Results were obtained from *E. coli* BL21(DE3) pET28a(+)celA2 wildtype cultivations in one 48-well Flowerplate. The experiments were conducted automatically by the RoboLector. Smoothing splines of the ScL curves were produced with MATLAB and subsequently the first derivatives were taken (dScL/dt). The indicator values (I) were calculated according to Eq. (6-1). The respective induction time and IPTG concentration are illustrated in the graph. The color and symbol code from **A)** and **B)** is identical. **A)** The experiments were categorized according to their dScL/dt pattern into three groups, **B)** determined final volumetric enzyme activity of the expressed cellulase celA2 as function of the indicator value (I). Cultivation conditions: sandwich membrane (m2p-labs), V_L = 800 µL, n = 1400 rpm, d_0 = 3 mm, 37°C.

It is important to mention, that in this case the volumetric enzyme activity [µU/mL] is proportional to the amount of formed target protein [mg], since the enzyme specific activity [µU/mg] is identical within all experiments of one induction profiling (same heterologous protein is produced). By means of the color coding of the three groups and the symbols from Figure 6-1 A the individual cultivations and groups are represented in Figure 6-1 B. A first general trend is obvious: lower I-values describe better production performance. Many non-induced or too low induced cultures (blue, triangle) have an I-value around 180 a.u.. The dScL/dt curves exhibit only one early single high peak at around 9 h. The lower the maximum of this single peak, the lower the I-value and the higher the product formation (blue-white/grey triangle). When the dScL/dt values over time show a plateau like pattern (green, square), best results are obtained. The I-value is very low, due to a relatively early and low dScL/dt maximum (compare Figure 5-2 C, chapter 5). If the dScL/dt peak is further shifted to later time points, the I-value becomes larger (red, circle). These cultures were induced too high, thus, have to sustain stronger metabolic burden. Hence, the product formation is strongly reduced.

The same procedure was applied for two other *E. coli* BL21 variants, one expressing the same cellulase but under control of the Tac-promoter and one expressing an improved variant of the cellulase (labeled as mutant – best variant from clone screening in section 3.3.2). In addition, experiments with the *E. coli* Tuner strain expressing the fluorescent protein FbFP at different temperatures were considered. The maximum reached FbFP fluorescence intensity obtained from online measurements in MTPs was used for the evaluation of expression performance. The calculated I-values for all 405 cultivations are presented in Figure 6-2. The expressed cellulase mutant has an increased specific enzyme activity. Thus, it was necessary to use a second y-axis in Figure 6-2 A. All cultures expressing cellulases follow the previously described trend of higher expression performance at lower I-values. This is transferrable to the FbFP expressing cultures, although the data scattering is significantly higher. The non-induced and too low induced cultures producing FbFP in the diagram cluster like cultures forming celA2 around an I-value of 200 a.u.. For both diagrams, a linear and a logistic regression curve were applied to describe the splitting in two trends. The first trend ending with the non-induced cultures and the second trend ending with the too high induced cultures (high I-values).

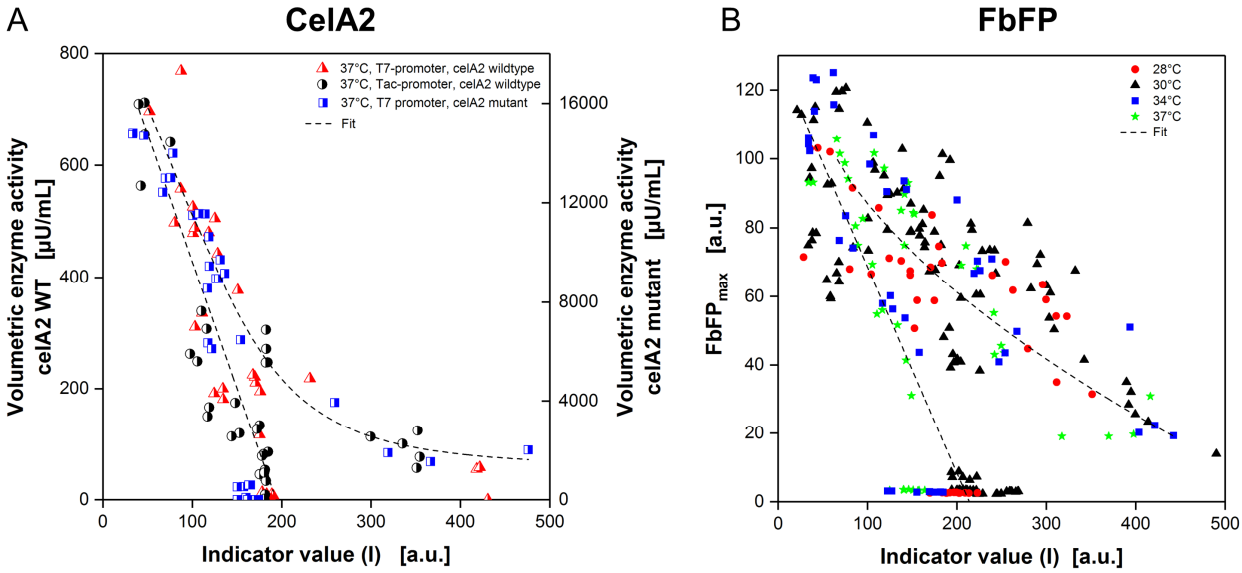

Figure 6-2: Prediction of the expression performance of strains producing the cellulase celA2 and the fluorescent protein FbFP. Results were obtained from 405 *E. coli* cultivations in 48-well Flowerplates with a BioLector device. The induction was automatically performed at 1-11 h with concentrations ranging from 0-1 mM IPTG. The indicator values (I) were calculated according to Eq. (6-1). **A)** *E. coli* BL21(DE3) pET28a(+) expressing either the cellulase wildtype or a variant under control of a T7-promoter or Tac-promoter and **B)** *E. coli* Tuner(DE3) expressing the fluorescent protein FbFP at four different temperatures. The formed protein amount was validated by the 4-MUC assay (A) or by using the maximal achieved online monitored fluorescence signal of FbFP (B). Linear and logistic fits describe the trend in both diagrams (equations are given in Table A- 1). Cultivation conditions: Wilms-MOPS mineral medium (20 g/L glucose), sandwich membrane (m2p-labs), V_L = 800 µL, n = 1400 rpm, d_0 = 3 mm, 28-37°C.

6.2 Predicted induction profiling

Results generated in induction profiling experiments are typically illustrated by colored contour plots. This enables a quick identification of the best induction time and inducer concentration. By means of the I-values according to Eq. (6-1), it is now possible to predict such a plot solely by using ScL measurements. In Figure 6-3 A the predicted induction profile of the strain *E. coli* BL21(DE3) pET-28a(+) expressing the cellulase celA2 wildtype is displayed. As I-value is inversely proportional to the recombinant protein production, the color bar is inverted in the graph. For confirmation purpose, the real volumetric enzyme activity was determined offline for each culture by the 4-MUC assay (Figure 6-3 B).

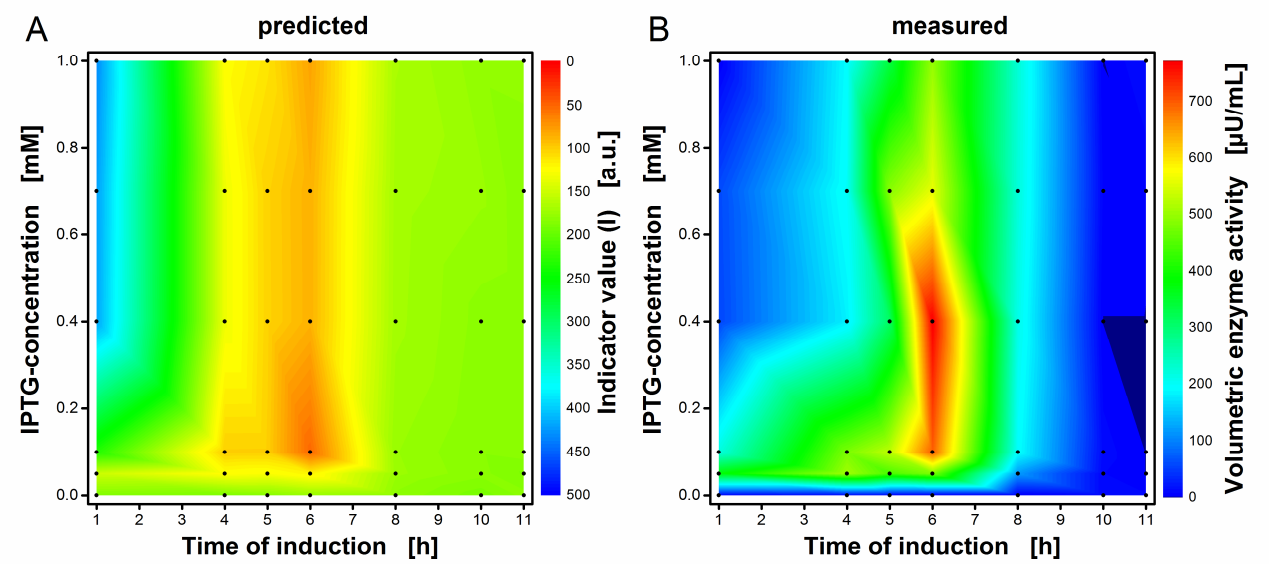

Figure 6-3: Induction profiles – predicted vs. measured data. Results were obtained from *E. coli* BL21(DE3) pET28a(+) expressing the wildtype cellulase celA2 under control of a T7-promoter. Induction profiling was conducted in a 48-well Flowerplate within a BioLector device. The induction took place automatically at 1-11 h with concentrations ranging from 0-1 mM IPTG. Black dots indicate the 42 individual cultivations. The indicator values (I) were calculated according to Eq. (6-1). **A)** A whole induction profile is predicted from dScL/dt data by the calculated indicator values (I). Since the indicator is inversely proportional to the product formation, the color code is inverted. **B)** Results of the offline conducted 4-MUC assay that was used to experimentally evaluate the volumetric enzyme activity for all induction conditions (end-point determination). Cultivation conditions: Wilms-MOPS mineral medium (20 g/L glucose), sandwich membrane (m2p-labs), V_L = 800 µL, n = 1400 rpm, d_0 = 3 mm, 37°C.

Both profiles have a very similar information content. In this case, the optimal predicted induction time to receive high product formation (red color) is 6 h. The predicted value fits perfectly to the measured optimal induction time. A fairly good agreement is also found for the inducer concentration. While the optimal IPTG concentration is predicted in between 0.1 and 1 mM, the measured data state 0.1 to 0.5 mM. This kind of comparison was also performed for the already in section 6.1 presented three other *E. coli* variants and is accessible in Figure A-11, Figure A- 13 and Figure A- 15. The optimal induction conditions could always be captured. Consequently, the predicted induction profiling is a very fast approach to narrow down reasonable induction conditions without labor intensive offline assays.

6.3 Time-resolved prediction of recombinant protein production

While the previous described prediction method (section 6.2) achieves assumptions about the final expression performance of recombinant proteins in *E. coli*, a time-resolved prediction of product formation is investigated in this section. The Eq. (5-5) can be solved for the product formation rate:

$$\frac{dP}{dt} = \frac{OTR - \frac{1}{Y_{X/O_2}} \cdot dScL/dt}{\frac{1}{Y_{P/O_2}}} \tag{6-2}$$

Integrating Eq. (6-2) reveals the product concentration (P) in dependency of the time. Thus, the product formation is calculated via the four parameters: OTR, dScL/dt, Y_{X/O_2} and Y_{P/O_2}. The OTR is monitored in the RAMOS or µRAMOS devices and dScL/dt is received by transformation of BioLector measurements. The other two yield coefficients will again be assumed constant for the whole cultivation time. Y_{X/O_2} is accessible by a non-induced reference cultivation where Eq. (5-4) is valid and can be written as:

$$\frac{1}{Y_{X/O_2}} = \frac{OTR}{dScL/dt} \tag{6-3}$$

The reciprocal of Y_{X/O_2} was determined in parity plots of dScL/dt versus OTR for non-induced cultivations in conventional RAMOS devices and simultaneous cultivations in the commercial BioLector device at 28, 30 and 37°C and is illustrated in Figure 6-4. A linear trend is apparent for all temperatures, although there are some deviations at lower OTR or dScL/dt values. The slopes of the linear fitting in Figure 6-4 represent the reciprocal yield coefficient, thus the highest yield is obtained for 30°C followed by 37°C and 28°C. This is in agreement with literature data. Shiloach and Bauer 1975 investigated the yield constant of biomass per oxygen for *E. coli* at 28°C, 31°C as well as 34°C and gained also the highest values for the middle temperature of 31°C. For further evaluations at 30°C, $\frac{1}{Y_{X/O_2}}$ was set to 4.50 which is the mean value for all cultivations at 30°C (rounded down).

The before mentioned discrepancies from the linear regression curves in Figure 6-4 may come from slight differences in the growth behavior within the independent cultivation systems and incubation chambers. Another explanation could be the disregard of cell maintenance.

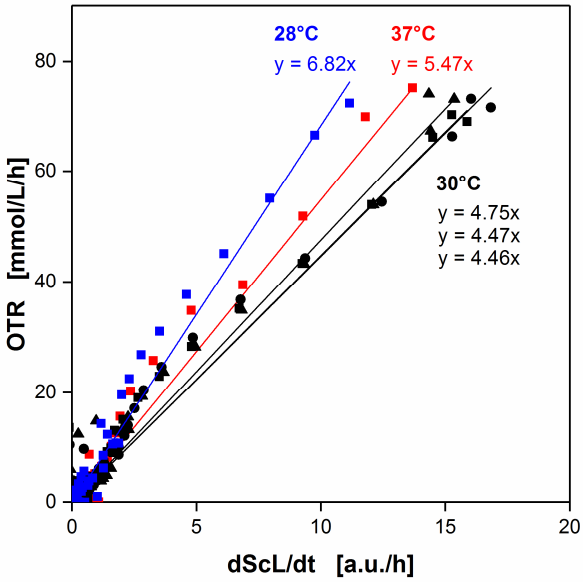

Figure 6-4: Parity plots of OTR vs. dScL/dt for non-induced *E. coli* cultures. The 5 RAMOS and BioLector cultivations were conducted for each temperature in parallel using the same *mastermix* (medium plus microorganisms). Smoothing splines of the ScL curves were produced with MATLAB and subsequently the first derivatives were taken (dScL/dt). Cultivation conditions for *E. coli* Tuner(DE3)/pRhotHi-2-EcFbFP in RAMOS device: Wilms-MOPS mineral medium, 250 mL flask, V_L = 8 mL, n = 350 rpm, d_0 = 50 mm, in BioLector device: Wilms-MOPS mineral medium, 48-well Flowerplate, sandwich membrane (m2p-labs), V_L = 800 µL, n = 1400 rpm, d_0 = 3 mm. Cultivation temperature for both devices: 28-37°C.

To accomplish a time-resolved quantitative prediction of the product formation, still the second yield constant is missing. Since this constant is dependent on the specific product and expression host, the value has to be found empirically for the first time. The strain *E. coli* Tuner(DE3) expresses the fluorescent protein FbFP, thus online product formation data are easily available by using the BioLector technology. Since $\frac{1}{Y_{P/O_2}}$ is assumed to be similar for one temperature, product and strain, it can afterwards be used for predictions without empirical determination in advance. $\frac{1}{Y_{P/O_2}}$ is obtained by using the solver-function to minimize the total sum of squares (TSS) of the difference of predicted and measured product concentration (ΔP(x)) for *m* different RAMOS and BioLector cultivations at one temperature with *n* time intervals at once (Eq. (6-4)).

$$TSS = \sum_{i=1}^{m}\sum_{j=1}^{n}\left[P(x)_{predicted} - P(x)_{measured}\right]^2 \quad (6\text{-}4)$$

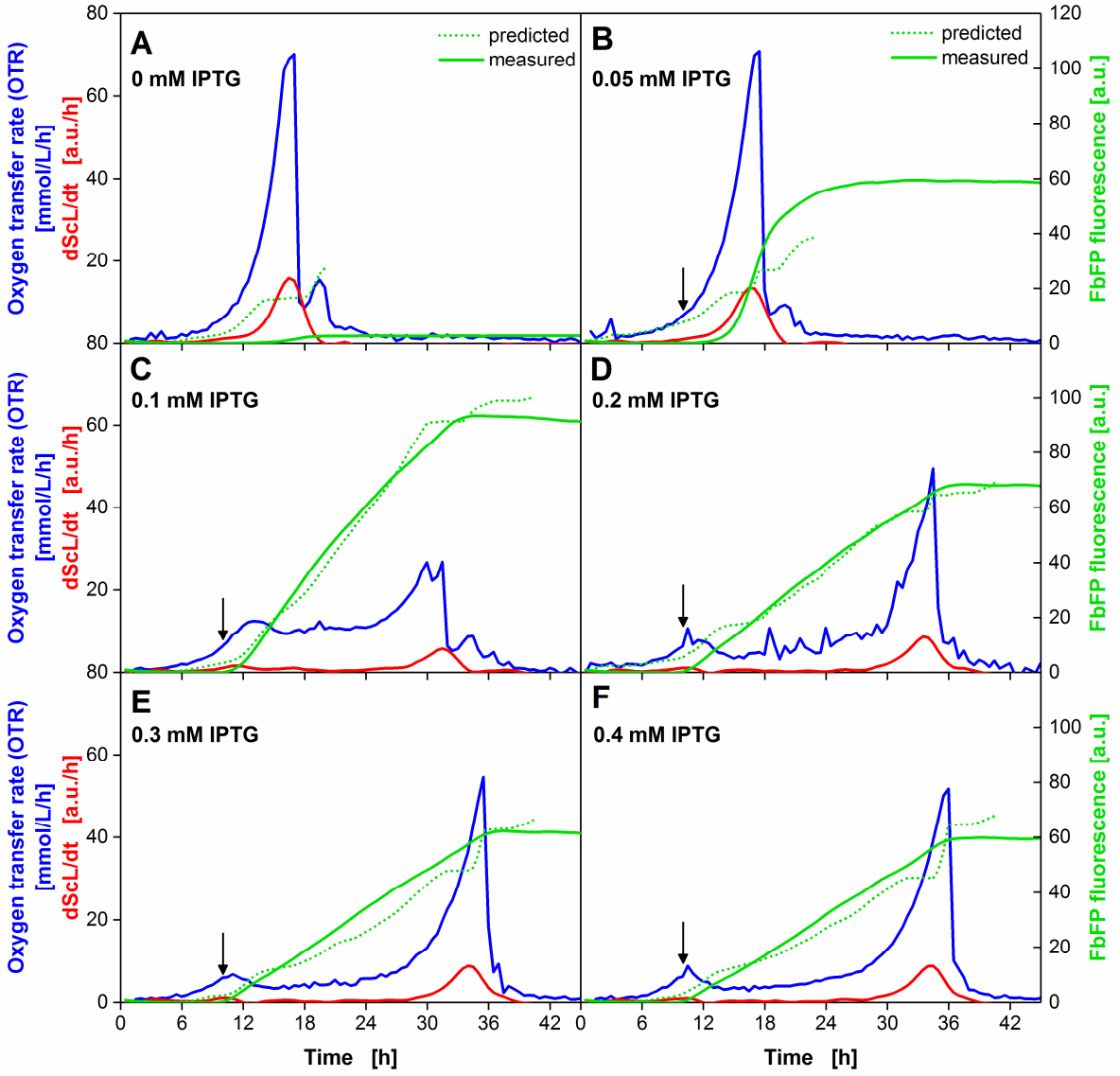

Figure 6-5: Time-resolved prediction of *E. coli* Tuner(DE3) FbFP at 30°C. Fixed parameter: $\frac{1}{Y_{X/O_2}} = 4.50$, parameter received by solver function: $\frac{1}{Y_{P/O_2}} = 1.77$. The 6 RAMOS and BioLector cultivations were conducted in parallel using the same *mastermix* (medium plus microorganisms). Smoothing splines of the ScL curves were produced with MATLAB and subsequently the first derivatives were taken (dScL/dt). Manual induction (shake flask) and automated induction (MTP) at 7 h with different inducer concentrations (0-0.4 mM IPTG). Cultivation conditions in RAMOS device: Wilms-MOPS mineral medium, 250 mL flask, V_L = 8 mL, n = 350 rpm, d_0 = 50 mm, in BioLector device: Wilms-MOPS mineral medium, 48-well Flowerplate, sandwich membrane (m2p-labs), V_L = 800 µL, n = 1400 rpm, d_0 = 3 mm.

Two constraints were made during the analysis, both the objective cell ($\frac{1}{Y_{P/O_2}}$) and the production rate from Eq. (6-2) were not allowed to be negative. The result for *E. coli* Tuner(DE3) FbFP with IPTG induction at concentrations of 0 - 0.4 mM is $\frac{1}{Y_{P/O_2}} = 1.77$.

The final predicted and fitted progresses are presented in Figure 6-5. For IPTG concentrations of at least 0.1 mM, a good agreement of the presented courses with the measured data is obtained. However, the prediction for the very low or non-induced cultures have neither the maximum FbFP fluorescence intensity nor the starting point of production with the measured data in common. Although, the here presented results reflect the adjusted progresses and absolute values in dependency of the empirically determined yield coefficient for $\frac{1}{Y_{P/O_2}}$, the qualitative trends are completely predicted.

The same analysis was conducted for other induction conditions at 30°C (Figure A- 17, Figure A- 18) as well as at 37°C (Figure A- 19) and 28°C (Figure A- 20). Some predicted progresses are not in an acceptable range, since the absolute values have strong deviations from the measured data. A summary of all used and obtained yield coefficients is illustrated in Table 6-1. All yield coefficients for the product per oxygen are roughly within the same range. However, the similarity for all experiments at 30°C is not satisfactory since identical values were expected.

Table 6-1: Overview of applied and obtained yield coefficients for the time-resolved prediction.

T [°C]	**28**	**30**	**30**	**30**	**37**
IPTG [mM]	**0 - 0.3**	**0 - 0.09**	**0 - 0.4**	**0 - 1**	**0 - 1**
$\frac{1}{Y_{X/O_2}}$ **[-]**	6.82	4.50	4.50	4.50	5.47
$\frac{1}{Y_{P/O_2}}$ **[-]**	1.39	1.41	1.77	1.84	1.66

Even though, there is a lot of room for improvement, the new prediction method serves as a first approach of a time-resolved prediction. When comparing this new technique with the previously described prediction method based solely on scattered light (section 6.1), only experiments that ran parallel in RAMOS and BioLector devices can be considered, because the

new prediction method requires both parameters (OTR and dScL/dt). Furthermore, only the predicted end-points can be evaluated, since no time-resolved results are available for the prediction presented in section 6.1. This comparison is illustrated in Figure 6-6. Although the scattering in both cases is quite large, the new method (B) allows a quantitative prediction of the final product when a determination of Y_{P/O_2} is conducted in prior.

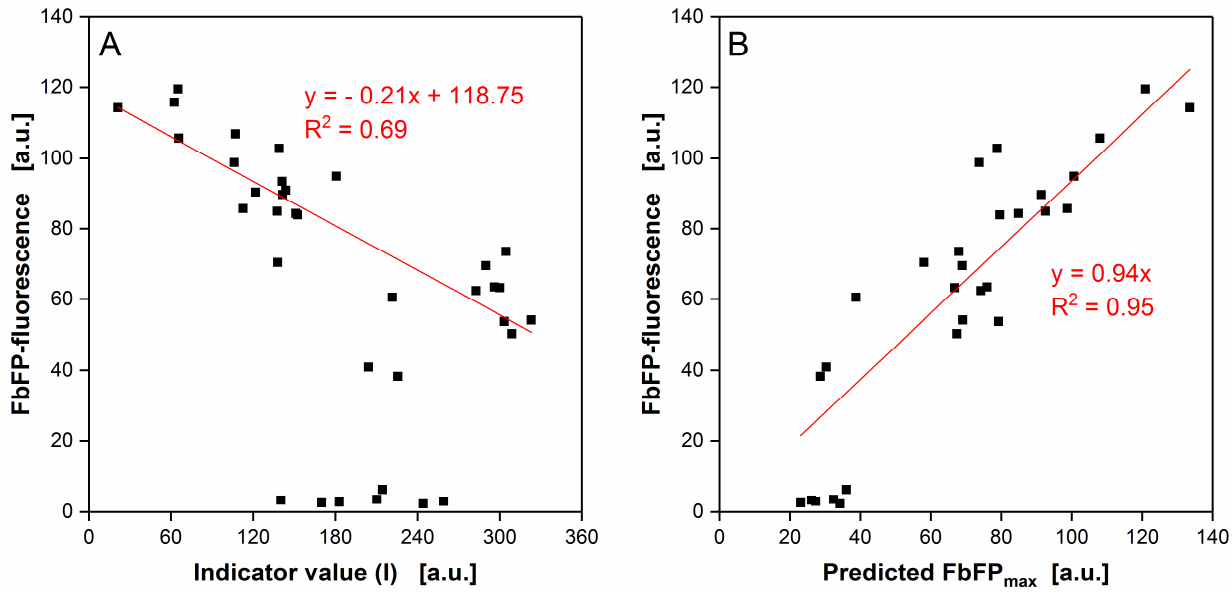

Figure 6-6: Comparison of old and new prediction method. A) Old prediction method (described in section 6.1), the indicator values (I) were calculated according to Eq. (6-1). **B)** New prediction method. For **A)** and **B)**: The 29 RAMOS and BioLector cultivations were conducted in parallel using the same *mastermix* (medium plus microorganisms). Additional 6 experiments were conducted only in the BioLector device and are considered only for the old prediction. Smoothing splines of the ScL curves were produced with MATLAB and subsequently the first derivatives were taken (dScL/dt). Manual induction (shake flask) and automated induction (MTP) at 7 h with different inducer concentrations (0-1 mM IPTG). Cultivation conditions for *E. coli* Tuner(DE3)/pRhotHi-2-EcFbFP in RAMOS device: Wilms-MOPS mineral medium, 250 mL flask, V_L = 8 mL, n = 350 rpm, d_0 = 50 mm, in BioLector device: Wilms-MOPS mineral medium, 48-well Flowerplate, sandwich membrane (m2p-labs), V_L = 800 µL, n = 1400 rpm, d_0 = 3 mm. Cultivation temperature for both devices: 28-37°C.

In order to improve the new method, some modifications were investigated. The solver function was used with two objective cells for both of the yield coefficients and a maintenance term was included (Eq.(6-5)).

$$\frac{dP}{dt} = \frac{OTR - \frac{1}{Y_{X/O_2}} \cdot dScL/dt - m_s \cdot X}{\frac{1}{Y_{P/O_2}}} \qquad (6\text{-}5)$$

However, both adaptions could not improve the outcome significantly. Absolute values still had strong deviations from the online monitored product formation. Consequently, the new prediction method has a lot of potential, but there is a need for further improvement. For the future research, a first approach could be to adapt the constraints or extend the equation with other biologically relevant terms. Integration of NADH formation might be an option.

6.4 NADH as indicator for metabolic burden

In the sections above, ScL was used as online signal to measure the biomass concentration of the culture broth in microtiter plates. It has been known for a long time, that also the fluorescence of NADH can serve as an alternative biomass signal (Duysens and Amesz 1957; Walker and Dhurjati 1989). NADH is a coenzyme abundantly available in each living cell and is involved in many redox reactions. It exists in two forms, the oxidized form NAD^+ that is reduced when it accepts electrons. The resulting oxidizing agent NADH can transfer electrons to other molecules (Figure 6-7). When cells are irradiated with ultraviolet light (λ_{ex}=365 nm), NADH is excited and the resulting maximum fluorescence signal can be detected at an emission wavelength of 450 nm (Andersson et al. 1998). On the contrary, NAD^+ is not fluorescent.

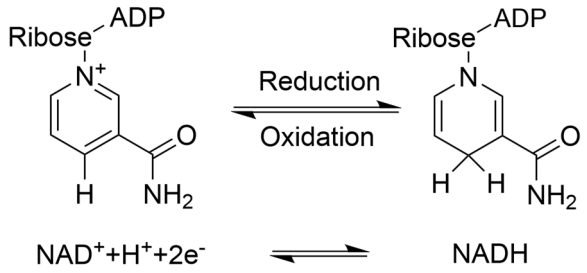

Figure 6-7: Redox balance of NADH.

The effect of recombinant protein production on NADH formation in *E. coli* BL21(DE3) and Tuner(DE3) is investigated in this section. Either the wildtype cellulase celA2 or the fluorescent protein FbFP were expressed after induction with IPTG. NADH fluorescence and ScL were detected in 48-well microtiter plates for non-induced and induced cultivations conditions. While the product formation of FbFP was monitored online, the volumetric enzyme activity of the cellulase celA2 was measured by using the 4-MUC assay at the end of each cultivation. All online measured data were pre-processed by subtracting the individual minimal value at the beginning of each cultivation. To enable a comparison of NADH and ScL, both signals were normalized by the maximum value of a non-induced (n.i.) culture and set into relation (see Eq.

(6-6)). Consequently, the ratio of both normalized signals will be exactly 1 throughout the cultivation time when NADH is equal or a multiple of ScL.

$$\left(\frac{NADH}{ScL}\right)_{norm} = \frac{\frac{NADH}{\overline{NADH(n.i.)_{max}}}}{\frac{ScL}{\overline{ScL(n.i.)_{max}}}} \tag{6-6}$$

Individually induced cultures of *E. coli* BL21(DE3) expressing the wildtype cellulase celA2 under control of the T7-promoter were classified according to their dScL/dt courses (compare chapter 5) in Figure 6-8. The non-induced and too low induced cultures are located in column one, the good induced cultures in column two and the too strong induced cultures in column three. The course of NADH for the first group looks like a typical biomass growth curve known from ScL measurements. There is no difference between the non-induced culture (black dotted line) and the other applied induction conditions. The ratio of NADH and ScL is around 1, consequently both signals reflect a typical growth curve as assumed. A very different effect is shown in group two. In comparison to the non-induced culture (black dotted line), significantly higher NADH fluorescence intensities were detected for the induced cultures. Therefore, the ratio of NADH and ScL exceeds the value of 1 by far. Higher NADH fluorescence intensities were also obtained in group three, however the trend is clearly distinguishable from group two. In all induced cases of group three, the NADH/ScL curves hold a wider peak whose maximum comes temporally at the rising part of the corresponding dScL/dt peak. These effects were reproducible also for *E. coli* BL21(DE3) expressing the wildtype cellulase celA2 under control of the Tac-promoter (Figure A- 21) and for *E. coli* Tuner(DE3) expressing FbFP at cultivation temperatures of 28°C (Figure A- 22) and 30°C (Figure A- 23).

One explanation for this phenomenon could be based on a shifted chemical equilibrium of NAD^+/NADH to NAD+ in each cell, thus lowering detectable NADH fluorescences in the whole cell broth. During the production of recombinant proteins the biomass growth was hampered and the consumption of oxygen was reduced, thus lower dScL/dt values were detected. NAD+ is regenerated from NADH within the electron transfer chain while oxygen is converted to water (Blank et al. 2010). Assuming an interference of the respiration through metabolic burden imposed by recombinant protein production, NADH would accumulate. The growth rates and the oxygen consumption of group two were low for the whole cultivation, while group three recovered at the end of the cultivation, noticeable by high dScL/dt values.

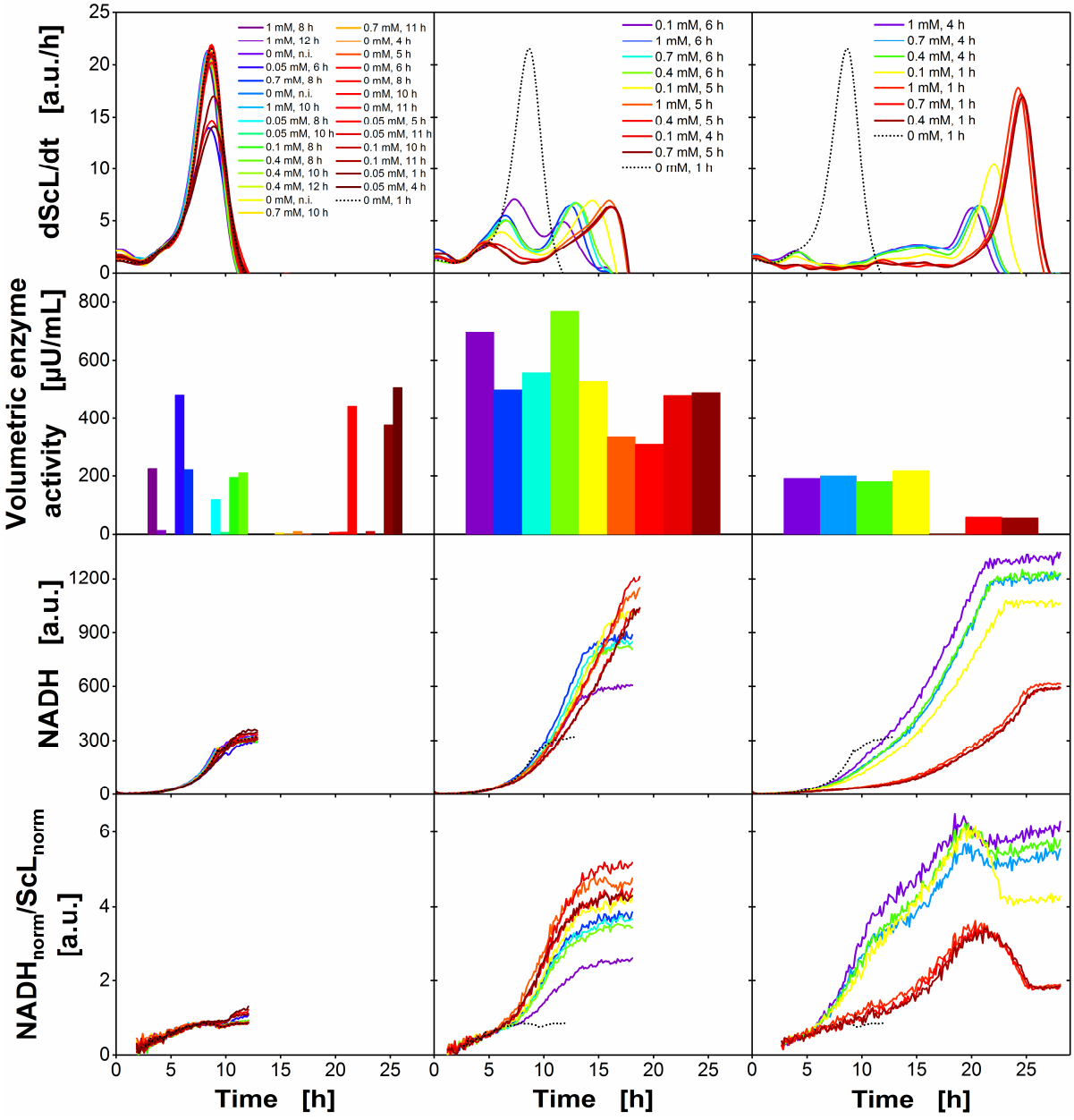

Figure 6-8: Impact of product expression on NADH formation classified in three groups. *E. coli* BL21(DE3) pET28a(+) expressing the wildtype cellulase celA2 under control of a T7-promoter. Induction profiling was conducted in a 48-well Flowerplate within a BioLector device. The induction took place automatically at 1-11 h with concentrations ranging from 0-1 mM IPTG. NADH and ScL were measured optically in the BioLector device. Smoothing splines of the ScL curves were produced with MATLAB and subsequently the first derivatives were taken (dScL/dt). The volumetric enzyme activity was determined by the 4-MUC assay (end-point determination). The ratio of NADH and ScL was calculated according to Eq. (6-6). Cultivation conditions in BioLector device: Wilms-MOPS mineral medium, 48-well Flowerplate, sandwich membrane (m2p-labs), V_L = 800 µL, n = 1400 rpm, d_0 = 3 mm, 37°C.

The electron transfer chain might work again normally during this time, which could explain the drop in the ratio of normalized NADH and ScL. The signal of single NADH seems to rise continuously during the later phase of cultivation of group three, but this is an overlay of

increased NADH due to biomass growth in the whole cell broth and equalization of the NADH/NAD^+ balance per cell (regeneration of NAD^+).

Consequently, NADH might act as an indicator for metabolic burden. Conclusions regarding product formations are rather difficult. Although there seems to be a link between the normalized ratio of NADH/ScL and product yields. Ratios slightly above 1 and without any peak seem to be an indicator for good product formation, while at ratios of 1 or below rather low product formation is expected. When the course of NADH/ScL exhibits a peak, a lot of C-source is consumed for the production of biomass after a longer phase of metabolic burden resulting mostly in lower product concentrations.

6.5 Conclusion

Two methods for the prediction of recombinant protein production performance in *E. coli* were presented in this chapter. A simpler qualitative prediction using only one online derived signal and a more complex but time-resolved prediction that requires more data. Additionally, it was demonstrated that dScL/dt and NADH courses of *E. coli* cultivations help indicating metabolic burden.

The first prediction approach is purely empirical and based on two characteristic parameters derived from transformed ScL curves (see chapter 5). Thus, an indicator value (I) was defined as the product of dScL/dt-maximum and the corresponding time. The production performance was predicted for a large variety of induction conditions for all before investigated *E. coli* strains and results were illustrated as dot plot and colored contour plot. Therewith, a direct comparison of predicted and actually achieved production performance was possible. A good estimation of optimal induction conditions without any offline assay was possible for all investigated strains and cultivation conditions.

The more mechanistic second approach allows a time-resolved prediction and was described by biological correlations. It requires the OTR as well as the dScL/dt courses of *E. coli* cultivations and their two yield coefficients of biomass/product per oxygen. While the first coefficient is accessible via the data of non-induced cultures, the yield coefficient of product per oxygen has to be estimated. The prediction was presented for selected *E. coli* Tuner(DE3) FbFP cultivations, to allow a comparison of results with online measured product formation data. The yield coefficient of product per oxygen was estimated by reduction of the total sum

of squares between the real and the predicted product formation using the solver function. The final predictions show great potential, however are not adequate for all considered cases, thus further development is necessary.

The online monitored NADH-fluorescence courses of induced *E. coli* cultivations showed an unusual trend which did not reflect the biomass growth as assumed in the beginning. To enable a comparison of the qualitative different ScL and NADH measurements, a ratio of both normalized parameters was generated. While non-induced cultures reached ratios of around 1, unexpected high ratios were obtained for induced *E. coli* cultures. A blockage of the electron transfer chain due to metabolic burden was supposed to explain the accumulation of NADH. The classification of cultivations according to the dScL/dt courses (chapter 5) was simultaneously a classification for the NADH/ScL ratios. The recovery of NADH to NAD^+ seemed to be coupled to increased growth rates. Thus, higher NADH/ScL ratios can indicate stronger metabolic burden.

Chapter 7

Conclusion and outlook

The overall objective of this thesis was to develop, extend and apply high-throughput (HT) methods on a robotic platform to screen for optimized clones and cultivation conditions in microscale to achieve high recombinant protein yields in *Escherichia coli* (*E. coli*). Therefore, the versatile RoboLector platform that combines the advantages of a liquid handling robot and the online monitoring device BioLector, was essential in each part of the work. The benefits of a liquid handling robot in high-throughput screenings (HTS) are obvious. It can reduce significantly the potential errors that come from repetitive manual tasks, saves time and allows scientists to concentrate on rational research. Therefore, its application in industry and academic research is continuously increasing.

The RoboLector proves to be a very suitable platform for the automation of several up- and downstream procedures. A modularly structured collection of automated methods was developed and can be applied depending on the respective requirements (chapter 3). Therewith, an advanced clone library screening was conducted. While HTS in drug discovery tries to find active chemical compounds against biological entities in rather short experiments, the here presented HTS is more complex, as it involves the cultivation of whole cells, the expression of recombinant proteins and the final analysis. Thus, new optimized strains and enzymes can be found and produced. The cultivation part of the screening was optimized by biomass triggered robot actions. Growth differences that can be assumed in conventional screenings, whether clones are picked from an agar plate or taken from frozen cryocultures, could be synchronized by the RoboLector. A successful and reliable screening with 46 *E. coli* variants expressing cellulases was presented. Nevertheless, the absorbance and fluorescence measurements for offline assays were still not automated due to a separate stand-alone photometer. Therefore, the

RoboLector platform has to be further extended to enable a complete automated process. To increase the throughput in future research, several approaches are conceivable. The here demonstrated procedure handles both: The preculture and the main culture in one 96-well plate. Thus only 48 different cultivations are possible to conduct in parallel. The synchronization step from the preculture into the main culture could also be realized in a new 96-well plate, resulting in twice as many cultivations. Furthermore, the robot could be combined with an extended BioLector device that is capable to measure many microtiter plates in parallel. Up to 384 cultivations would be accomplishable when the set-up presented by Wandrey et al. 2016 is used within a robotic platform. Another possibility is to combine the robot with a 2D BioLector to allow for advanced analysis like chemometrics (Ladner et al. 2016a). When oxygen limitation is known to be an issue in the production of a specific recombinant protein, two strategies can be pursued: The media can be adapted by reducing the C-source concentration or the cultivation system needs to be changed. A switch from 96-well plates to 48-well Flowerplates is suited to achieve higher oxygen transfer capacities.

A complete different approach is the screening in fed-batch mode that can avoid both, oxygen limitations and catabolite repression. This can be realized either by an automated feeding strategy of the robot (Hemmerich et al. 2014), with feeding plates (Panula-Perälä et al. 2008; Huber et al. 2009a), soluble slow release substrates (Krause et al. 2010) or a microfluidic BioLector (Funke et al. 2010; Blesken et al. 2016). However, all of these solutions bring diverse disadvantages such as numerous interruptions caused by feeding, prohibiting the measurement of optical signals through the plate bottom, restrictions to single slow release substrates or expensive single-use articles.

Apart from screening for improved variants, screening for optimal cultivation parameters can also increase the product formation. A broad study of the influencing factors - induction time, inducer concentration and temperature - on the recombinant protein production within *E. coli* was conducted (chapter 4). Induction profiling experiments have shown that optimal induction conditions can result in high product formation independent of the temperatures investigated (28°C - 37°C). Further conclusions regarding metabolic burden could be drawn by interpretation of parallel microtiter plate and shake flask cultivations. When the metabolism of the microorganism was interfered by induction with IPTG, strong effects on biomass growth and oxygen consumption could be detected. The impact on fast growing cultures was thereby much higher than for slow growing cultures.

The above-mentioned study was a comprehensive and linear investigation of three parameters. Indeed, this approach is ideally suited for detailed analysis of a small selection of factors. When thinking about more variables to be examined, the experimental effort would strongly increase, thus design of experiment (DOE) would be the method of choice. However, it can only be applied reliably when enough knowledge about the investigated biological system is available. Otherwise, wrong factors and levels will be defined or too little iterations will be conducted. Consequently, optima could be overlooked.

Nearly all raw data obtained in this thesis come from online monitored signals in small scale. The oxygen transfer rate (OTR) signal was known to be very useful for various interpretations of the microbial metabolism. Its measurement was only feasible in shake flasks of the Respiration Activity MOnitoring System (RAMOS) device or in 48-well microtiter plates of the not yet commercially available µRAMOS device. The latter is further restricted to round-well microtiter plates and is inaccessible for robot interactions. The establishment of a method that transforms the optical scattered light signal from BioLector measurements into a signal that is proportional to the OTR (first derivative of scattered light (dScL/dt), chapter 5), opened new routes for the interpretation of large data sets coming from HT experiments. Additionally, the measurement of the scattered light signal is independent of the type of a microtiter plate. The proof of concept was demonstrated for the model organism *E. coli*. The transformed BioLector data were verified by parallel OTR measurements in the RAMOS device. The feasibility study for other microorganisms is still outstanding. In particular, morphological changes during cultivations have to be considered. They could strongly interfere with the optical scattered light signal and falsify the biomass growth curve and thus the dScL/dt signal.

The transformed ScL signal served additionally as a starting point to predict the production performance in *E. coli*. Two different approaches were demonstrated in chapter 6. The first one predicts relative amounts of maximum achieved recombinant proteins and needs only two key parameters of the dScL/dt course for calculation. It is based on the changing peak maximum which is dependent on the metabolic burden that the cells experience upon induction (compare Figure A- 10). The evaluation is independent from the used BioLector device and was successfully applied for different compositions of the mineral Wilms-MOPS medium. Whether this prediction method is transferrable to other cultivation media and organisms is part of future research. The second presented approach allows for a time-resolved prediction and is based on the mathematical relation of OTR and dScL/dt. It is not yet fully developed, however predicted

product concentrations can already compete with results from the first prediction method. To realize the full potential of the method, other relevant metabolic processes have to be considered. An extension by a maintenance term seems to be apparent, however preliminary results were not promising since no improvement of the outcome could be achieved. Another starting point would be the incorporation of more parameters regarding the phenomenon of metabolic burden. OTR, ScL, NADH and temperature were analyzed in this thesis with respect to the interference of microbial metabolism caused by recombinant protein expression. However, there are many other parameters that can help to understand this process. One of them is acetate, which is known to have several negative effects on protein production (Eiteman and Altman 2006; Basan et al. 2015). The field of systems biology is becoming more and more important with increasing complexity of considered parameters. Mathematical models can then help to understand complex interactions of molecular systems (Kremling and Saez-Rodriguez 2007).

The further developed prediction method based on ScL could then be applied in prospective fully automated optimization procedures. The aim would be to achieve a biomass growth that is as linear as possible after induction, since this is known to be ideal for high recombinant protein production (Ladner et al. 2017). It could be applied within a secondary clone screening (~ 10-100 clones) where tailored optimal induction conditions will be identified and used for the final clone ranking. In all screening procedures deployed so far, equal inducer concentrations and times of induction or equal biomass concentrations at time of induction were used for each clone. However, small modifications in the gene sequence can already change optimal induction conditions for high recombinant protein production (Rahmen et al. 2015b; Rahmen et al. 2015a). In contrast to that, the tailored procedure would allow a comparison of the maximum expression performance for each clone. In this fictitious approach, the online monitored ScL data of the main cultures will be evaluated automatically with respect to the predicted production performance. As long as there is potential for improvement, new induction conditions will be determined individually by an algorithm and tested in a new run. This controlled-loop is illustrated in Figure 7-1.

Finally, it can be stated that the RoboLector platform is a versatile and powerful tool for various tasks in the bioprocess development. It was successfully extended and employed in many HT applications. Online monitoring was the prerequisite to demonstrate procedures like the advanced clone library screening, the optimization of induction conditions and to develop new

methods for the prediction of production performance in *E. coli*. The established methods can be regarded as fundamental tools for future high-quality development in small scale.

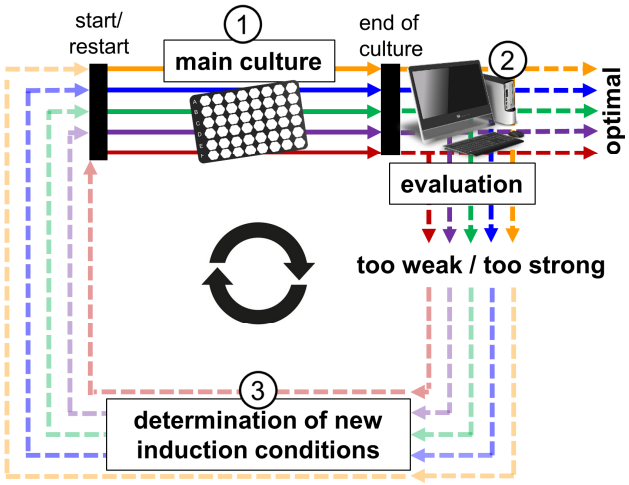

Figure 7-1: Controlled-loop for the automated optimization of recombinant protein production. Different clones will be cultivated for recombinant protein expression in a MTP (main cultivation, (1)) and obtained ScL courses will be evaluated and categorized into one of the three groups: Too weak induction, too strong induction or optimal induction (2). Subsequently, new optimized induction conditions will be determined (3) and a new cycle with new cultivations will start.

Bibliography

Anderlei T, Büchs J (2001) Device for sterile online measurement of the oxygen transfer rate in shaking flasks. Biochemical Engineering Journal 7:157–162

Anderlei T, Zang W, Papaspyrou M, Büchs J (2004) Online respiration activity measurement (OTR, CTR, RQ) in shake flasks. Biochemical Engineering Journal 17:187–194

Andersson H, Baechi T, Hoechl M, Richter C (1998) Autofluorescence of living cells. Journal of microscopy 191:1–7

Back A, Rossignol T, Krier F, Nicaud J-M, Dhulster P (2016) High-throughput fermentation screening for the yeast *Yarrowia lipolytica* with real-time monitoring of biomass and lipid production. Microbial Cell Factories 15:147

Bareither R, Pollard D (2011) A review of advanced small-scale parallel bioreactor technology for accelerated process development: current state and future need. Biotechnology progress 27:2–14

Basan M, Hui S, Okano H, Zhang Z, Shen Y, Williamson JR, Hwa T (2015) Overflow metabolism in *Escherichia coli* results from efficient proteome allocation. Nature 528:99–104

Baumann P, Hahn T, Hubbuch J (2015) High-throughput micro-scale cultivations and chromatography modeling: Powerful tools for integrated process development. Biotechnology and Bioengineering 112:2123–2133

Bentley WE, Mirjalili N, Andersen DC, Davis RH, Kompala DS (1990) Plasmid-encoded protein: The principal factor in the “metabolic burden” associated with recombinant bacteria. Biotechnology and Bioengineering 35:668–681

Berrow NS, Büssow K, Coutard B, Diprose J, Ekberg M, Folkers GE, Levy N, Lieu V, Owens RJ, Peleg Y, Pinaglia C, Quevillon-Cheruel S, Salim L, Scheich C, Vincentelli R, Busso D (2006) Recombinant protein expression and solubility screening in *Escherichia coli*: a comparative study. Acta Crystallographica Section D 62:1218–1226

Betenbaugh MJ, Beaty C, Dhurjati P (1989) Effects of plasmid amplification and recombinant gene expression on the growth kinetics of recombinant *E. coli*. Biotechnology and Bioengineering 33:1425–1436

Bhattacharya SK, Dubey AK (1995) Metabolic burden as reflected by maintenance coefficient of recombinant *Escherichia coli* overexpressing target gene. Biotechnology Letters 17:1155–1160

Bienick MS, Young KW, Klesmith JR, Detwiler EE, Tomek KJ, Whitehead TA (2014) The interrelationship between promoter strength, gene expression, and growth rate. PloS one 9:e109105

Blank LM, Ebert BE, Buehler K, Bühler B (2010) Redox Biocatalysis and Metabolism:Molecular Mechanisms and Metabolic Network Analysis. Antioxidants & Redox Signaling 13:349–394

Blesken C, Olfers T, Grimm A, Frische N (2016) The microfluidic bioreactor for a new era of bioprocess development: m2p. Engineering in Life Sciences 16:190–193

Bradford MM (1976) A rapid and sensitive method for the quantitation of microgram quantities of protein utilizing the principle of protein-dye binding. Analytical biochemistry 72:248–254

Chandel AK, Chandrasekhar G, Silva MB, Silverio da Silva S (2012) The realm of cellulases in biorefinery development. Critical reviews in biotechnology 32:187–202

Dalibor Mijaljica, Mark Prescott, Daniel J. Klionsky, Rodney J. Devenish (2007) Autophagy and vacuole homeostasis: A case for self-degradation? Autophagy 3:417–421

Davids T, Schmidt M, Bottcher D, Bornscheuer UT (2013) Strategies for the discovery and engineering of enzymes for biocatalysis. Current opinion in chemical biology 17:215–220

Decker SR, Adney WS, Jennings E, Vinzant TB, Himmel ME (2003) Automated filter paper assay for determination of cellulase activity. Applied Biochemistry and Biotechnology 107:689–703

Dellomonaco C, Fava F, Gonzalez R (2010) The path to next generation biofuels: successes and challenges in the era of synthetic biology. Microbial Cell Factories 9:1–15

Diederichs S, Korona A, Staaden A, Kroutil W, Honda K, Ohtake H, Büchs J (2014) Phenotyping the quality of complex medium components by simple online-monitored shake flask experiments. Microbial Cell Factories 13:137

Donovan RS, Robinson CW, Glick BR (1996) Review: Optimizing inducer and culture conditions for expression of foreign proteins under the control of the lac promoter. Journal of Industrial Microbiology 16:145–154

Dörr M, Fibinger MPC, Last D, Schmidt S, Santos-Aberturas J, Böttcher D, Hummel A, Vickers C, Voss M, Bornscheuer UT (2016) Fully automatized high-throughput enzyme library screening using a robotic platform. Biotechnology and Bioengineering 113:1421–1432

Dragosits M, Frascotti G, Bernard-Granger L, Vázquez F, Giuliani M, Baumann K, Rodríguez-Carmona E, Tokkanen J, Parrilli E, Wiebe MG, Kunert R, Maurer M, Gasser B, Sauer M, Branduardi P, Pakula T, Saloheimo M, Penttilä M, Ferrer P, Luisa Tutino M, Villaverde A, Porro D, Mattanovich D (2011) Influence of growth temperature on the production of antibody Fab fragments in different microbes: A host comparative analysis. Biotechnology Progress 27:38–46

Drepper T, Huber R, Heck A, Circolone F, Hillmer A-K, Büchs J, Jaeger K-E (2010) Flavin mononucleotide-based fluorescent reporter proteins outperform green fluorescent protein-like proteins as quantitative in vivo real-time reporters. Applied and Environmental Microbiology 76:5990–5994

Durrschmid K, Reischer H, Schmidt-Heck W, Hrebicek T, Guthke R, Rizzi A, Bayer K (2008) Monitoring of transcriptome and proteome profiles to investigate the cellular response of *E. coli* towards recombinant protein expression under defined chemostat conditions. Journal of Biotechnology 135:34–44

Duysens LNM, Amesz J (1957) Fluorescence spectrophotometry of reduced phosphopyridine nucleotide in intact cells in the near-ultraviolet and visible region. Biochimica et Biophysica Acta 24:19–26

Eiteman MA, Altman E (2006) Overcoming acetate in *Escherichia coli* recombinant protein fermentations. Trends in Biotechnology 24:530–536

F.William Studier, Barbara A. Moffatt (1986) Use of bacteriophage T7 RNA polymerase to direct selective high-level expression of cloned genes. Journal of Molecular Biology 189:113–130

FDA (1982) Human insulin receives FDA approval. FDA drug bulletin 12:18–19

Fiorentino G, Ripa M, Ulgiati S (2016) Chemicals from biomass: technological versus environmental feasibility. A review. Biofuels, Bioproducts and Biorefining

Flitsch D, Ladner T, Lukacs M, Büchs J (2016a) Easy to use and reliable technique for online dissolved oxygen tension measurement in shake flasks using infrared fluorescent oxygen-sensitive nanoparticles. Microbial Cell Factories 15:91

Flitsch D, Krabbe S, Ladner T, Beckers M, Schilling J, Mahr S, Conrath U, Schomburg WK, Büchs J (2016b) Respiration activity monitoring system for any individual well of a 48-well microtiter plate. Journal of Biological Engineering 10:21

Freyer SA, König M, Künkel A (2004) Validating shaking flasks as representative screening systems. Biochemical Engineering Journal 17:169–173

Funke M, Diederichs S, Kensy F, Müller C, Büchs J (2009) The baffled microtiter plate: Increased oxygen transfer and improved online monitoring in small scale fermentations. Biotechnology and Bioengineering 103:1118–1128

Funke M, Buchenauer A, Schnakenberg U, Mokwa W, Diederichs S, Mertens A, Müller C, Kensy F, Büchs J (2010) Microfluidic biolector-microfluidic bioprocess control in microtiter plates. Biotechnology and Bioengineering 107:497–505

Garcia-Ochoa F, Gomez E (2009) Bioreactor scale-up and oxygen transfer rate in microbial processes: an overview. Biotechnology advances 27:153–176

Garcia-Ochoa F, Gomez E, Santos VE, Merchuk JC (2010) Oxygen uptake rate in microbial processes: An overview. Biochemical Engineering Journal 49:289–307

Garvey M, Klose H, Fischer R, Lambertz C, Commandeur U (2013) Cellulases for biomass degradation: comparing recombinant cellulase expression platforms. Trends in Biotechnology 31:581–593

Hahn-Hagerdal B, Karhumaa K, Larsson CU, Gorwa-Grauslund M, Gorgens J, van Zyl WH (2005) Role of cultivation media in the development of yeast strains for large scale industrial use. Microbial Cell Factories 4:31

Hayes DJM (2013) Second-generation biofuels: why they are taking so long. Wiley Interdisciplinary Reviews: Energy and Environment 2:304–334

Hemmerich J, Kensy F (2014) Automated microbioreactor systems for pharmaceutical bioprocessing: profiling of seeding and induction conditions in high-throughput fermentations. Pharmaceutical Bioprocessing 2:227–235

Hemmerich J, Adelantado N, Barrigón J, Ponte X, Hörmann A, Ferrer P, Kensy F, Valero F (2014) Comprehensive clone screening and evaluation of fed-batch strategies in a microbioreactor and lab scale stirred tank bioreactor system: application on *Pichia pastoris* producing *Rhizopus oryzae* lipase. Microbial Cell Factories 13:36

Hitchman ML (1978) Measurement of dissolved oxygen. Chemical Analysis :a series of monographs on analytical chemistry and its applications, vol. 49. John Wiley & Sons, New York

Hortsch R, Weuster-Botz D (2011) Growth and recombinant protein expression with Escherichia coli in different batch cultivation media. Applied Microbiology and Biotechnology 90:69–76

Hsu W-T, Aulakh RPS, Traul DL, Yuk IH (2012) Advanced microscale bioreactor system: a representative scale-down model for bench-top bioreactors. Cytotechnology 64:667–678

Huber R, Scheidle M, Dittrich B, Klee D, Buchs J (2009a) Equalizing growth in high-throughput small scale cultivations via precultures operated in fed-batch mode. Biotechnology and Bioengineering 103:1095–1102

Huber R, Ritter D, Hering T, Hillmer A-K, Kensy F, Müller C, Wang L, Büchs J (2009b) Robo-Lector – a novel platform for automated high-throughput cultivations in microtiter plates with high information content. Microbial Cell Factories 8:42

Huber R, Palmen TG, Ryk N, Hillmer A-K, Luft K, Kensy F, Büchs J (2010) Replication methods and tools in high-throughput cultivation processes - recognizing potential variations of growth and product formation by on-line monitoring. BMC Biotechnology 10:22

Huber R, Roth S, Rahmen N, Büchs J (2011) Utilizing high-throughput experimentation to enhance specific productivity of an *E.coli* T7 expression system by phosphate limitation. BMC Biotechnology 11:22

Ilmberger N, Meske D, Juergensen J, Schulte M, Barthen P, Rabausch U, Angelov A, Mientus M, Liebl W, Schmitz RA, Streit WR (2012) Metagenomic cellulases highly tolerant towards the presence of ionic liquids--linking thermostability and halotolerance. Applied Microbiology and Biotechnology 95:135–146

Jäger V, Apati G, Konisch N (2012) Optimisation of cell growth and recombinant protein production in small-scale culture vessels by using optical sensors for on-line measurement of dissolved oxygen. In: Jenkins N, Barron N, Alves P (eds) Proceedings of the 21st Annual Meeting of the European Society for Animal Cell Technology (ESACT), Dublin, Ireland, June 7-10, 2009. Springer Netherlands, Dordrecht, pp 379–382

Jensen EB, Carlsen S (1990) Production of recombinant human growth hormone in *Escherichia coli*: expression of different precursors and physiological effects of glucose, acetate, and salts. Biotechnology and Bioengineering 36:1–11

John GT, Klimant I, Wittmann C, Heinzle E (2003) Integrated optical sensing of dissolved oxygen in microtiter plates: A novel tool for microbial cultivation. Biotechnology and Bioengineering 81:829–836

Katzke N, Arvani S, Bergmann R, Circolone F, Markert A, Svensson V, Jaeger K-E, Heck A, Drepper T (2010) A novel T7 RNA polymerase dependent expression system for high-level protein production in the phototrophic bacterium *Rhodobacter capsulatus*. Protein Expression and Purification 69:137–146

Kensy F, John GT, Hofmann B, Buchs J (2005) Characterisation of operation conditions and online monitoring of physiological culture parameters in shaken 24-well microtiter plates. Bioprocess and Biosystems Engineering 28:75–81

Kensy F, Engelbrecht C, Büchs J (2009a) Scale-up from microtiter plate to laboratory fermenter: evaluation by online monitoring techniques of growth and protein expression in *Escherichia coli* and *Hansenula polymorpha* fermentations. Microbial Cell Factories 8:68

Kensy F, Zang E, Faulhammer C, Tan R-K, Büchs J (2009b) Validation of a high-throughput fermentation system based on online monitoring of biomass and fluorescence in continuously shaken microtiter plates. Microbial Cell Factories 8:31

Knepper A, Heiser M, Glauche F, Neubauer P (2014) Robotic platform for parallelized cultivation and monitoring of microbial growth parameters in microwell plates. Journal of Laboratory Automation 19:593–601

Koepff J, Keller M, Tsolis KC, Busche T, Rückert C, Hamed MB, Anné J, Kalinowski J, Wiechert W, Economou A, Oldiges M (2017) Fast and reliable strain characterization of *Streptomyces lividans* through micro-scale cultivation. Biotechnology and Bioengineering 114:2011–2022

Krause M, Ukkonen K, Haataja T, Ruottinen M, Glumoff T, Neubauer A, Neubauer P, Vasala A (2010) A novel fed-batch based cultivation method provides high cell-density and improves yield of soluble recombinant proteins in shaken cultures. Microbial Cell Factories 9:11

Kremling A, Saez-Rodriguez J (2007) Systems biology--an engineering perspective. Journal of Biotechnology 129:329–351

Kunze M, Huber R, Gutjahr C, Müllner S, Büchs J (2012) Predictive tool for recombinant protein production in *Escherichia coli* Shake-Flask cultures using an on-line monitoring system. Biotechnology Progress 28:103–113

Kunze M, Lattermann C, Diederichs S, Kroutil W, Büchs J (2014) Minireactor-based high-throughput temperature profiling for the optimization of microbial and enzymatic processes. Journal of Biological Engineering 8:22

Ladd Effio C, Baumann P, Weigel C, Vormittag P, Middelberg A, Hubbuch J (2016) High-throughput process development of an alternative platform for the production of virus-like particles in *Escherichia coli*. Journal of Biotechnology 219:7–19

Ladner T, Flitsch D, Schlepütz T, Büchs J (2015) Online monitoring of dissolved oxygen tension in microtiter plates based on infrared fluorescent oxygen-sensitive nanoparticles. Microbial Cell Factories 14:161

Ladner T, Beckers M, Hitzmann B, Büchs J (2016a) Parallel online multi-wavelength (2D) fluorescence spectroscopy in each well of a continuously shaken microtiter plate. Biotechnology Journal 11:1605–1616

Ladner T, Held M, Flitsch D, Beckers M, Büchs J (2016b) Quasi-continuous parallel online scattered light, fluorescence and dissolved oxygen tension measurement combined with monitoring of the oxygen transfer rate in each well of a shaken microtiter plate. Microbial Cell Factories 15:206

Ladner T, Mühlmann M, Schulte A, Wandrey G, Büchs J (2017) Prediction of *Escherichia coli* expression performance in microtiter plates by analyzing only the temporal development of scattered light during culture. Journal of Biological Engineering 11:20

Lan Tee K, Schwaneberg U (2007) Directed evolution of oxygenases: screening systems, success stories and challenges. Combinatorial chemistry & high throughput screening 10:197–217

Lara AR, Jaén KE, Sigala J-C, Mühlmann M, Regestein L, Büchs J (2017) Characterization of Endogenous and Reduced Promoters for Oxygen-Limited Processes Using *Escherichia coli*. ACS synthetic biology 6:344–356

Lehmann C, Sibilla F, Maugeri Z, Streit WR, Domínguez de María P, Martinez R, Schwaneberg U (2012) Reengineering CelA2 cellulase for hydrolysis in aqueous solutions of deep eutectic solvents and concentrated seawater. Green Chemistry 14:2719

Lesley SA (2001) High-throughput proteomics: Protein expression and purification in the postgenomic world. Protein Expression and Purification 22:159–164

Losen M, Frölich B, Pohl M, Büchs J (2004) Effect of oxygen limitation and medium composition on *Escherichia coli* fermentation in shake-flask cultures. Biotechnology progress 20:1062–1068

Maier U, Büchs J (2001) Characterisation of the gas–liquid mass transfer in shaking bioreactors. Biochemical Engineering Journal 7:99–106

Marbach A, Bettenbrock K (2012) lac operon induction in *Escherichia coli*: Systematic comparison of IPTG and TMG induction and influence of the transacetylase LacA. Journal of Biotechnology 157:82–88

Marini G, Luchese MD, Argondizzo APC, de Goes, Ana Carolina Magalhaes Andrade, Galler R, Alves TLM, Medeiros MA, Larentis AL (2014) Experimental design approach in recombinant protein expression: determining medium composition and induction conditions for expression of pneumolysin from Streptococcus pneumoniae in *Escherichia coli* and preliminary purification process. BMC Biotechnology 14:1

Marques MPC, Cabral JMS, Fernandes P (2010) Bioprocess scale-up: quest for the parameters to be used as criterion to move from microreactors to lab-scale. Journal of Chemical Technology & Biotechnology 85:1184–1198

Meier K, Klöckner W, Bonhage B, Antonov E, Regestein L, Büchs J (2016) Correlation for the maximum oxygen transfer capacity in shake flasks for a wide range of operating conditions and for different culture media. Biochemical Engineering Journal 109:228–235

Meng J, Walter J-G, Kökpinar Ö, Stahl F, Scheper T (2008) Automated Microscale His-tagged Protein Purification Using Ni-NTA Magnetic Agarose Beads. Chemical Engineering & Technology 31:463–468

Miao F, Kompala DS (1992) Overexpression of cloned genes using recombinant *Escherichia coli* regulated by a T7 promoter: I. Batch cultures and kinetic modeling. Biotechnology and Bioengineering 40:787–796

Morowvat MH, Babaeipour V, Rajabi Memari H, Vahidi H (2014) Optimization of fermentation conditions for recombinant human interferon beta production by *Escherichia coli* using the response surface Methodology. Jundishapur Journal of Microbiology 8:e16236

Mühlmann M, Büchs J (2018) Automatisiertes Klonscreening und Vorhersage der Expressionsleistung. BioSpektrum 24:46–49

Mühlmann M, Kunze M, Ribeiro J, Geinitz B, Lehmann C, Schwaneberg U, Commandeur U, Büchs J (2017a) Cellulolytic RoboLector - towards an automated high-throughput screening platform for recombinant cellulase expression. Journal of Biological Engineering 11:1

Mühlmann M, Forsten E, Noack S, Büchs J (2017b) Optimizing recombinant protein expression via automated induction profiling in microtiter plates at different temperatures. Microbial Cell Factories 16:220

Navarro D, Couturier M, da Silva G, Berrin J-G, Rouau X, Asther M, Bignon C (2010) Automated assay for screening the enzymatic release of reducing sugars from micronized biomass. Microbial Cell Factories 9:58

Panula-Perälä J, Siurkus J, Vasala A, Wilmanowski R, Casteleijn MG, Neubauer P (2008) Enzyme controlled glucose auto-delivery for high cell density cultivations in microplates and shake flasks. Microbial Cell Factories 7:31

Percival Zhang Y-H, Himmel ME, Mielenz JR (2006) Outlook for cellulase improvement: screening and selection strategies. Biotechnology advances 24:452–481

Peter CP, Lotter S, Maier U, Büchs J (2004) Impact of out-of-phase conditions on screening results in shaking flask experiments. Biochemical Engineering Journal 17:205–215

Ragauskas AJ, Williams CK, Davison BH, Britovsek G, Cairney J, Eckert CA, Frederick WJ, Hallett JP, Leak DJ, Liotta CL, Mielenz JR, Murphy R, Templer R, Tschaplinski T (2006) The path forward for biofuels and biomaterials. Science 311:484–489

Rahmen N, Schlupp CD, Mitsunaga H, Fulton A, Aryani T, Esch L, Schaffrath U, Fukuzaki E, Jaeger K-E, Büchs J (2015a) A particular silent codon exchange in a recombinant gene greatly influences host cell metabolic activity. Microbial Cell Factories 14:15

Rahmen N, Fulton A, Ihling N, Magni M, Jaeger K-E, Büchs J (2015b) Exchange of single amino acids at different positions of a recombinant protein affects metabolic burden in *Escherichia coli*. Microbial Cell Factories 14:10

Rischbieter E, Schumpe A (1996) Gas solubilities in aqueous solutions of organic substances

Rohe P, Venkanna D, Kleine B, Freudl R, Oldiges M (2012) An automated workflow for enhancing microbial bioprocess optimization on a novel microbioreactor platform. Microbial Cell Factories 11:144

Rosano G¡nL, Ceccarelli EA (2014) Recombinant protein expression in *Escherichia coli*: advances and challenges. Frontiers in Microbiology 5:116

Samorski M, Müller-Newen G, Büchs J (2005) Quasi-continuous combined scattered light and fluorescence measurements: A novel measurement technique for shaken microtiter plates. Biotechnology and Bioengineering 92:61–68

Sanchez-Garcia L, Martin L, Mangues R, Ferrer-Miralles N, Vazquez E, Villaverde A (2016) Recombinant pharmaceuticals from microbial cells: a 2015 update. Microbial Cell Factories 15:33

Santos-Aberturas J, Dörr M, Waldo GS, Bornscheuer UT (2015) In-depth high-throughput screening of protein engineering libraries by split-GFP direct crude cell extract data normalization. Chemistry & Biology 22:1406–1414

Sarder P, Maji D, Achilefu S (2015) Molecular probes for fluorescence lifetime imaging. Bioconjugate Chemistry 26:963–974

Scheich C, Sievert V, Büssow K (2003) An automated method for high-throughput protein purification applied to a comparison of His-tag and GST-tag affinity. BMC Biotechnology 3:1–8

Schein CH, Noteborn MHM (1988) Formation of soluble recombinant proteins in *Escherichia coli* is favored by lower growth temperature. Nat Biotech 6:291–294

Sharma B, Ingalls RG, Jones CL, Khanchi A (2013) Biomass supply chain design and analysis: Basis, overview, modeling, challenges, and future. Renewable and Sustainable Energy Reviews 24:608–627

Shiloach J, Bauer S (1975) High-yield growth of *E. coli* at different temperatures in a bench scale fermentor. Biotechnology and Bioengineering 17:227–239

Sieben M, Giese H, Grosch J-H, Kauffmann K, Buchs J (2016) Permeability of currently available microtiter plate sealing tapes fail to fulfil the requirements for aerobic microbial cultivation. Biotechnology Journal

Siepert E-M, Gartz E, Tur MK, Delbrück H, Barth S, Büchs J (2012) Short-chain fluorescent tryptophan tags for on-line detection of functional recombinant proteins. BMC Biotechnology 12:65

Studier FW, Moffatt BA (1986) Use of bacteriophage T7 RNA polymerase to direct selective high-level expression of cloned genes. Journal of Molecular Biology 189:113–130

Suresh S, Srivastava VC, Im Mishra (2009) Techniques for oxygen transfer measurement in bioreactors: A review. Journal of Chemical Technology & Biotechnology 84:1091–1103

Tartof KD, Hobbs CA (1987) Improved media for growing plasmid and cosmid clones. Bethesda Research Laboratories Focus 9:12

Terpe K (2006) Overview of bacterial expression systems for heterologous protein production: from molecular and biochemical fundamentals to commercial systems. Applied Microbiology and Biotechnology 72:211

Tolosa L, Kostov Y, Harms P, Rao G (2002) Noninvasive measurement of dissolved oxygen in shake flasks. Biotechnology and Bioengineering 80:594–597

Unthan S, Radek A, Wiechert W, Oldiges M, Noack S (2015) Bioprocess automation on a Mini Pilot Plant enables fast quantitative microbial phenotyping. Microbial Cell Factories 14:32

Vera A, González-Montalbán N, Arís A, Villaverde A (2007) The conformational quality of insoluble recombinant proteins is enhanced at low growth temperatures. Biotechnology and Bioengineering 96:1101–1106

Walker CC, Dhurjati P (1989) Use of culture fluorescence as a sensor for on-line discrimination of host and overproducing recombinant Escherichia coli. Biotechnology and Bioengineering 33:500–505

Wandrey G, Bier C, Binder D, Hoffmann K, Jaeger K-E, Pietruszka J, Drepper T, Büchs J (2016) Light-induced gene expression with photocaged IPTG for induction profiling in a high-throughput screening system. Microbial Cell Factories 15:145

Wang W, Malcolm BA (1999) Two-stage PCR protocol allowing introduction of multiple mutations, deletions and insertions using QuikChange Site-Directed Mutagenesis. Biotechniques 26:680–682

Wang M, Si T, Zhao H (2012) Biocatalyst development by directed evolution. Bioresource technology 115:117–125

Weuster-Botz D, Puskeiler R, Kusterer A, Kaufmann K, John GT, Arnold M (2005) Methods and milliliter scale devices for high-throughput bioprocess design. Bioprocess and Biosystems Engineering 28:109–119

Wewetzer S, Kunze M, Ladner T, Luchterhand B, Roth S, Rahmen N, Kloß R, Costa e Silva A, Regestein L, Büchs J (2015) Parallel use of shake flask and microtiter plate online measuring devices (RAMOS and BioLector) reduces the number of experiments in laboratory-scale stirred tank bioreactors. Journal of Biological Engineering 9:2

Wilhelm E, Battino R, Wilcock R (1976) Low pressure solubility of gases. Chemical Reviews 77:219–262

Wilms B, Hauck A, Reuss M, Syldatk C, Mattes R, Siemann M, Altenbuchner J (2001) High-cell-density fermentation for production of L-N-carbamoylase using an expression system based on the *Escherichia coli* rhaBAD promoter. Biotechnology and Bioengineering 73:95–103

Yang J, Ruff AJ, Hamer SN, Cheng F, Schwaneberg U (2016) Screening through the PLICable promoter toolbox enhances protein production in *Escherichia coli*. Biotechnology Journal 11:1639–1647

Zimmermann HF, Anderlei T, Büchs J, Binder M (2006) Oxygen limitation is a pitfall during screening for industrial strains. Applied Microbiology and Biotechnology 72:1157–1160

Appendix

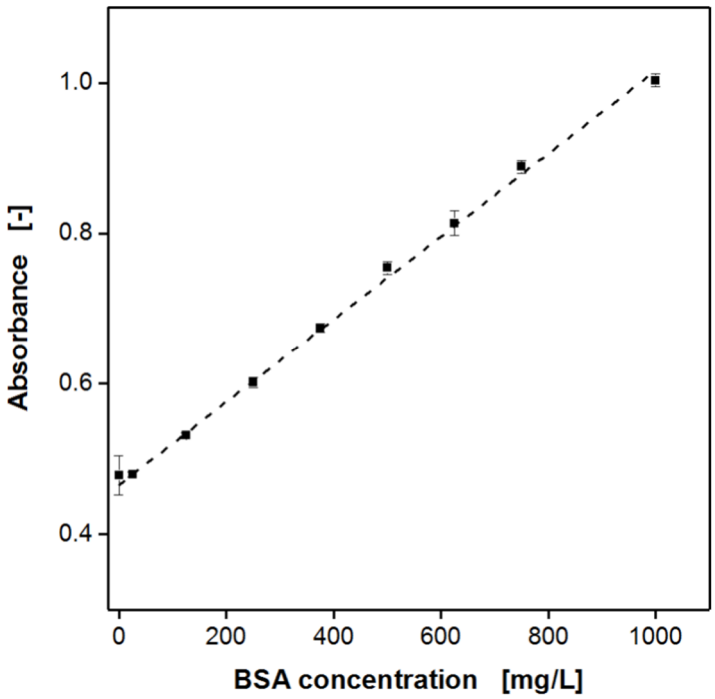

Figure A- 1: Calibration curve for Bradford-assay.

Triplicate determination of each BSA concentration with standard deviation in between of 0.4 – 2.6%. Linear regression curve: $y = 0.0005x + 0.471$ ($R^2 = 0.998$). Assay conditions: automated serial dilution of BSA stock solution (1 g/L) by the RoboLector from a reservoir plate standing on the platform, 96-well plate, V_L = 260 µL (10 µL sample + 250 µL Bradford reagent), 10 min incubation time, n = 800 rpm, final absorbance measurement at 595 nm, RT.

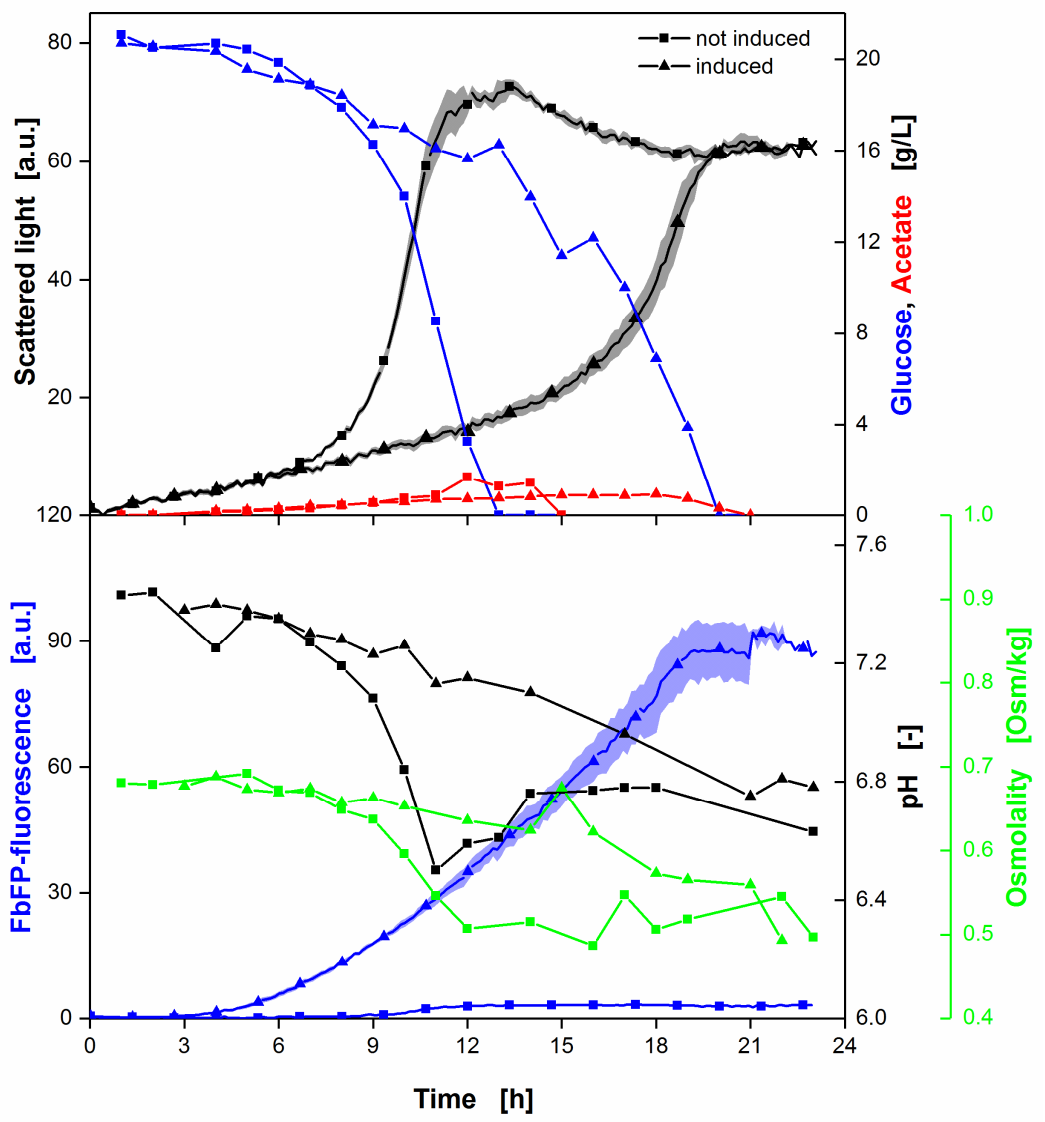

Figure A- 2: **Online and offline analytics of *E. coli* Tuner(DE3) FbFP in an automated sampling experiment.** Half of the 48 samples were induced with 0.05 mM IPTG at start of the cultivation. Standard deviations were calculated for ScL and FbFP from all wells that were not sampled up to the respective time (shaded areas). Sampling procedure: two wells (not-induced and induced) were sacrificed every hour by sampling 200 µL culture broth, respectively and storing them in a 96-well MTP sealed with X-pierce film on the cooling carrier. Offline measurement of glucose and acetate via HPLC after sterile filtration. pH and osmolality were measured offline when sufficient volume was left. Cultivation conditions: Wilms-MOPS mineral medium, 48-well Flowerplate, sandwich membrane (m2p-labs), V_L = 800 µL, n = 1400 rpm, d_0 = 3 mm, 37°C.

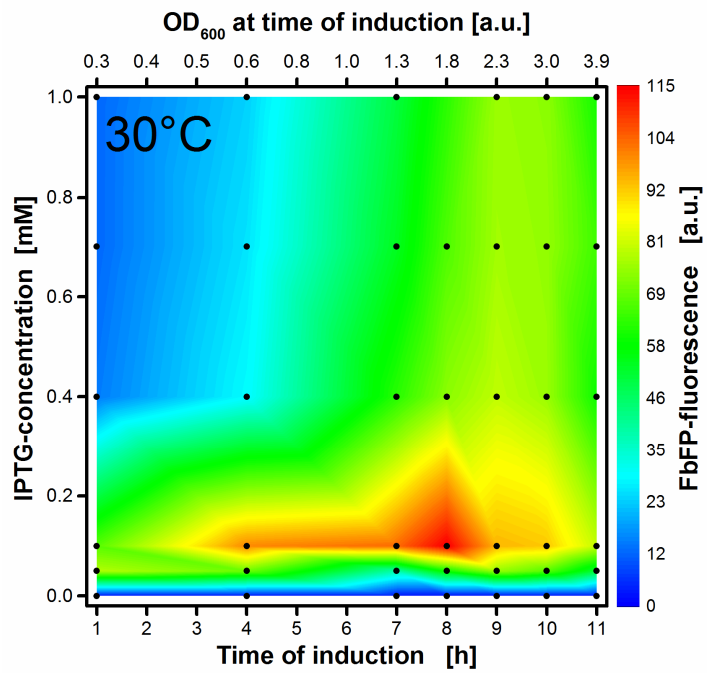

Figure A- 3: **Induction profile with automated addition of 0 - 1 mM IPTG solution after 1 - 10 h of cultivation time at 30°C.** Colors from blue to red indicate maximal reached FbFP intensities at the end of each cultivation. Black dots indicate the 36 individual cultivations. The upper x-axis reflects the corresponding optical density of the cultures at the time of induction. It is calculated from the mean scattered light values of the cultures that have not been induced until the respective induction time and a calibration curve that was previously prepared (see Figure A- 7). Cultivation conditions for *E. coli* Tuner(DE3)/pRhotHi-2-EcFbFP: Wilms-MOPS mineral medium, 48-well Flowerplate, sandwich membrane (m2p-labs), V_L = 800 µL, n = 1400 rpm, d_0 = 3 mm, 30°C.

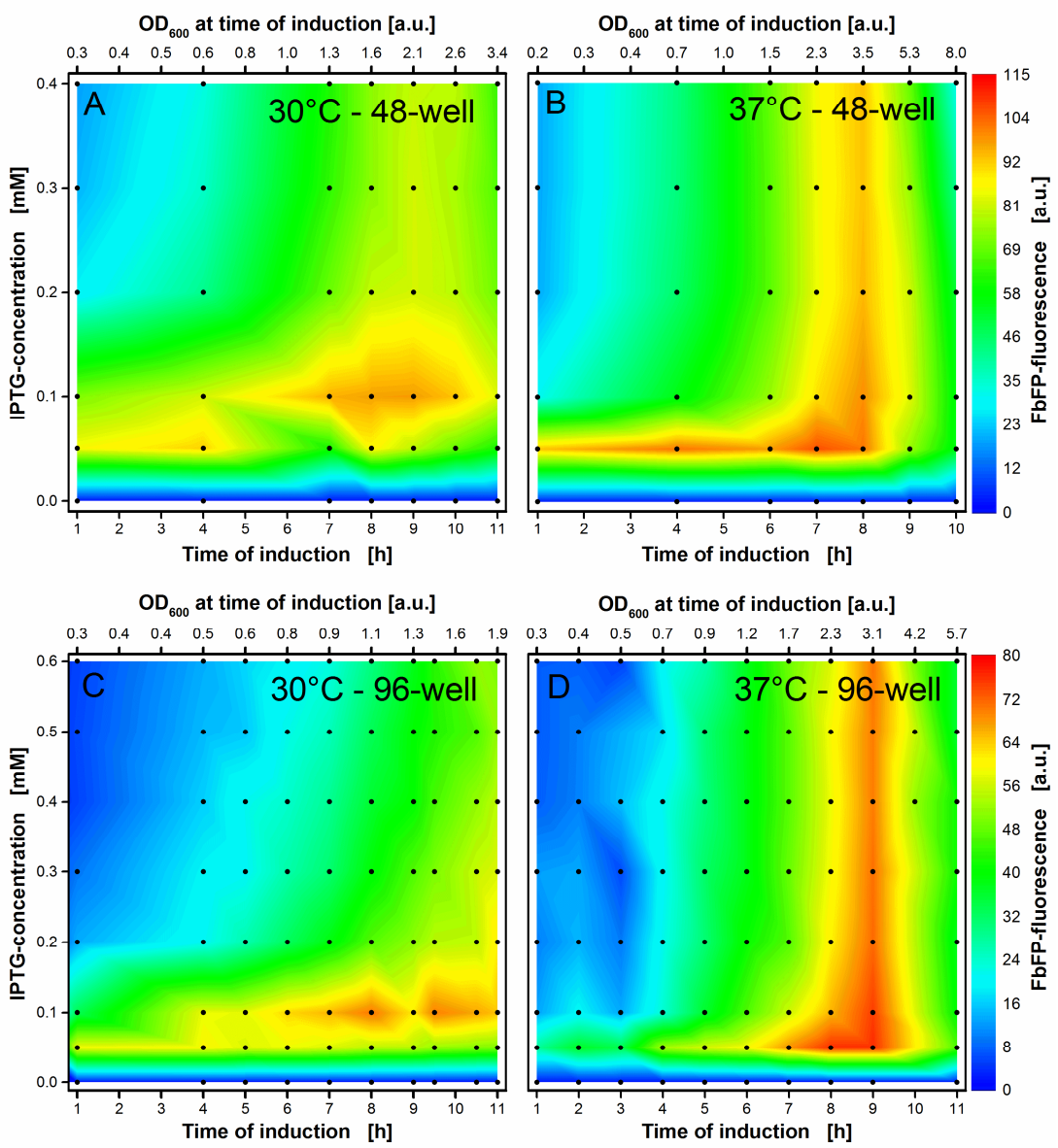

Figure A- 4: **Comparison of induction profiles at 30°C and 37°C in 48-well plates and 96-well plates.** Colors from blue to red indicate maximal reached FbFP intensities at the end of each culture. Black dots indicate the 42-80 individual cultivations for each induction profile. The upper x-axes reflect the corresponding optical density of the cultures at the time of induction. It is calculated from the mean scattered light values of cultures that have not been induced until the respective induction time and a calibration curve that was previously prepared (see Appendix). **A)** 30°C, 48-well plate, induction after 1 - 11 h, **B)** 37°C, 48-well plate, induction after 1 - 10 h, **C)** 30°C, 96-well plate, induction after 1 - 11 h, **D)** 37°C, 96-well plate, induction after 1 - 11 h. Cultivation conditions for *E. coli* Tuner(DE3)/pRhotHi-2-EcFbFP in 48-well Flowerplates: Wilms-MOPS mineral medium, sandwich membrane (m2p-labs), V_L = 800 µL, n = 1400 rpm, d_0 = 3 mm. For standard 96-well plates: Wilms-MOPS mineral medium, AeraSeal membrane, V_L = 200 µL, n = 1000 rpm, d_0 = 3 mm.

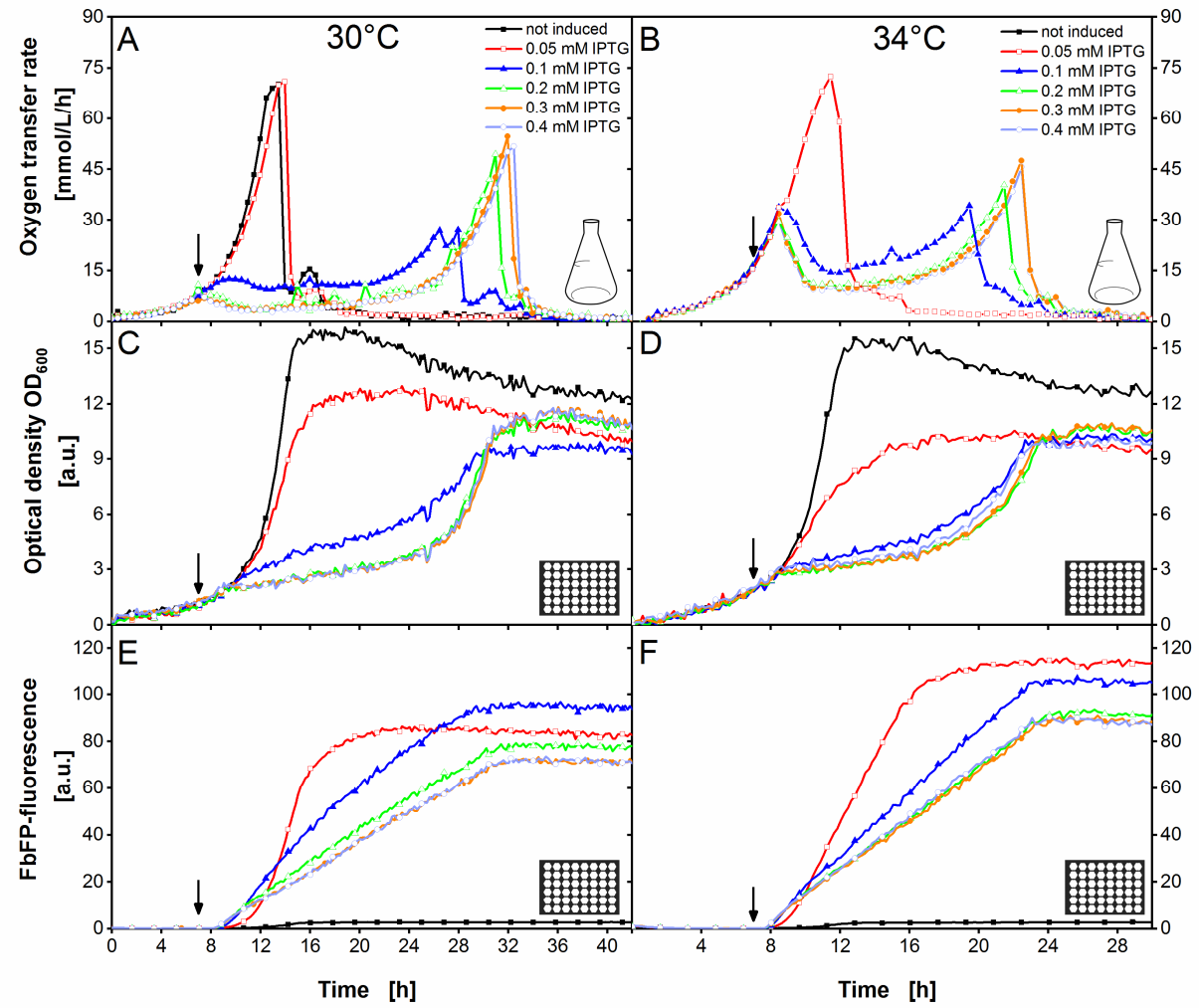

Figure A- 5: **Comparison of selected induction conditions at 30°C and 34°C measured in a RAMOS and a BioLector device.** Manual induction (shake flask) and automated induction (MTP) after 7 h with 0-0.4 mM IPTG (indicated by black arrow). Cultivation temperature was 30°C for the graphs in the left column and 34°C for the graphs in the right column. RAMOS and BioLector cultivations were conducted for each temperature in parallel using the same 'mastermix' (medium plus microorganisms). **A), B)** Oxygen-transfer rate of RAMOS cultivations in 250 mL shake flasks, **C), D)** Scattered light signal from BioLector cultivations, **E), F)** FbFP-fluorescence. Cultivation conditions for *E. coli* Tuner(DE3)/pRhotHi-2-EcFbFP in RAMOS device: Wilms-MOPS mineral medium, 250 mL flask, V_L = 8 mL, n = 350 rpm, d_0 = 50 mm, in BioLector device: Wilms-MOPS mineral medium, 48-well Flowerplate, sandwich membrane (m2p-labs), V_L = 800 µL, n = 1400 rpm, d_0 = 3 mm.

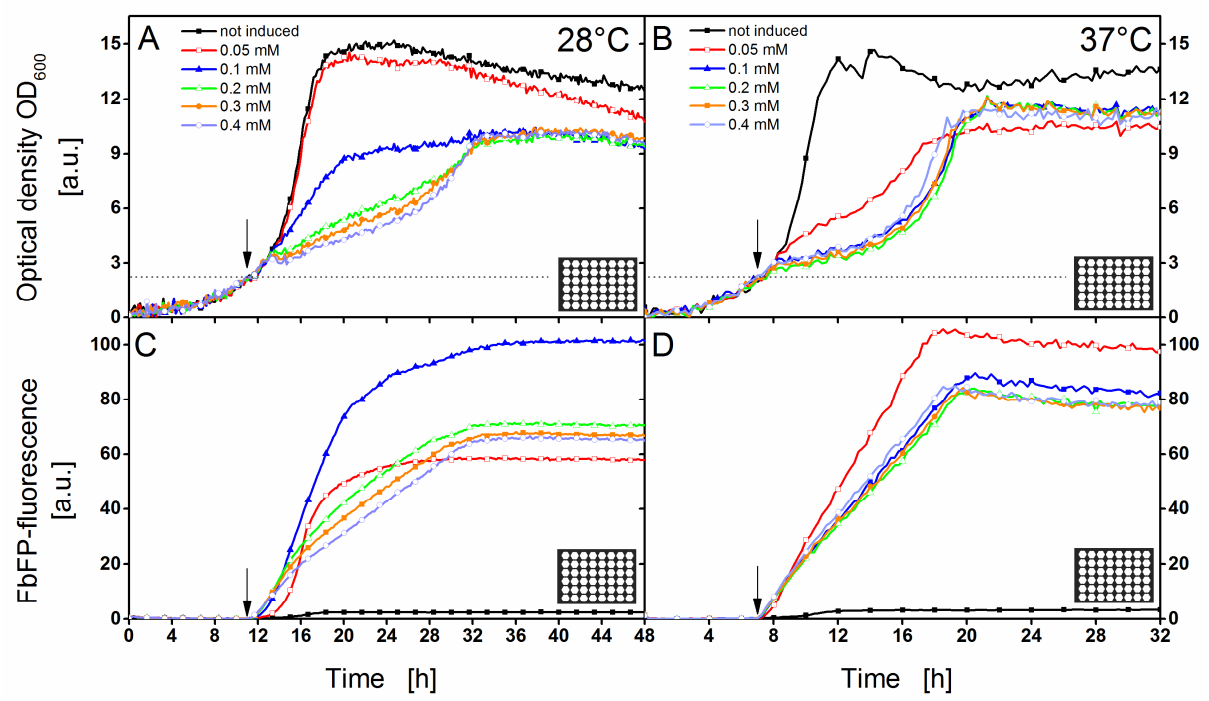

Figure A- 6: **Comparison of selected induction conditions at 28°C and 37°C at same optical density measured in BioLector device.** Automated induction after 11 h (A, C) and 7 h (B, D) with 0 - 0.4 mM IPTG (indicated by black arrow). Dotted line visualizes induction at same biomass concentration. Cultivation temperature was 28°C for the graphs in the left column and 37°C for the graphs in the right column. **A), B)** Scattered light signal and **C), D)** FbFP-fluorescence. Cultivation conditions for *E. coli* Tuner(DE3)/pRhotHi-2-EcFbFP in BioLector device: Wilms-MOPS mineral medium, 48-well Flowerplate, sandwich membrane (m2p-labs), V_L = 800 µL, n = 1400 rpm, d_0 = 3 mm.

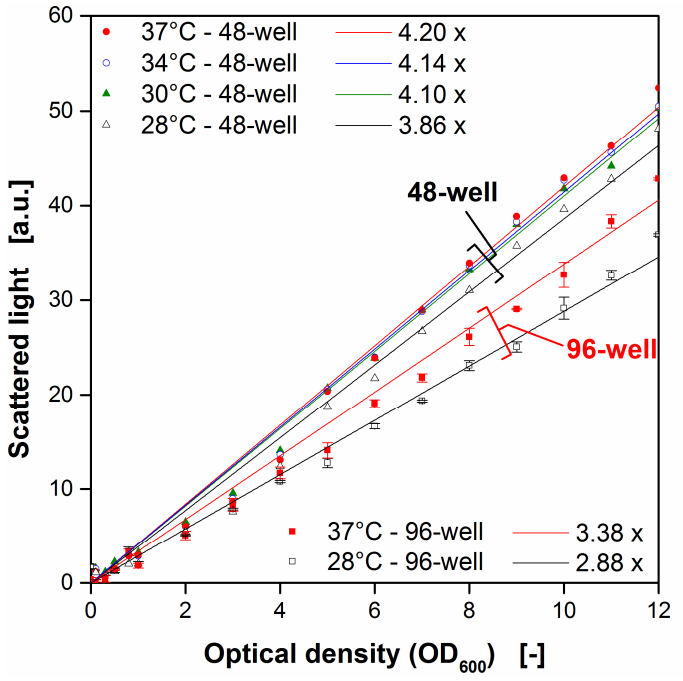

Figure A- 7: **Calibration curves for conversion of scattered light to standard optical density in 48-well and 96-well plates.** Calibration was performed with cells from stationary phase. Optical densities from 0.1-12 were prepared. Standard deviations are only available for 96-well plates and were derived from three independent measurements. Equations from linear fits can be found in the figure. Cultivation conditions: *E. coli* Tuner(DE3)/pRhotHi-2-EcFbFP dilutions were measured in BioLector device in 48-well Flowerplates: Wilms-MOPS mineral medium, sandwich membrane (m2p-labs), V_L = 800 µL, n = 1400 rpm, d_0 = 3 mm. In 96-well standard plates: Wilms-MOPS mineral medium, AeraSeal membrane, V_L = 200 µL, n = 1000 rpm, d_0 = 3 mm. For both MTPs: 28-37°C.

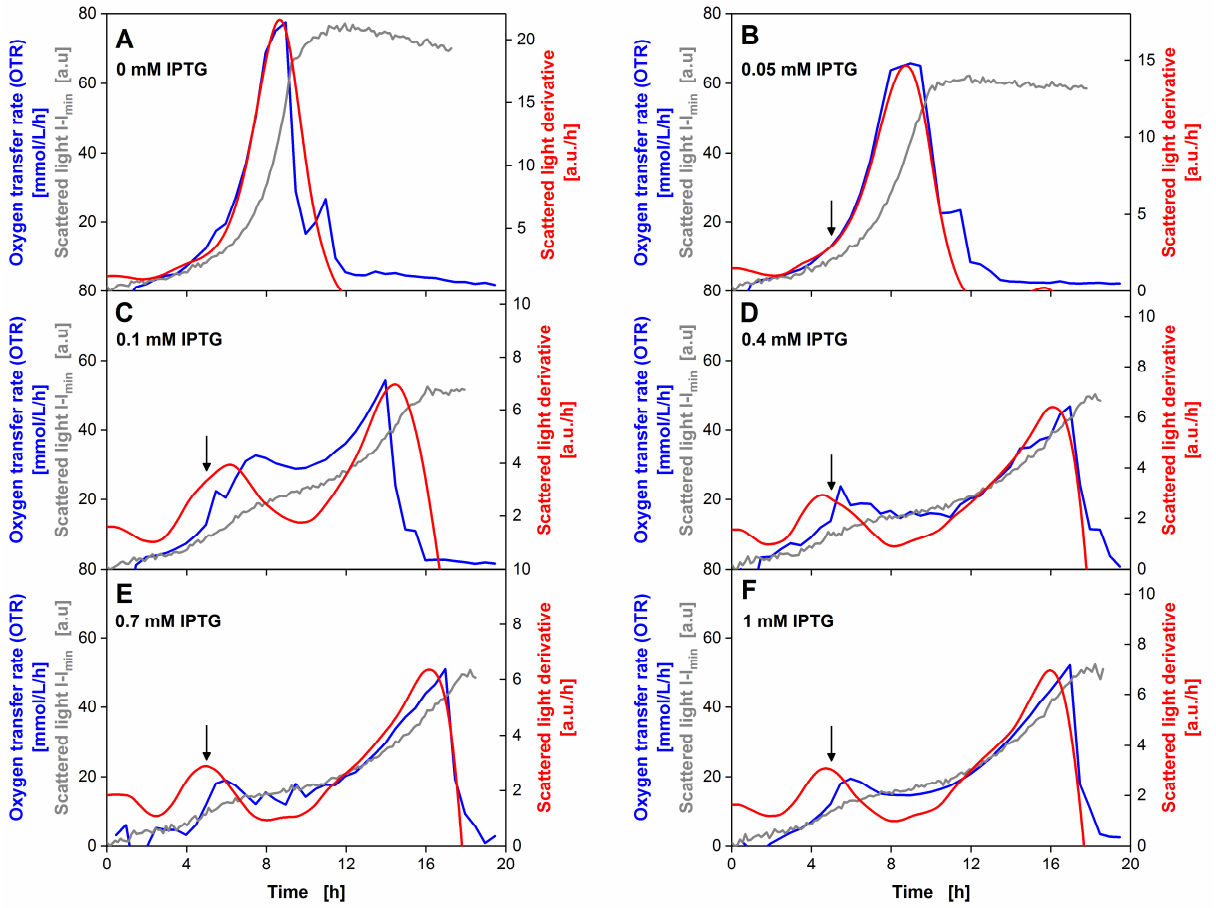

Figure A- 8: **Simultaneous experiments of *E. coli* BL21(DE3) pET28a(+) expressing the cellulase celA2 wildtype under control of the T7-promoter in a RAMOS device and a BioLector device.** The cultures were prepared from one *mastermix* and were started simultaneously in both devices in Wilms-MOPS mineral medium (20 g/L glucose). OTRs were obtained from RAMOS measurements in shake flasks. ScL values were received from BioLector measurements in a 48-well Flowerplate. Smoothing splines of the ScL curves were produced with MATLAB and subsequently the first derivative was taken (dScL/dt). Induction was manually performed for shake flasks and automatically for the MTP after 5 h with 0-1 mM IPTG (**A-F**). Cultivation conditions for shake flasks: 250 mL flask, V_L = 8 mL, n = 350 rpm, d_0 = 50 mm, 37°C. Cultivation conditions for MTPs: 48-well Flowerplate, sandwich membrane (m2p-labs), V_L = 800 µL, n = 1400 rpm, d_0 = 3 mm, 37°C.

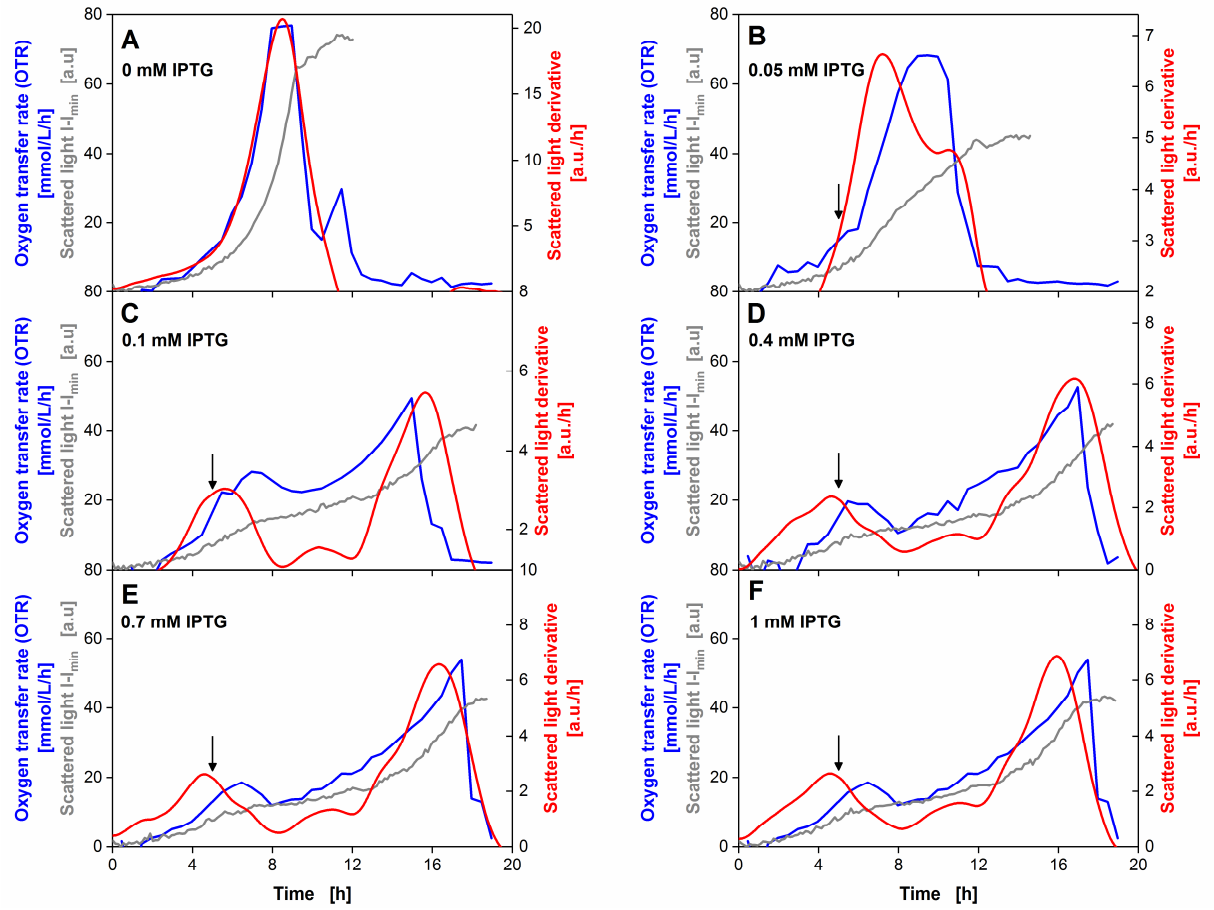

Figure A- 9: **Simultaneous experiments of *E. coli* BL21(DE3) pET28a(+) expressing the cellulase celA2 mutant under control of the T7-promoter in a RAMOS device and a BioLector device.** The cultures were prepared from one *mastermix* and were started simultaneously in both devices in Wilms-MOPS mineral medium (20 g/L glucose). OTRs were obtained from RAMOS measurements in shake flasks. ScL values were received from BioLector measurements in a 48-well Flowerplate. Smoothing splines of the ScL curves were produced with MATLAB and subsequently the first derivative was taken (dScL/dt). Induction was manually performed for shake flasks and automatically for the MTP after 5 h with 0-1 mM IPTG (**A-F**). Cultivation conditions for shake flasks: 250 mL flask, V_L = 8 mL, n = 350 rpm, d_0 = 50 mm, 37°C. Cultivation conditions for MTPs: 48-well Flowerplate, sandwich membrane (m2p-labs), V_L = 800 µL, n = 1400 rpm, d_0 = 3 mm, 37°C.

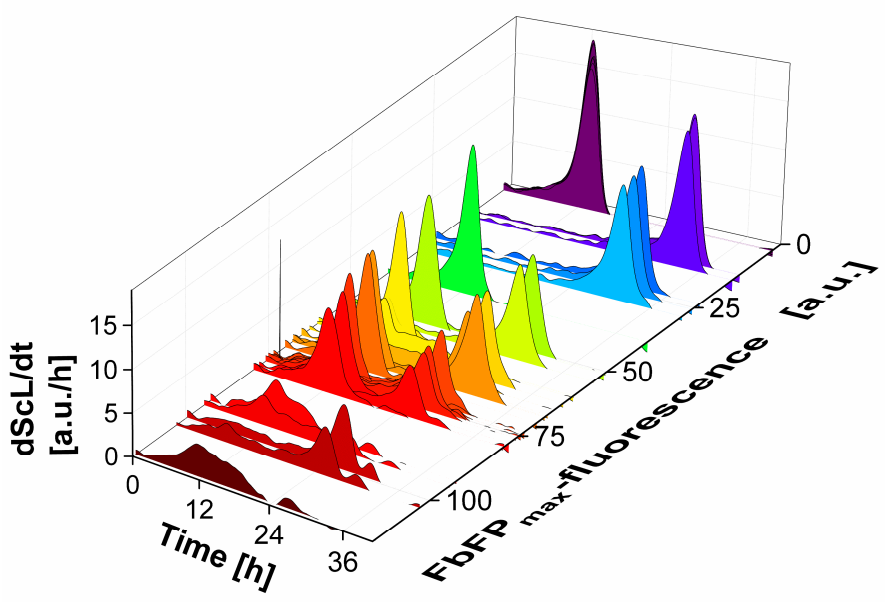

Figure A- 10: 3D-plot of dScL/dt courses over time vs. achieved product maximum.
Results were derived from 45 *E. coli* Tuner(DE3) FbFP cultivations. Smoothing splines of the ScL curves were produced with MATLAB and subsequently the first derivatives were taken (dScL/dt). Automated induction of cultures at 7 h with different inducer concentrations (0-1 mM IPTG). Cultivation conditions in BioLector device: Wilms-MOPS mineral medium, 48-well Flowerplate, sandwich membrane (m2p-labs), V_L = 800 µL, n = 1400 rpm, d_0 = 3 mm, 30°C.

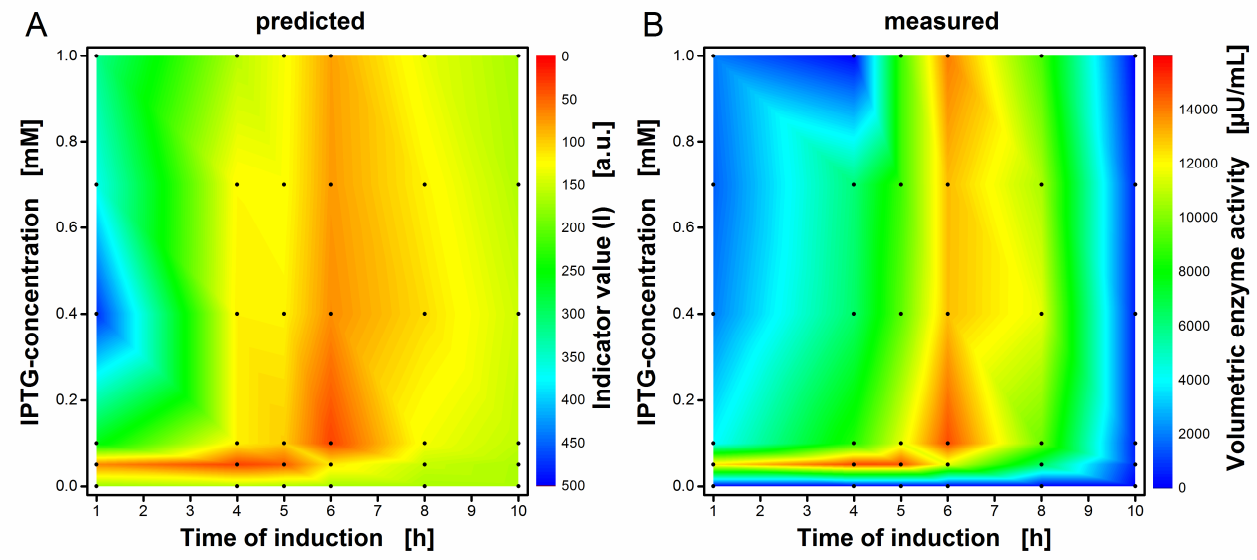

Figure A- 11: Induction profiles – predicted vs. measured data.
Results were obtained from *E. coli* BL21(DE3) pET28a(+) expressing the cellulase celA2 mutant under control of a T7-promoter. Induction profiling was conducted in a 48-well Flowerplate with a BioLector device. The induction took was automatically performed at 1-10 h with concentrations ranging from 0-1 mM IPTG. Black dots indicate the 36 individual cultivations. The indicator values (I) were calculated according to Eq. (6-1). **A)** A whole induction profile is predicted from dScL/dt data by the calculated indicator values. Since the indicator is inversely proportional to the product formation, the color code is inverted. **B)** Results of the offline conducted 4-MUC assay that was used to experimentally evaluate the volumetric enzyme activity for all induction conditions (end-point determination). Cultivation conditions: Wilms-MOPS mineral medium (20 g/L glucose), sandwich membrane (m2p-labs), V_L = 800 µL, n = 1400 rpm, d_0 = 3 mm, 37°C.

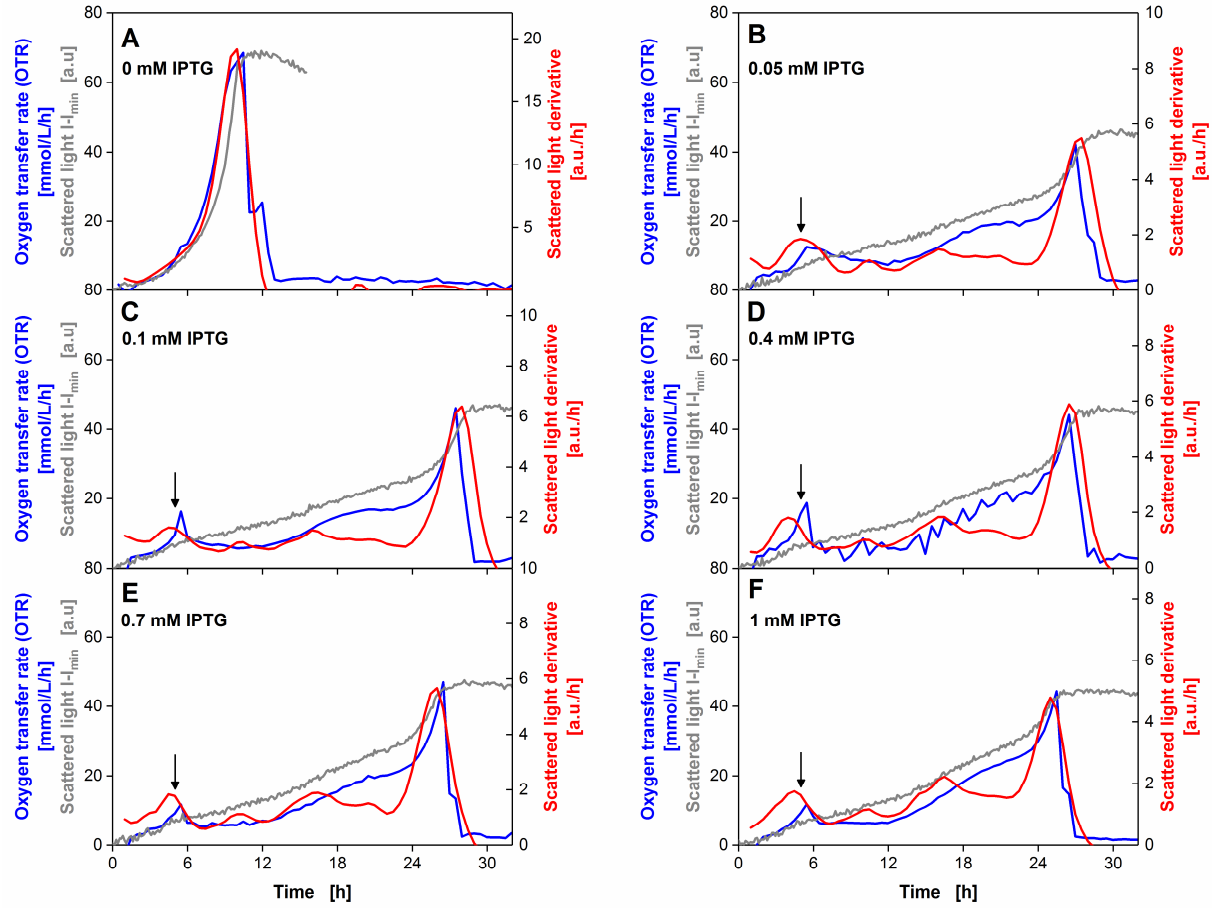

Figure A- 12: Simultaneous experiments of *E. coli* BL21(DE3) pET28a(+) celA2 expressing the cellulase celA2 wildtype under control of the Tac-promoter in a RAMOS device and a BioLector device. The cultures were prepared from one *mastermix* and were started simultaneously in both devices in Wilms-MOPS mineral medium (20 g/L glucose). OTRs were obtained from RAMOS measurements in shake flasks. ScL values were received from BioLector measurements in a 48-well Flowerplate. Smoothing splines of the ScL curves were produced with MATLAB and subsequently the first derivative was taken (dScL/dt). Induction was manually performed for shake flasks and automatically for the MTP after 5 h with 0-1 mM IPTG (**A-F**). Cultivation conditions for shake flasks: 250 mL flask, V_L = 8 mL, n = 350 rpm, d_0 = 50 mm, 37°C. Cultivation conditions for MTPs: 48-well Flowerplate, sandwich membrane (m2p-labs), V_L = 800 µL, n = 1400 rpm, d_0 = 3 mm, 37°C.

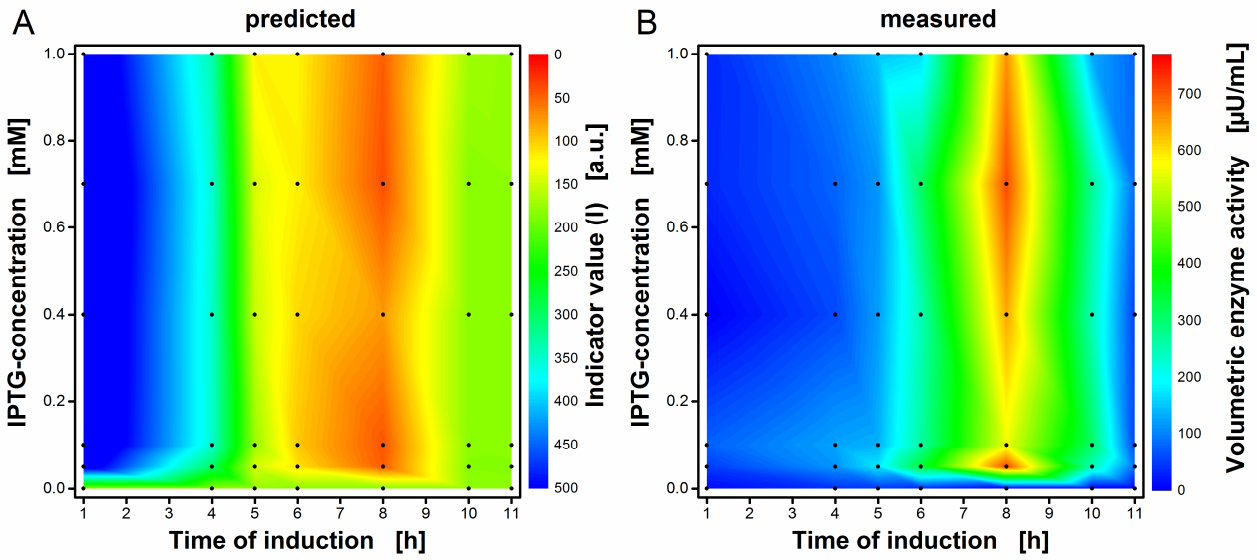

Figure A- 13: Induction profiles – predicted vs. measured data.
Results were obtained from *E. coli* BL21(DE3) pET28a(+) expressing the cellulase celA2 wildtype under control of a Tac-promoter. Induction profiling was conducted in a 48-well Flowerplate with a BioLector device. The induction was automatically performed at 1-11 h with concentrations ranging from 0-1 mM IPTG. Black dots indicate the 42 individual cultivations. The indicator values (I) were calculated according to Eq. 8. **A)** A whole induction profile is predicted from dScL/dt data by the calculated indicator values. Since the indicator is inversely proportional to the product formation, the color code is inverted. **B)** Results of the offline conducted 4-MUC assay that was used to experimentally evaluate the volumetric enzyme activity for all induction conditions (end-point determination). Cultivation conditions: Wilms-MOPS mineral medium (20 g/L glucose), sandwich membrane (m2p-labs), V_L = 800 µL, n = 1400 rpm, d_0 = 3 mm, 37°C.

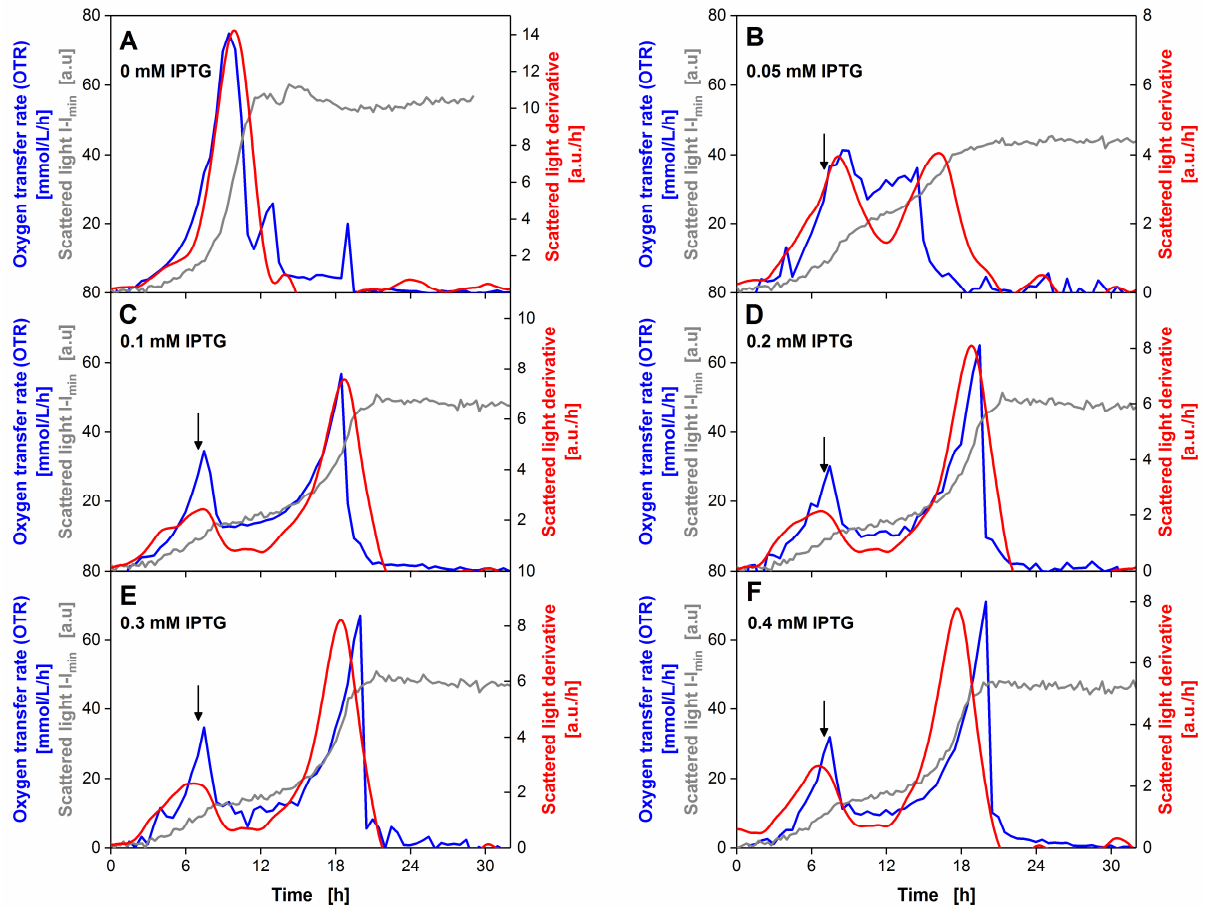

Figure A- 14: Simultaneous experiments of *E. coli* Tuner(DE3) FbFP in a RAMOS device and a BioLector device. The cultures were prepared from one *mastermix* and were started simultaneously in both devices in Wilms-MOPS mineral medium (20 g/L glucose). OTRs were obtained from RAMOS measurements in shake flasks. ScL values were received from BioLector measurements in a 48-well Flowerplate. Smoothing splines of the ScL curves were produced with MATLAB and subsequently the first derivative was taken (dScL/dt). Induction was manually performed for shake flasks and automatically for the MTP after 7 h with 0-0.4 mM IPTG (**A-F**). The expression of FbFP was under control of the T7 promoter. Cultivation conditions for shake flasks: Cultivation conditions for shake flasks: 250 mL flask, V_L = 8 mL, n = 350 rpm, d_0 = 50 mm, 37°C. Cultivation conditions for MTPs: 48-well Flowerplate, sandwich membrane (m2p-labs), V_L = 800 µL, n = 1400 rpm, d_0 = 3 mm, 37°C.

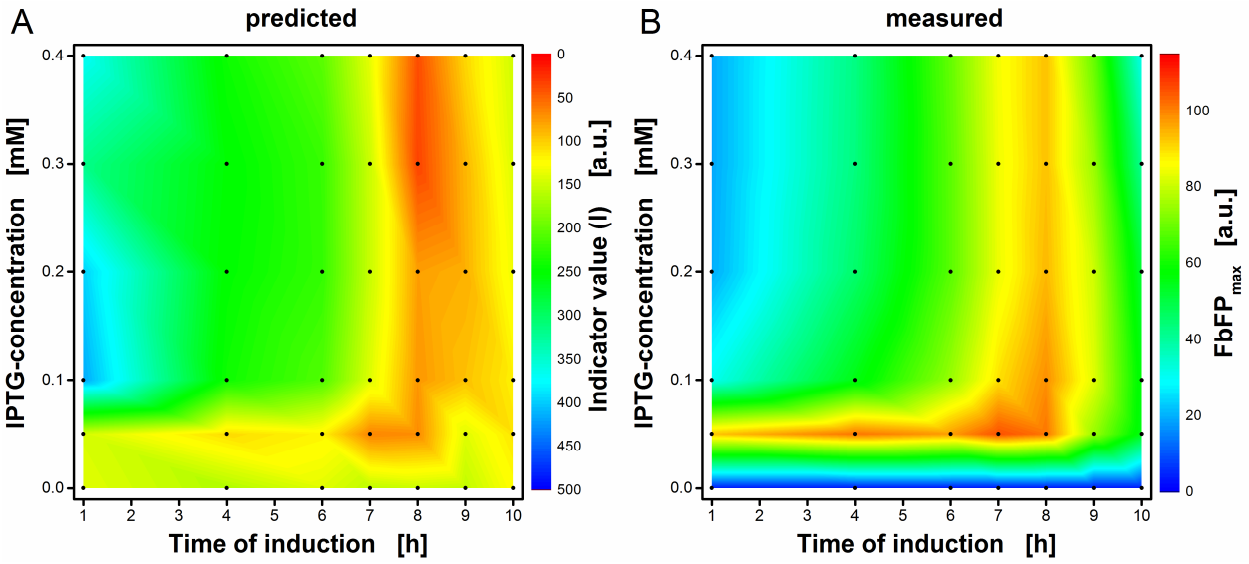

Figure A- 15: Induction profiles – predicted vs. measured data.
Results were obtained from *E. coli* Tuner(DE3) expressing the fluorescent protein FbFP under control of a T7-promoter. Induction profiling was conducted in a 48-well Flowerplate with a BioLector device. The induction was automatically performed at 1-10 h with concentrations ranging from 0-0.4 mM IPTG. Black dots indicate the 42 individual cultivations. The indicator values (I) were calculated according to Eq. 8. **A)** A whole induction profile is predicted from dScL/dt data by the calculated indicator values. Since the indicator is inversely proportional to the product formation, the color code is inverted. **B)** Results of the maximum measured FbFP fluorescence intensity for each induction condition. Cultivation conditions: Wilms-MOPS mineral medium (20 g/L glucose), sandwich membrane (m2p-labs), V_L = 800 µL, n = 1400 rpm, d_0 = 3 mm, 37°C.

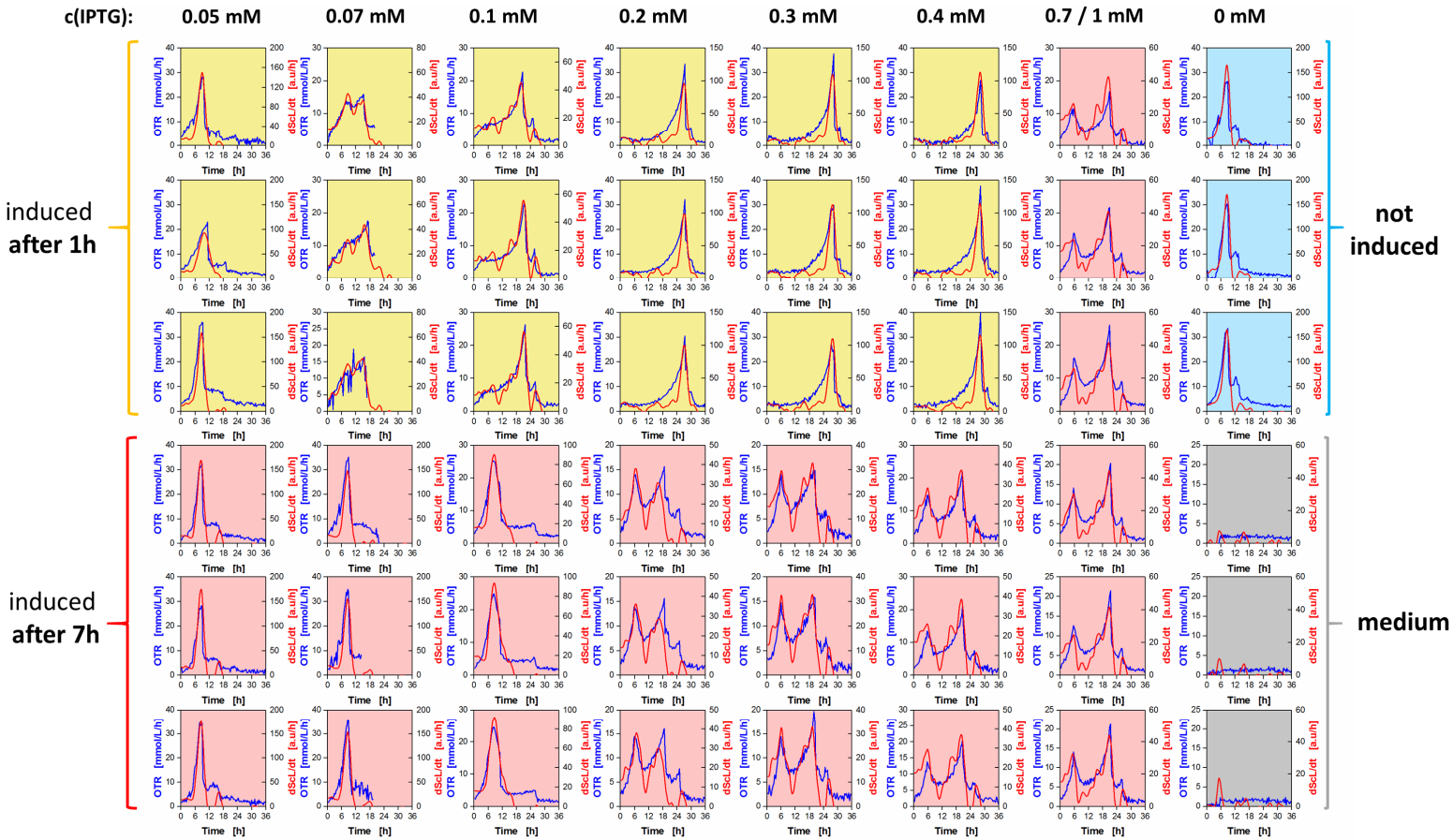

Figure A- 16: **48 simultaneous experiments of *E. coli* Tuner(DE3) FbFP in a device that combines the µRAMOS with the BioLector technology** (Ladner et al. 2016b). OTRs were obtained from µRAMOS measurements in a 48-roundwell plate. ScL values were received simultaneously from BioLector measurements in the identical plate. A smoothing spline of the ScL curve is produced with MATLAB and subsequently the first derivative is taken (dScL/dt). Induction was manually performed after 1 or 7 h with 0-1 mM IPTG. Each induction condition was performed as triplicate. 6 wells were used for a non-induced reference and plain medium. Cultivation conditions: Wilms-MOPS mineral medium (10 g/L glucose), V_L = 800 µL, n = 1000 rpm, d_0 = 3 mm, 30°C.

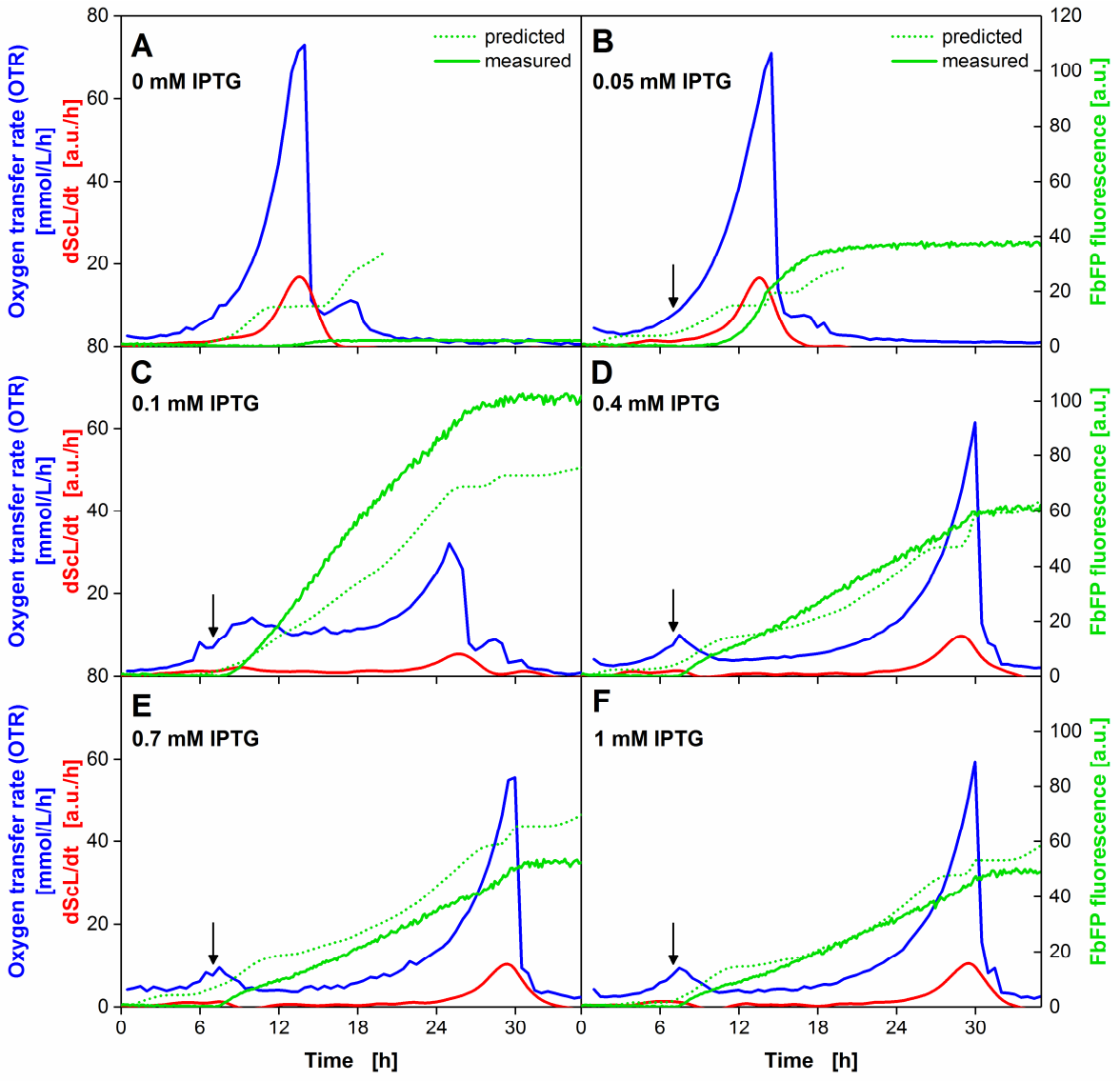

Figure A- 17: Time-resolved prediction of *E. coli* Tuner(DE3) FbFP at 30°C (0-1 mM IPTG).

Fixed parameter: $\frac{1}{Y_{X/O_2}} = 4.50$, parameter received by solver function: $\frac{1}{Y_{P/O_2}} = 1.84$. The 6 RAMOS and BioLector cultivations were conducted in parallel using the same mastermix (medium plus microorganisms). Smoothing splines of the ScL curves were produced with MATLAB and subsequently the first derivatives were taken (dScL/dt). Manual induction (shake flask) and automated induction (MTP) at 7 h with different inducer concentrations (0-1 mM IPTG). Cultivation conditions in RAMOS device: Wilms-MOPS mineral medium, 250 mL flask, V_L = 8 mL, n = 350 rpm, d_0 = 50 mm, in BioLector device: Wilms-MOPS mineral medium, 48-well Flowerplate, sandwich membrane (m2p-labs), V_L = 800 µL, n = 1400 rpm, d_0 = 3 mm.

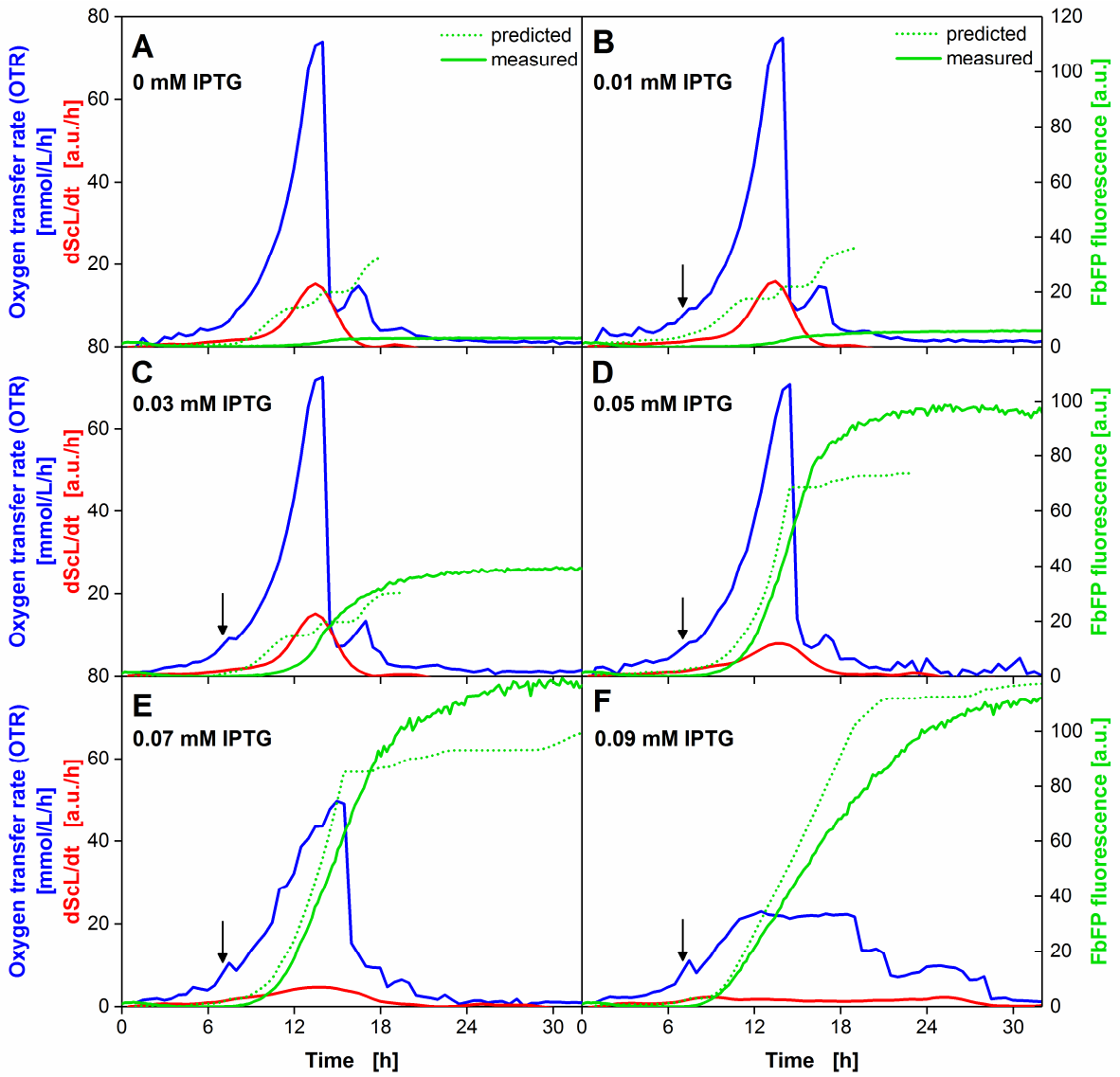

Figure A- 18: Time-resolved prediction of *E. coli* Tuner(DE3) FbFP at 30°C (0-0.09 mM IPTG). Fixed parameter: $\frac{1}{Y_{X/O_2}} = 4.50$, parameter received by solver function: $\frac{1}{Y_{P/O_2}} = 1.41$. The 6 RAMOS and BioLector cultivations were conducted in parallel using the same mastermix (medium plus microorganisms). Smoothing splines of the ScL curves were produced with MATLAB and subsequently the first derivatives were taken (dScL/dt). Manual induction (shake flask) and automated induction (MTP) at 7 h with different inducer concentrations (0-0.09 mM IPTG). Cultivation conditions in RAMOS device: Wilms-MOPS mineral medium, 250 mL flask, V_L = 8 mL, n = 350 rpm, d_0 = 50 mm, in BioLector device: Wilms-MOPS mineral medium, 48-Flowerplate, sandwich membrane (m2p-labs), V_L = 800 µL, n = 1400 rpm, d_0 = 3 mm.

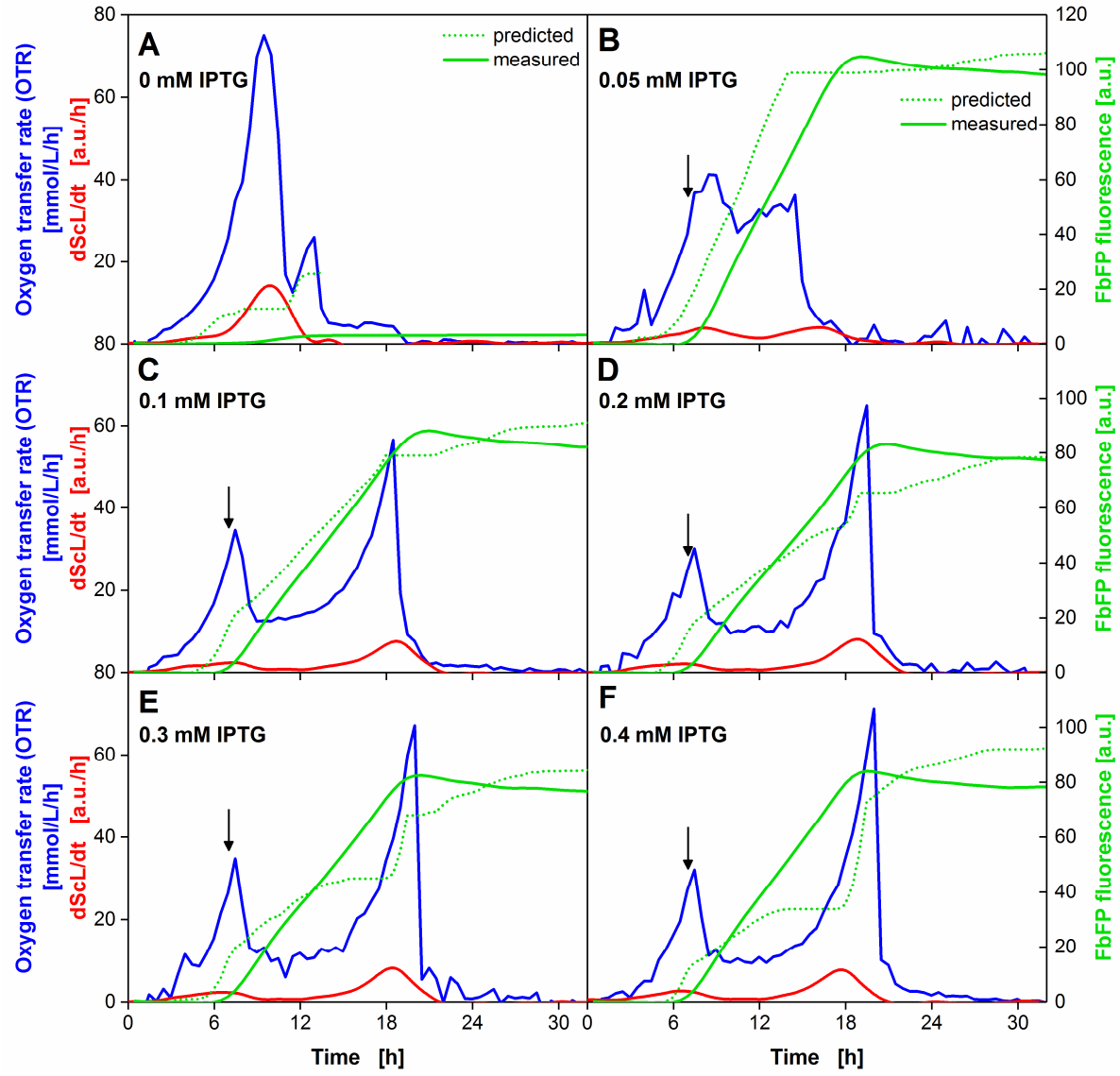

Figure A- 19: **Time-resolved prediction of *E. coli* Tuner(DE3) FbFP at 37°C.**
Fixed parameter: $\frac{1}{Y_{X/O_2}} = 5.47$, parameter received by solver function: $\frac{1}{Y_{P/O_2}} = 1.66$. The 6 RAMOS and BioLector cultivations were conducted in parallel using the same mastermix (medium plus microorganisms). Smoothing splines of the ScL curves were produced with MATLAB and subsequently the first derivatives were taken (dScL/dt). Manual induction (shake flask) and automated induction (MTP) at 7 h with different inducer concentrations (0-0.4 mM IPTG). Cultivation conditions in RAMOS device: Wilms-MOPS mineral medium, 250 mL flask, V_L = 8 mL, n = 350 rpm, d_0 = 50 mm, in BioLector device: Wilms-MOPS mineral medium, 48-well Flowerplate, sandwich membrane (m2p-labs), V_L = 800 µL, n = 1400 rpm, d_0 = 3 mm.

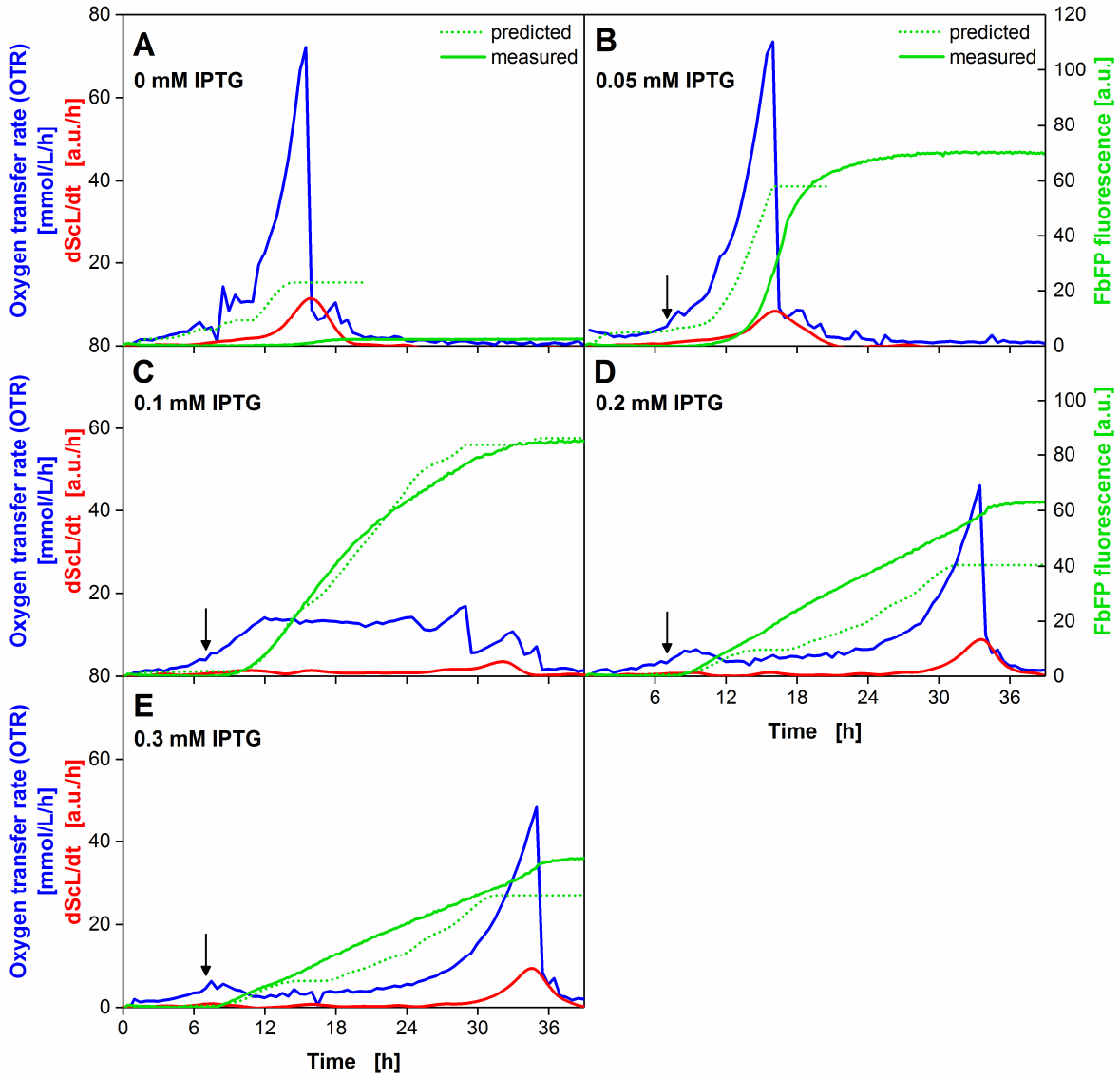

Figure A- 20: **Time-resolved prediction of *E. coli* Tuner(DE3) FbFP at 28°C.**
Fixed parameter: $\frac{1}{Y_{X/O_2}} = 6.82$, parameter received by solver function: $\frac{1}{Y_{P/O_2}} = 1.39$. The 5 RAMOS and BioLector cultivations were conducted in parallel using the same mastermix (medium plus microorganisms). Smoothing splines of the ScL curves were produced with MATLAB and subsequently the first derivatives were taken (dScL/dt). Manual induction (shake flask) and automated induction (MTP) at 7 h with different inducer concentrations (0-0.3 mM IPTG). Cultivation conditions in RAMOS device: Wilms-MOPS mineral medium, 250 mL flask, V_L = 8 mL, n = 350 rpm, d_0 = 50 mm, in BioLector device: Wilms-MOPS mineral medium, 48-well Flowerplate, sandwich membrane (m2p-labs), V_L = 800 µL, n = 1400 rpm, d_0 = 3 mm.

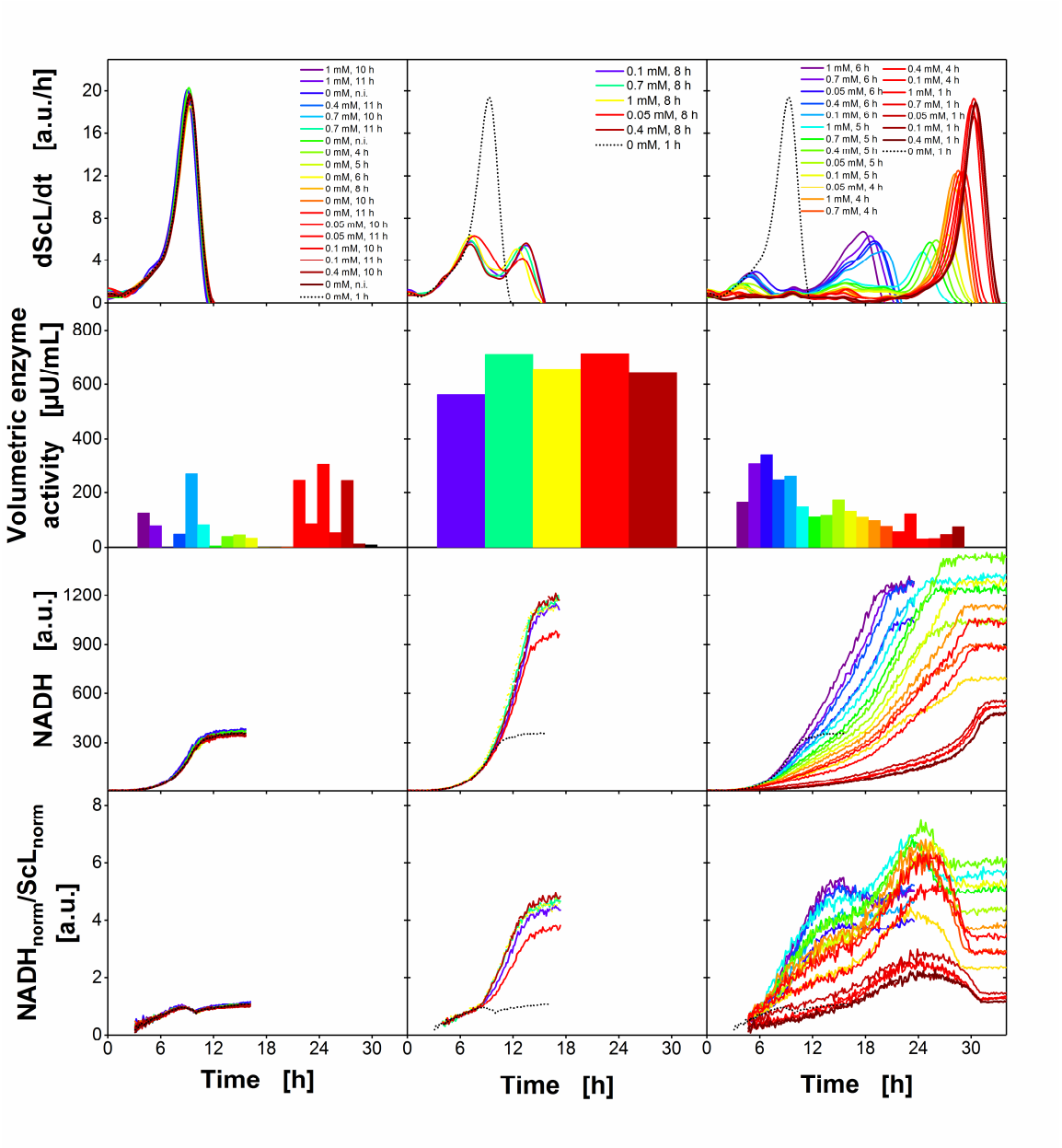

Figure A- 21: Impact of product expression on NADH formation classified in three groups for *E. coli* BL21(DE3)pET28a(+) celA2 wildtype under control of a Tac-promoter. Induction profiling was conducted in a 48-well Flowerplate with a BioLector device. The induction was automatically performed at 1-11 h with concentrations ranging from 0-1 mM IPTG. Black dots indicate the 42 individual cultivations. NADH and ScL were measured optically in the BioLector device. Smoothing splines of the ScL curves were produced with MATLAB and subsequently the first derivatives were taken (dScL/dt). The volumetric enzyme activity was determined by the 4-MUC assay (end-point determination). Cultivation conditions in BioLector device: Wilms-MOPS mineral medium, 48-well Flowerplate, sandwich membrane (m2p-labs), V_L = 800 µL, n = 1400 rpm, d_0 = 3 mm, 37°C.

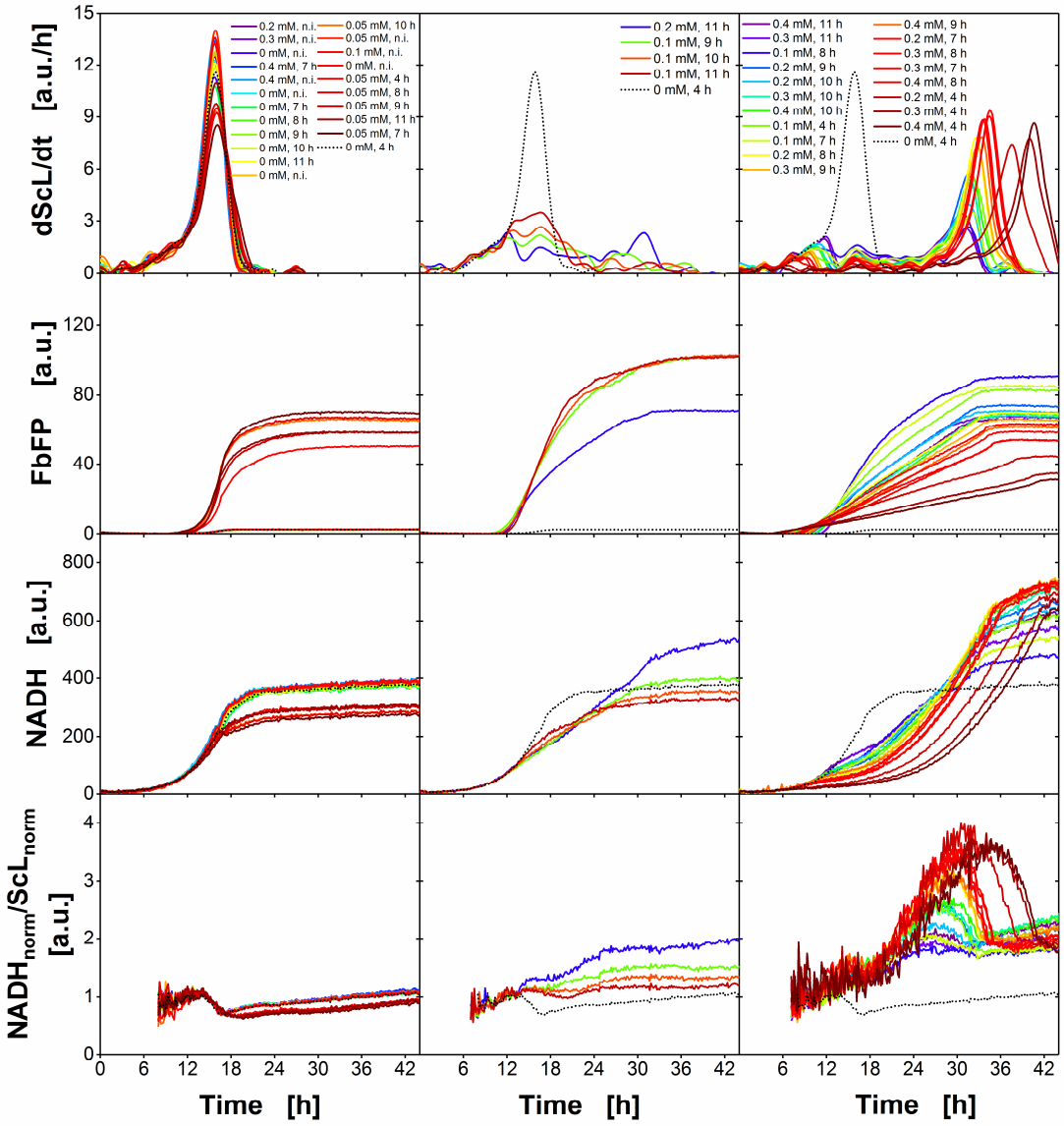

Figure A- 22: Impact of product expression on NADH formation classified in three groups for *E. coli* Tuner(DE3)FbFP at 28°C. Induction profiling was conducted in a 48-well Flowerplate with a BioLector device. The induction was automatically performed at 1-11 h with concentrations ranging from 0-0.4 mM IPTG. Black dots indicate the 42 individual cultivations. FbFP, NADH and ScL were measured optically in the BioLector device. Smoothing splines of the ScL curves were produced with MATLAB and subsequently the first derivatives were taken (dScL/dt). Cultivation conditions in BioLector device: Wilms-MOPS mineral medium, 48-well Flowerplate, sandwich membrane (m2p-labs), V_L = 800 µL, n = 1400 rpm, d_0 = 3 mm, 28°C.

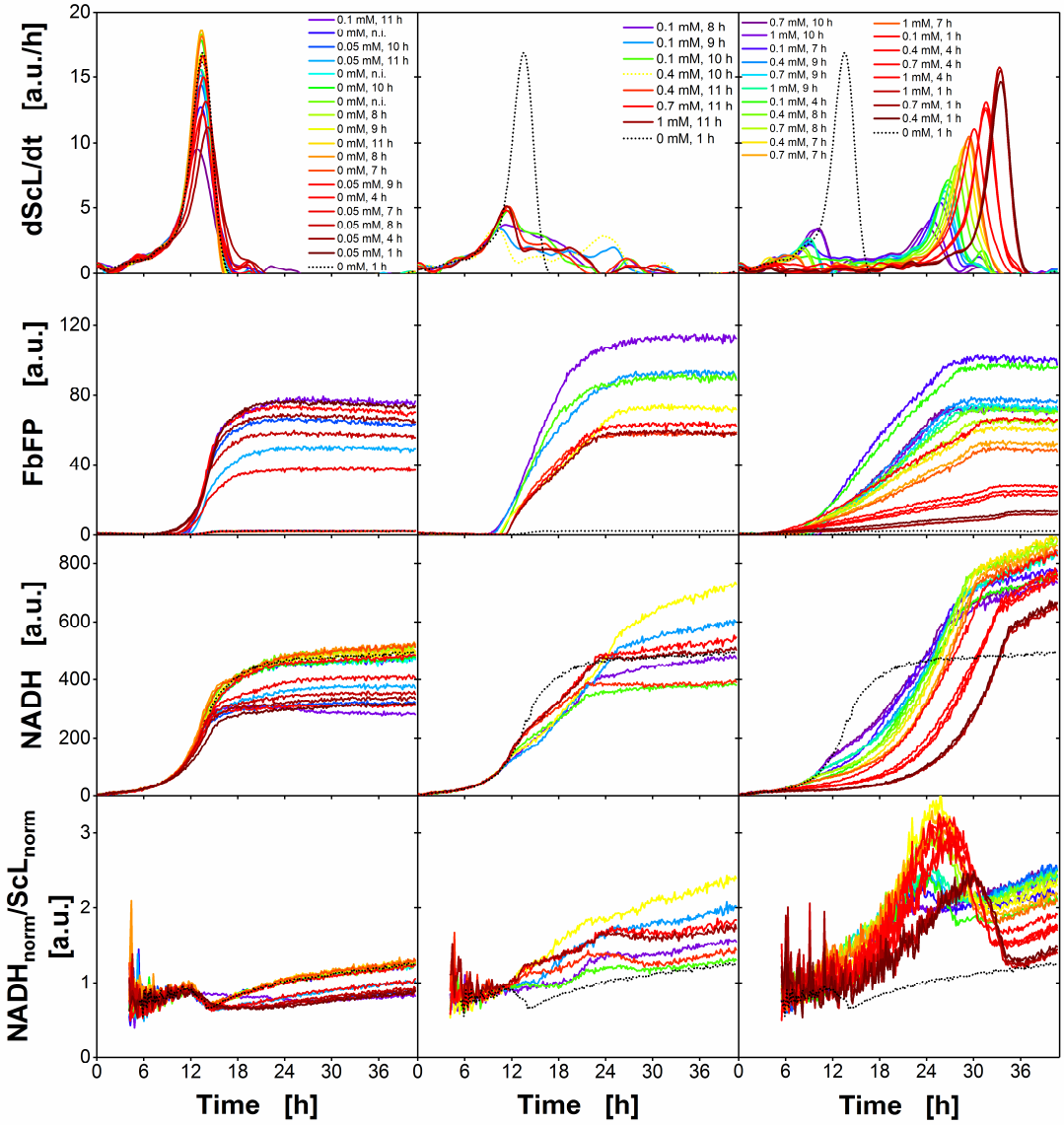

Figure A- 23: Impact of product expression on NADH formation classified in three groups for *E. coli* Tuner(DE3)FbFP at 30°C. Induction profiling was conducted in a 48-well Flowerplate with a BioLector device. The induction was automatically performed at 1-11 h with concentrations ranging from 0 - 1 mM IPTG. Black dots indicate the 42 individual cultivations. FbFP, NADH and ScL were measured optically in the BioLector device. Smoothing splines of the ScL curves were produced with MATLAB and subsequently the first derivatives were taken (dScL/dt). Cultivation conditions in BioLector device: Wilms-MOPS mineral medium, 48-well Flowerplate, sandwich membrane (m2p-labs), V_L = 800 µL, n = 1400 rpm, d_0 = 3 mm, 30°C.

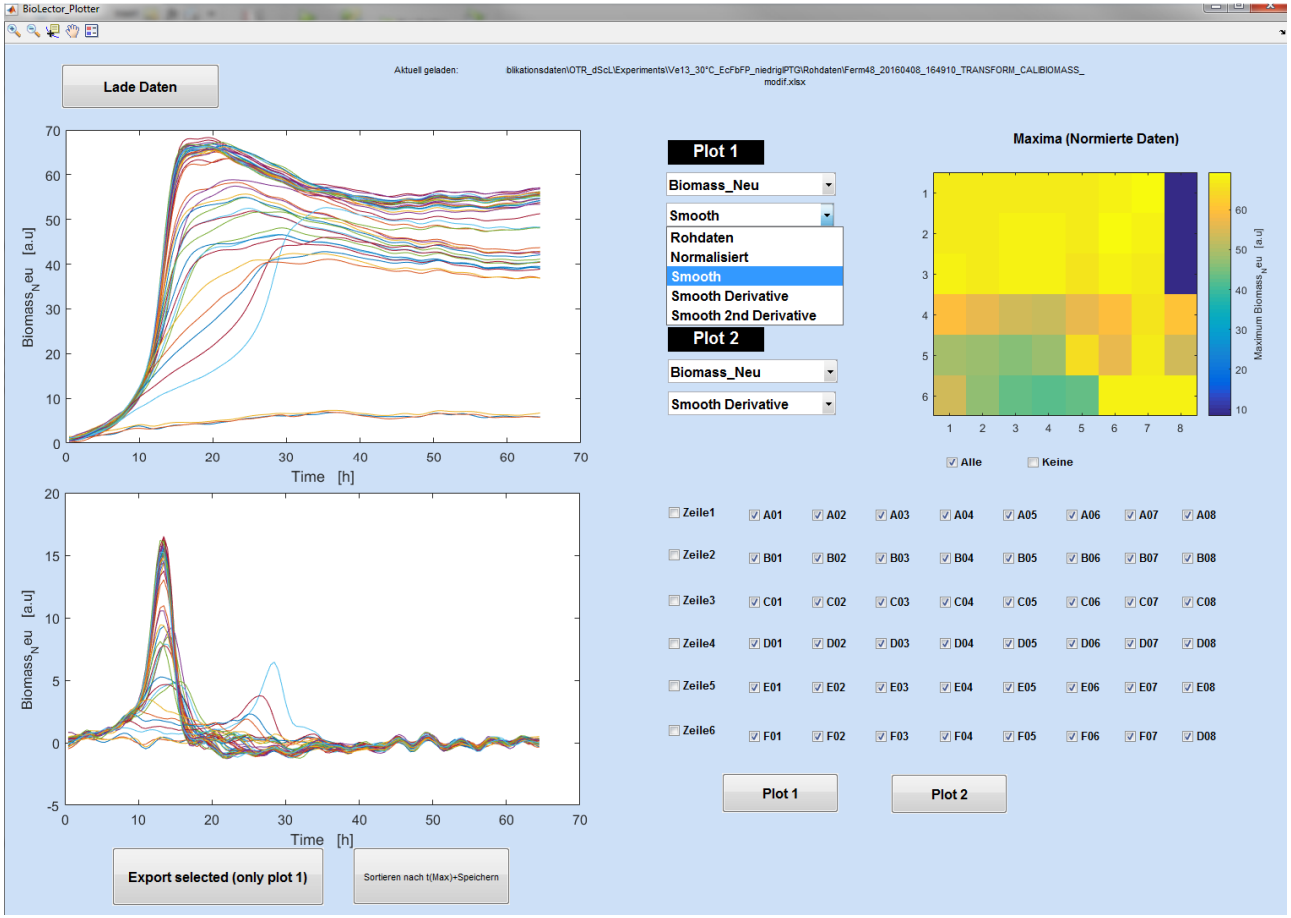

Figure A- 24: Screenshot of the programmed BioLector plotter in MATLAB for 48-well cultivations. m2p-Biolector raw files can be loaded and processed depending on the selected properties in the user interface. After selecting the desired filter, the user can select between 5 data processing possibilities: Raw data; normalized data, smoothed data, first derivative of smoothed data or second derivative of smoothed data. In dependency of the selected wells of a 48-well plate, two different plots can be created. Plotted data in graph 1 can also be saved automatically in an excel-file. The data can be saved and sorted either by alphabet or by the time when the maximum of the respective courses is reached.

Table A- 1: Equations for regression curves in Figure 6-2

	Figure 6-2 A	**Figure 6-2 B**
Linear regression	$y = -4.6x + 883.9$	$y = -0.6x + 128.9$
Logistic regression	$y = 1298.1 + \frac{14773.3 - 1298.1}{1 + \left(\frac{x}{144.2}\right)^{3.1}}$	$y = -4274.4 + \frac{151.2 + 4274.4}{1 + \left(\frac{x}{490844.7}\right)^{0.5}}$

Eq. A1-A2: Calculation of the mean change of dissolved oxygen per hour of an *E. coli* batch cultivation

When the DOT has a value of ~100% air saturation at the beginning of a cultivation (equals an oxygen concentration of 0.22 mmol/L (Wilhelm et al. 1976) and when assuming that the oxygen limitation is reached after ~ 14 h of cultivation (DOT = 0% air saturation), the mean change of dissolved oxygen tension per hour of cultivation can be considered as:

$$\frac{100\%}{14\ h} = 7.14\ \frac{\%}{h} \tag{A1}$$

Proportionally calculated for the oxygen concentration:

$$7.14\ \frac{\%}{h} \cdot 0.22\ \frac{mmol}{L} \cdot \frac{1}{100\%} = 0.0157\ \frac{mmol}{L \cdot h} \tag{A2}$$

The mean change of dissolved oxygen concentration per hour is ~0.02 mmol/L/h during an *E. coli* batch cultivation.